



# **UNIVERSITÀ DEGLI STUDI DI TORINO**

Department of Molecular Sciences and Biotechnologies

## **PhD Programme in Biomedical Sciences and Oncology Cycle XXXII**

Molecular and metabolic characterization of cancer  
cachexia-related muscle wasting

Thesis' author: Elisabeth Wyart

Supervisor: Prof. Paolo Porporato

PhD Programme Co-ordinator : Prof. Emilio Hirsch

Academic years of enrolment : 2016/2020

# Index

|   |    |
|---|----|
| Summary .....   | 2  |
| Introduction.....   | 4  |
| I Cancer Cachexia: A debilitating disease .....                               | 4  |
| I.1 Definition and prevalence .....   | 4  |
| I.2 Classification of cachectic stages.....                                   | 4  |
| I.3 Experimental models of cachexia.....                                      | 5  |
| II Mechanisms of skeletal muscle wasting in cachexia.....                     | 6  |
| II.1 Altered protein homeostasis .....  | 6  |
| II.2 Mediators and signaling pathways inducing skeletal muscle wasting .....  | 7  |
| III Metabolic dysfunction in cancer cachexia .....                            | 10 |
| III.1 Systemic metabolic dysfunction.....                                     | 10 |
| III.2 Skeletal muscle metabolism & mitochondrial dysfunction in cachexia..... | 15 |
| IV Iron metabolism in cachexia .....  | 16 |
| IV.1 Cellular iron metabolism .....   | 16 |
| IV.2 Iron metabolism in cancer.....   | 17 |
| IV.3 Iron and muscle function: Implication in cachexia?.....                  | 18 |
| V References Introduction.....  | 19 |
| Aims of the work .....  | 26 |
| Chapter 1 .....   | 26 |
| Chapter 2 .....   | 27 |
| Chapter 1 .....   | 28 |
| I Introduction.....   | 29 |
| II Materials and Methods .....  | 30 |
| III Results .....   | 35 |
| IV Discussion.....  | 40 |
| V References Chapter 1 .....  | 42 |
| Chapter 2 .....   | 44 |
| I Introduction.....   | 45 |
| II Material and methods.....  | 46 |
| III Results .....   | 53 |
| IV Discussion.....  | 63 |
| V References chapter 2 .....  | 65 |
| VI Supplementary Material .....   | 75 |
| General Conclusion .....  | 80 |

# Summary

Cancer cachexia is a complex metabolic syndrome occurring in the majority of terminal cancer patients. Cachexia is characterized by a progressive loss of adipose tissue and skeletal muscle mass that cannot be reversed by conventional nutritional support. It is associated with bad prognosis and diminished quality of life, and to date, it is lacking effective therapies. Mechanisms responsible for cancer cachexia are still poorly understood and research in this field is hampered by the lack of satisfactory models to study the complexity of wasting in cachexia-inducing tumors.

To answer this need, the first part of my PhD project consisted in the establishment and characterization of two different models of pancreatic cancer-induced muscle wasting to promote efficient muscular wasting *in vitro* and *in vivo*, respectively. *In vitro*, treatment with conditioned medium from pancreatic cancer cells led to induction of atrophy in C2C12 derived myotubes. *In vivo*, The inoculation of a specific KPC cell clone (derived from primary tumor arising in C57BL/6 KRAS<sup>G12D</sup> P53<sup>R172H</sup>Pdx-Cre<sup>+/+</sup>) resulted in a clear reduction of muscular function and weight in C57BL/6 mice. Interestingly the atrophic phenotype was accompanied by several metabolic alterations in skeletal muscle such as excessive fatty acid oxidation or mitochondrial Reactive Oxygen Species (ROS) production supporting the implication of mitochondrial dysfunction in the pathogenesis of cachexia. Importantly the kinetic of wasting happened to be much slower than current available models, making it a model specific for pre-cachexia, allowing us to study early phases of the disease.

Subsequently, we investigated on the role of iron metabolism in cancer cachexia, as iron deficiency anemia is frequently diagnosed in cancer patients, especially in advanced cancer. Hence, we wondered if the disruption of systemic iron metabolism could have an impact on muscle mass maintenance in cachexia. Importantly, we found that altered skeletal muscle iron metabolism was a signature of the wasting process in several mouse model of cancer related muscle wasting, (C26, LLC, Baf) as reflected by the depletion of iron importer transferrin receptor (TFR1) coupled to an upregulation of the iron exporter ferroportin in skeletal muscle. We identified a mis-compartmentalization of iron in the muscle with a decrease in iron bioavailability and a decrease in mitochondrial iron. Coherently, we found profound alterations in iron-dependant mitochondrial enzymes such as a strong decrease in aconitase activity or succinate dehydrogenase activity. Interestingly, the reduction of iron availability by several means (both genetic and pharmacological) triggered skeletal myotube atrophy *in vitro* while iron supplementation was sufficient to prevent and even rescue myotube atrophy induced by different cancer cell lines. Consistently, intravenous injection of iron (ferric

carboxymaltose) in mice bearing C26 colon-carcinoma significantly decreased skeletal muscle atrophy and prolonged survival in mice. In particular, we observed in skeletal muscle of C26 mice injected with iron a maintenance of mitochondrial function and muscle strength, a normalization of phosphorylation of AMPK and of fatty acid oxidation machinery, both common markers for mitochondrial dysfunction in cachexia, and a decrease in the glucocorticoid response (known to promote atrophy in cachexia). Finally, iron injection was sufficient to promote strength increase in a small cohort of iron deficient cancer patients.

Taken together, these results suggest that dysregulated iron homeostasis contributes to cancer related muscle wasting and represent a potential new therapeutic target to prevent cancer related skeletal muscle atrophy.

# Introduction

## I Cancer Cachexia: A debilitating disease

### I.1 Definition and prevalence

Cancer cachexia (from the greek *kakos* and *hexis* meaning literally bad condition) is a multi-organ disorder characterized by aberrant skeletal muscle wasting (with or without adipose tissue wasting) resulting in progressive total body weight loss that cannot be fully recovered by conventional nutritional support [2]. This syndrome leads to progressive functional impairment and negatively affects the quality of life by interfering with the ability to move, breathe or even swallow food. Moreover, debilitated muscles decreased responsiveness to chemotherapy and therefore account for a decreased survival of cancer patients. [3]. Indeed the presence of cancer cachexia indicates a poor prognosis associated with a shorter survival time [4]. Cachexia is a common syndrome affecting about half of all cancer patients. However, the prevalence and severity of cachexia vary across tumor types and are generally higher in patients with tumors in the gastrointestinal tracts and the lung (85%) than in those with breast cancer, thyroid cancer, or hematological malignancies (30%). It's prevalence also rises with the progression of the disease and is present in 80% of terminally ill cancer patients [5]. As early as 1932, cachexia has been estimated to be responsible for 20% of all cancer related death [6], very few epidemiologic studies give a more actual estimation, partially because of the lack of a precise definition of cancer cachexia and the complexity of it's diagnostic. Nevertheless, cachexia contributes significantly in a direct or indirect way to cancer mortality. Weight loss in cancer patients has long been considered as a side effect of tumor growth and is rarely recognized and assessed by physicians. Due to the complexity of its diagnostic and to the lack of approved therapeutic strategy, cancer cachexia remains an unmet medical need.

### I.2 Classification of cachectic stages

Cancer cachexia evolves through a spectrum of different stages defined by an international Delphi consensus in 2011 including: Pre-cachexia, characterized by early metabolic alterations such as glucose intolerance, loss of appetite and  $\leq 5\%$  body weight loss ; cachexia, characterized by unintended body weight loss  $>5\%$  over the past 6 months, or a body mass index of  $<20$  and ongoing weight loss  $>2\%$ , or sarcopenia and ongoing weight loss  $>2\%$ ; and refractory cachexia characterized by a state of hypercatabolism, where clinical

management of weight loss is no longer possible due to rapid cancer progression. In the latter stage, cancer patients are usually unresponsive to anticancer therapy, they have a low performance score (WHO score of 3 or 4) and a life expectancy generally inferior to 3 months. [2]. However, not all patients will experience the full spectrum of the disease and the risk of progression depends not only on the cancer type and stage but also on food intake and systemic inflammation level. The classification of cachexia into different stages represents a first step toward a better understanding of the disease development and provides context for an early multimodal intervention (pre-cachexia) or a symptom control intervention (refractory cachexia) [2].

### **I.3 Experimental models of cachexia**

Most of our understanding of the molecular mechanisms leading to cachexia is based on experimental data obtained in rodents. Indeed, human data are scarce, in part because a clear definition on how to classify of human patients is still missing, but also because of the complexity of the diagnostic and the difficulty to recruit cachectic patients for clinical studies due to their vulnerability. Cancer cachexia has been studied in animals using mostly tumor models produced by transplanting tumor cells. The most widely used models are the Walker 256 carcinosarcoma and the Yoshida ascites hepatoma 130 in rats and the Lewis Lung carcinoma (LLC) and the C26 colorectal adenocarcinoma (C26) in mice. More recently, cachexia has also been studied in genetically engineered mouse models (GEMMs). These models are based on mutations leading to loss of function of tumor-suppressor genes such as APC and p53 or gain of function of proto-oncogenes such as KRAS. Commonly used GEMMs for the study of cachexia are APC<sup>Min/+</sup> and KPC mouse. These models are compared in **table 1**.

| Model         | Specie strain                | GEMM | Metastasis | Experime ntal period | Tumor mass (%BW) | Body weight loss | Muscle loss | anorexia | Ref        |
|---------------|------------------------------|------|------------|----------------------|------------------|------------------|-------------|----------|------------|
| Walker 256    | Rat Sprague - Dawley /Wistar | no   | no         | 10-20 days           | 10-20            | ~6%-15%          | 7-10%       | yes      | [7]<br>[8] |
| Yoshida AH130 | rat Wistar                   | no   | no         | 14-21 days           | < 3              | ~20%             | 13%         | yes      | [9]        |
| C26           | Mouse Balb/c                 | no   | no         | 13-21 days           | 2-6              | ~30%             | 30-40%      | yes      | [10]       |
| LLC           | mouse C57BL/6j               | no   | yes        | 20-30 days           | 20-30            | ~7%              | 20%         | yes      | [11]       |
| APCMin/+      | mouse                        | yes  | no         | 4months              | ND               | ~10%             | 35%         | no       | [12]       |
| KPC           | mouse                        | yes  | yes        | 5 months             | ND               | ~20%             | ~25-30%     | yes      | [13]       |

**Table 1 – Comparison of commonly used animal models of cancer cachexia.** BW: Body Weight; ND: not determined.

## II Mechanisms of skeletal muscle wasting in cachexia

### II.1 Altered protein homeostasis

The loss of skeletal muscle mass represents the most prominent feature of cachexia and accounts largely for the decreased quality of life and the worsened prognosis. Experimental studies of parabiotic transfer using tumor-bearing rats shed light on the humoral nature of cachexia-inducing factors, indeed pro-cachectic factors were transferred through the circulation between surgically connected rats [14]. Subsequent studies determined that pro-cachectic humoral factors could be either secreted directly by tumor cells or secreted by non-tumor cells in the tumor microenvironment or from distant organs. Investigators identified numerous humoral mediators of cachexia with very different origins and functions including pro-inflammatory cytokines, hormones, growth factors, and metal ions [15]. Cachectic mediators are known to impair protein homeostasis in skeletal muscle. Both decreased protein

synthesis and increased protein degradation have been observed and contribute to the decrease of muscle mass in cachexia [16]. Most studies emphasize the contribution of pathways involved in protein breakdown. In particular, the hyperactivation of the Ubiquitin-Proteasome Pathway (UPP) due to transcriptional upregulation of genes encoding for key E3 ligases, such as the muscle-specific RING finger protein 1 (MURF1) or the muscle atrophy F-box protein (MAFbx), increase the turnover of myofibrillar proteins [17]. However an increase in the activity of the autophagy-lysosome system in cachectic muscles also contributes to protein degradation [18]. The anabolic system also appears to be affected in cachexia, the reduced level of IGF-1 and the development of insulin resistance decreases PI3K-AKT signaling leading to a subsequent decrease of mTOR dependent protein synthesis. Moreover, in anabolic conditions, PI3K-AKT signaling not only promotes protein synthesis but is also able to inhibit Forkhead box O (FOXO) mediated induction of MURF1 and MAFbx therefore inhibiting muscle atrophy. Finally, in cachexia, the decrease in PI3K-AKT signaling hampers protein homeostasis affecting both protein synthesis and protein breakdown [19].

## **II.2 Mediators and signaling pathways inducing skeletal muscle wasting**

### **II.2.1 TNFA**

TNFA is a proinflammatory cytokine strongly secreted in animal models of cancer cachexia [20]. While it is still unclear if it is secreted by the tumor or by cells of the tumor microenvironment, TNFA, initially called “cachectin”, potently induces protein breakdown in skeletal muscle. TNFA binds to TNF receptor and directly activates the classical Nuclear factor KB (NFKB) pathway which successively activates E3 ligases and induces UPP mediated protein degradation. Similarly, TNF-related weak inducer of apoptosis (TWEAK), another cytokine belonging to the TNF superfamily, promotes Myosin Heavy Chain degradation by activating the same pathways [21]. In addition, it is also reported that NFKB activation inhibits skeletal muscle differentiation by suppressing MyoD mRNA post-transcriptionally [22].

### **II.2.2 IL6, LIF**

IL6 is another important driver of systemic inflammation in cancer cachexia. While in normal biology, IL6 is required for a correct immune response and for muscle growth and regeneration, high levels of IL6 have been observed in cancer patients and correlate with weight loss and decreased survival [23] [24]. A large body of evidence confirms the ability of IL6 to directly promote skeletal muscle atrophy. The wasting effect observed in animal models of cachexia such as *Apc*<sup>Min/+</sup> and C26 tumor bearing mice appears to be highly dependent on IL6 action [10,25]. Administration of high doses of IL6 in rodents also induced skeletal muscle



protein breakdown [26]. IL6 signals via its membrane bound receptor and activates the JAK/STAT pathway leading to the nuclear translocation of activated STAT [27] ultimately promoting protein degradation through enhanced transcription of E3 ligases such as MURF1. Activated STAT stimulates E3 ligases transcription in a direct or indirect way via AAT/enhancer-binding protein  $\delta$  (C/EBP $\delta$ ). Leukemia inhibitory factor (LIF) is another interleukin 6 class cytokine involved in cancer induced skeletal muscle atrophy. LIF activates similarly to IL6 the JAK/STAT pathway, moreover C26<sup>Lif<sup>-/-</sup></sup> mice revealed that IL6 secretion in C26 seems to depend on the secretion of LIF by the tumor [28].

### **II.2.3 TgfB, activin, myostatin**

Several members of the Transforming Growth Factor B (TGFB) superfamily have been involved in cancer cachexia. In particular, circulating activin A levels are elevated in cachectic cancer patients [29]. It was demonstrated in studies *in vivo* that activin A promotes skeletal muscle atrophy [30]. Activin A and other TGFB members such as myostatin signal through the activin type II receptor to activate the smad2 and smad3 transcription factor complex. Activation of the smad2/3 signaling pathway is known to induce skeletal muscle atrophy through activation of E3 ligases such as MURF1, MAFbx, or Muscle Ubiquitin ligase of SCF complex in atrophy-1 (Musa1). Pharmacological blockade of the ActRIIB was sufficient to suppress UPP activity and reversed cachexia in C26 mouse model highlighting the importance of TGFB signaling in the development of cancer induced muscle wasting [31]. Recently other TGFB superfamily members such as GDF15 and GDF11 were found to be elevated in cachexia and to promote muscle wasting [32].

### **II.2.4 Extracellular vesicles**

Extracellular vesicles (EVs) isolated from conditioned medium of cachexia inducing cancer cells such as Lewis Lung Carcinoma (LLC), were shown to induce catabolic activity in skeletal muscle. [33] EVs from LLC cells contain and release high level of extracellular heat shock proteins HSP90 and HSP70 triggering the activation of Toll-Like Receptor 4 (TLR4) and activating the p38 MAPK pathway, which is known to promote muscle atrophy through activation of E3 ligases [34]. Interestingly, HSP70/90 have been found in EVs isolated from conditioned medium of other cachexia inducing cancer cells from both mouse and human origin such as C26 or H1299 but also in the serum of different models of cancer cachexia in mice [33]. Tumor derived EVs from a cachexia inducing human pancreatic cancer cell line were also shown to induce myoblast cell death via activation of Toll-Like Receptor 7 signaling pathway and blockage of TLR7/8/9 with an antagonist was sufficient to attenuate cachexia [35].

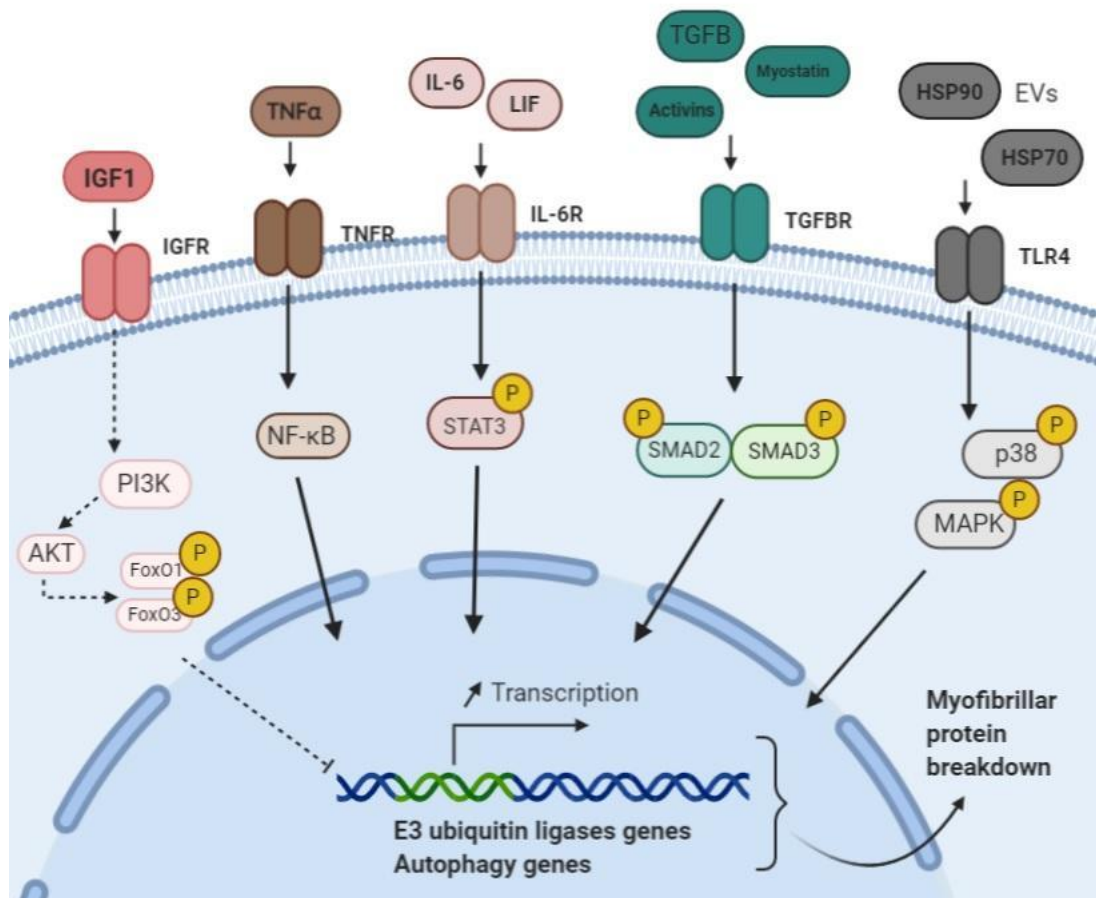


**Figure 1 | Signaling pathways involved in tumor-induced skeletal muscle atrophy.** Skeletal muscle wasting in cancer cachexia results from the activation of multiple signaling pathways by cytokines secreted by the tumor but also by stromal cell of tumor microenvironment and from cells of the host immune system. These factors signal through their respective receptor activating selective transcription factors which consecutively bind to promoters of genes encoding for ubiquitin ligases and component of the autophagy system. The activation of these systems results in selective degradation of myofibrillar protein ultimately promoting skeletal muscle atrophy. Alternatively, the inhibitory activity of FoxO1 and FoxO3 through PI3K signaling activation by IGF1 is suppressed (indicated by dashed lines) in cachexia, leading to transcription of genes encoding E3 ligases and autophagy components. *IGF1*, Insulin Growth Factor 1; *IGFR*, Insulin Growth Factor Receptor; *PI3K*; phosphatidylinositol 3-kinases, *AKT*; Protein kinase B, *FOXO1*; Forkhead box protein O1, *FOXO3*; Forkhead box protein O3, *TNFα*; Tumor necrosis factors, *TNFR*; tumor necrosis factor receptor, *NF-κB*; nuclear factor kappa-light-chain-enhancer of activated B cells, *IL-6*; Interleukin 6, *LIF*; Leukemia Inhibiting Factor; *IL-6R*; Interleukin-6 Receptor, *STAT3*; Signal transducer and activator of transcription 3, *TGFβ*; Transforming Growth Factor beta, *TGFBR*; Transforming Growth Factor beta Receptor, *smad2/3*; Mothers against decapentaplegic homolog 2/3, *HSP70/90*; Heat Shock Protein 70/90, *TLR4*; Toll like Receptor 4, *MAPK*; Mitogen-activated protein kinases,

Despite a growing understanding of the pathophysiology of cachexia and significant progresses in the identification of targetable mediators and biological pathways (**Figure 1**), there is currently no effective drug approved for the treatment of cancer cachexia. While the use of agents targeting cytokines appear as an attractive strategy, most of the clinical trials evaluating anti-cytokines therapies did not report a positive outcome [36]. Indeed, targeting a single putative mediator may have been shown to attenuate skeletal muscle wasting in cachexia but not to entirely restore muscle mass. This is probably due to the complexity of the mechanisms driving skeletal muscle wasting in cancer involving multiple signaling pathways all converging to myofibrillar protein breakdown. [37]

### **III Metabolic dysfunction in cancer cachexia**

#### **III.1 Systemic metabolic dysfunction**

The wasting phenotype observed in cancer cachexia results from a complex interplay of pathologic energy wasting circuits coupled to a strong decrease in food intake. The increasing energy need required by cancer cell rapid growth disturbs the homeostatic regulation of energy metabolism of the host. As a consequence, cachectic cancer patients experience systemic metabolic dysfunction with alterations in glucose, fat, and protein metabolism [38]. A study estimated that about 50% of cancer patients are hypermetabolic, meaning that they have an Elevated Resting Energy Expenditure (REE) [39]. Hypermetabolism in cancer patients correlates with clinical and biological markers of cancer cachexia such as the presence of C Reactive Protein (CRP) which is a marker of inflammation, or a weight loss >5%. It also associates with a shorter survival in metastatic cancer patients [39]. Tumor secreted factors or tumor/host interactions stimulate energy wasting processes in several organs by acting not only on skeletal muscle but also on adipose tissue, liver, bone, heart, or brain (**Figure 2**).

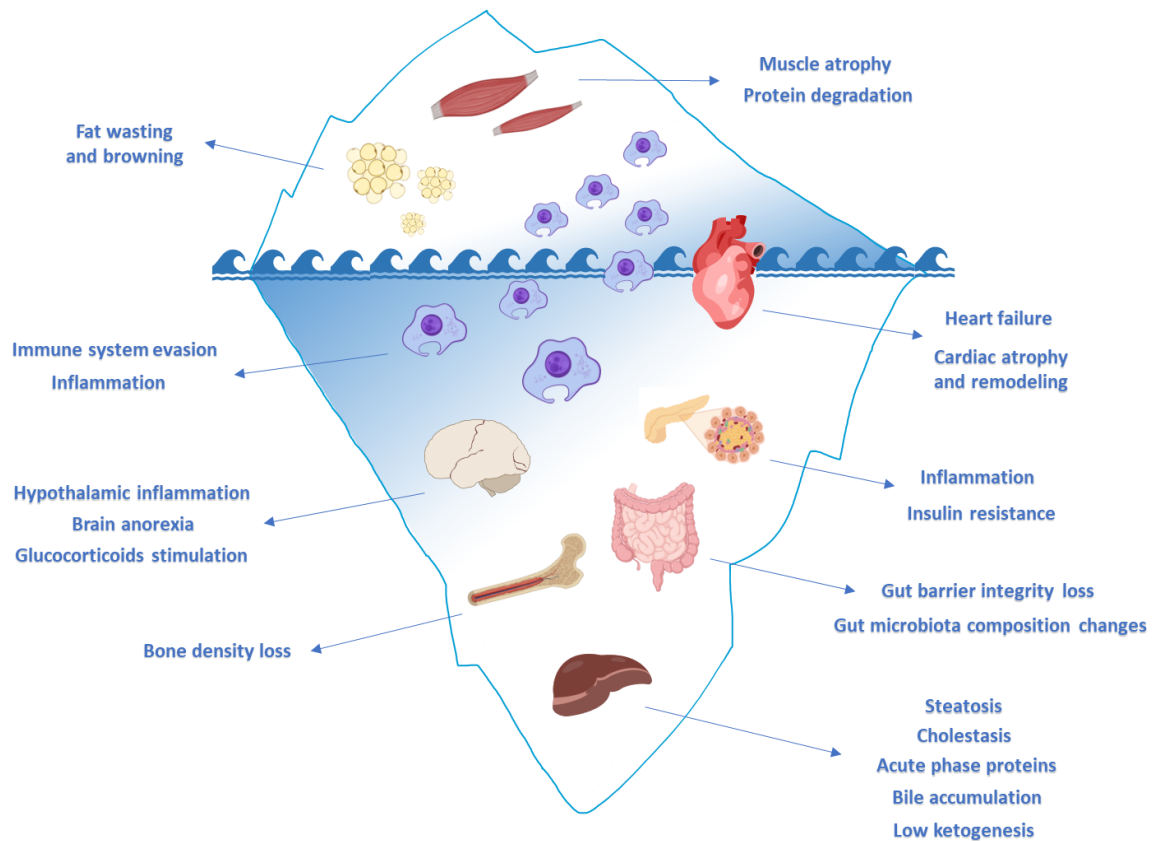


**Figure 2 | Muscle cachexia is the tip of the iceberg.** A growing body of evidence clearly indicates that cancer-induced muscle atrophy is only the tip of the iceberg. Indeed, multi-organ dysfunctions are parallelly ongoing during tumor growth and, in turn, their dysfunction is promoting muscle wasting in cachexia. Figure from Wyart et al. (2020) [1]

### III.1.1 Adipose tissue

Skeletal muscle loss in cachexia is often accompanied by White Adipose Tissue (WAT) loss. Studies focusing on pre-cachexia suggest that an increase in lipolysis is generally observed already in the early phases of the disease [40]. Interestingly, it was shown that by silencing a gene coding for adipose triglyceride lipase (ATGL), an enzyme catalyzing the first step of triacylglycerol hydrolysis, tumor bearing mice were protected from WAT loss but also from skeletal muscle atrophy [41]. In addition to elevated lipolysis, the phenomenon of “browning” from WAT takes place in early phases of cachexia mice model, before the onset of skeletal muscle atrophy. WAT browning contributes to the increased energy expenditure because of the increased expression of Uncoupling Protein 1 (UCP1) which uncouples oxidative phosphorylation from ATP synthesis to induce thermogenesis [42]. WAT browning is initiated by inflammatory molecules like IL6 or, in the LLC model, by the tumor derived

Parathyroid Hormone related Protein (PTHrP). Neutralization of PTHrP successfully preserved muscle mass and function and highlighted the importance of the tumor-adipose tissue-muscle axis in cachexia [43].

### **III.1.2 Brain Dysfunction and Neuroinflammation**

Anorexia is a frequent co-morbidity of cancer cachexia and considerably contributes to the negative energy balance observed in cachectic patients [78]. Appetite regulation is a complex process involving a broad variety of signals (hormones, nutrients, neuronal) converging to the hypothalamus. Those signals, either orexigenic (stimulating food intake, such as ghrelin) or anorexigenic (inhibiting food intake, such as leptin, insulin cholecystokinin, peptide YY, glucagon-like peptide 1, pancreatic polypeptide) stimulate distinct neuronal populations. Orexigenic signals stimulate neurons expressing NPY and Agouti-Related Peptide (AgRP), while anorexigenic hormones stimulate neurons expressing the cocaine and Amphetamine-Regulated Transcript (CART) and Pro-Opiomelanocortin (POMC) [79].

There is consistent evidence that increased hypothalamic inflammation is involved in the disruption of homeostatic regulation of appetite [80]. The privileged connection of hypothalamus to peripheral circulation (via the hypophyseal portal system) makes it very sensitive and reactive to the massive secretion of inflammatory cytokines occurring in cachexia. In addition to directly promoting muscle wasting and lipolysis, cytokines such as IL-1b and TNF- $\alpha$  have been shown to strongly decrease food intake when injected intracerebroventricularly in rodents [81,82]. Interestingly, blockages of TNF- $\alpha$  signaling with neutralizing antibodies, or administration of an IL-1b receptor antagonist were both able to prevent anorexia [83,84]. Mechanistically, pro-inflammatory cytokines such as IL-1b have been shown to overstimulate anorexigenic POMC neurons [85]. Similarly, the tumor-derived Leukaemia Inhibiting Factor (LIF), identified as a driver of cancer cachexia [86] activates anorexigenic POMC neurons [87]. Consistently, targeting the melanocortin system through central administration of an antagonist to the Melanocortin 4 Receptor (MCR4) appeared to be an efficient strategy for counteracting anorexia and cachexia in a murine cancer model [88,89].

Although the anorexigenic circuit is overactivated in cachexia, contrarily, the orexigenic axis appears to be dysfunctional as suggested by the decreased level of circulating NPY in anorexic cancer patients [90]. Coherently, alterations in the NPY system were also found in a rat model bearing a methylcolantrene-induced sarcoma as the expression of the NPY receptor was decreased in the hypothalamus [91]. Interestingly, tumor resection was sufficient to restore the hypothalamic expression of NPY [92,93]. It has been suggested that increased levels of serotonin were responsible for the inhibition of hypothalamic NPY secretion [93,94]. It is likely that elevation of ghrelin levels is a compensatory response to cancer-induced anorexia [94,95], however it is not sufficient to restore appetite and reveals a mechanism

described as “ghrelin-resistance” [96]. Finally, another emerging factor contributing to anorexia is the Growth Differentiation Factor 15 (GDF15), which has been linked to cancer-induced emesis [97].

Decreased food intake is an important feature of cachexia, however nutritional strategies aiming to reverse anorexia turned out to be inefficient for preventing body weight loss [98]. In addition to food intake regulation, the hypothalamus can also contribute to skeletal muscle catabolism through the hypothalamic–pituitary–adrenal (HPA) axis. Several studies have reported elevated circulating glucocorticoids in both animal models of cancer cachexia and cancer patients [72,75,102]. Glucocorticoids are well known inducers of skeletal muscle atrophy [103] and their secretion by the adrenal gland is placed under the control of the HPA axis, which can be stimulated by pro-inflammatory cytokines such as IL-1 $\beta$ , leading to the secretion of glucocorticoids by the adrenal gland ultimately promoting skeletal muscle and adipose tissue wasting [81].

### **III.1.3 Liver dysfunction**

Liver function is strongly altered by circulating factors in cancer cachexia. Since hepatic function exerts a major control on the whole-body energy expenditure, it is an important player in the etiology of cachexia. It has long been known that tumor ATP production heavily relies on glycolysis and therefore cancer cells consume high amount of glucose and release high levels of lactate [44]. In C26 bearing mice livers an increase in Lactate dehydrogenase A chain (LDHa) and an increase in the lactate transporter MCT1 have been found, suggesting a strong alteration of hepatic lactate metabolism [45]. Indeed, high circulating lactate gives rise to the “Cori cycle” in the liver: Hepatic cells reconvert circulating lactate into glucose through neoglucogenesis. This interorgan lactate cycling is a very inefficient metabolic process resulting in a negative energy balance. Lactate is not the only substrate fueling hepatic gluconeogenesis and it was postulated that amino acids mobilized from the catabolism of skeletal muscle can serve as an alternative source for energy production and sustain liver gluconeogenesis further contributing to energetic inefficiency [46] [47] [47]. Moreover, similarly to adipose tissue, it was suggested that uncoupling of mitochondrial oxidative phosphorylation occurs also in cachectic livers. Indeed, cachectic livers were found to present a reduced respiratory control ratio (an index of OXPHOS coupling efficiency) and an elevated LEAK respiration generating an increase in hepatic heat production and therefore further contributing to the increased REE and the weight loss [48].

The liver is involved in the acute phase response (APR) to tissue injury and inflammation by synthesizing acute phase proteins such as fibrinogen or Serum Amyloid A (SAA). In cachexia, the production of APR proteins is strongly upregulated [49]. It is likely that, to allow

a rapid and efficient synthesis of APR protein, skeletal muscle undergoes a catabolic process to mobilize and supply the liver in the necessary amino acids [49]. This process is mediated by the activation of the IL6/STAT3 signaling pathway.

Ketogenesis is another hepatic metabolic process altered in lung and pancreatic cancer cachexia models [47,50]. Ketones bodies are produced from fatty acid oxidation in the liver and can be used for energy production in skeletal muscle, heart or brain especially in case of starvation. Unexpectedly, serum levels of ketones are low in a mouse model of lung cancer cachexia, despite the strong decrease in food intake [47]. Reduced ketogenesis (likely induced by IL6) impede the physiological response to low food intake and prevent an efficient systemic energy production [50]. Consequently, low ketogenesis in cachexia results in elevated glucocorticoid levels triggering both strong catabolic program and an anti-anabolic program in skeletal muscle, ultimately leading to atrophy [50] [51]. Targeting ketogenesis using a PPAR $\alpha$  agonist (fenofibrate) resulted in less circulating glucocorticoid and therefore a reduced muscle atrophy in a cancer cachexia mouse model [47].

Collectively, a growing amount of evidence indicates that liver dysfunction and skeletal muscle degradation are intrinsically linked and contribute to tumor progression in cachexia.

#### **III.1.4 Insulin resistance**

Insulin resistance is often present in cancer patients suffering from cachexia [52]. In addition to be the main controller of systemic glucose metabolism, insulin also regulates muscle protein synthesis and breakdown. Insulin released from the pancreatic cells decreases blood glucose level and suppresses proteolysis. Therefore, insulin resistance might favor muscle proteolysis through the suppression of the anabolic PI3K-AKT pathway and activation of the UPP pathway [53]. Decreased insulin sensitivity have been found also in diverse models of cancer cachexia such as in C26 tumor bearing mice, Walker 256 tumor bearing rat, or even the tumor bearing fruit fly *Drosophila melanogaster* [54-56]. Treatment with the insulin sensitizer rosiglitazone reduced the weight loss in several models of cancer cachexia confirming the link between disrupted insulin sensitivity and decreased muscle mass in the context of cancer [57,58].

Taken together, the multi-organ involvement underlines the highly complex nature of cachexia whereby multiple mechanisms of metabolic disturbances contribute to the development of the syndrome and negatively affect skeletal muscle mass.

### III.2 Skeletal muscle metabolism & mitochondrial dysfunction in cachexia

Skeletal muscle metabolism is greatly affected by tumor growth whether it is because of direct mediators released by the tumor (as seen in part II), or indirect consequences of secondary organ reprogramming (as seen in part III.1). Skeletal muscle mitochondrial dysfunction has been reported in both cachectic cancer patients and in animal models of cachexia [59]. It was even demonstrated that mitochondrial degeneration precedes the onset of atrophy in the muscle of tumor bearing mice [60]. Accordingly, decreased oxidative capacity in muscle has emerged as an inducer of atrophy in cancer [61] but also in other forms of muscle wasting [62] [63] and the critical role of mitochondria in atrophy is currently actively investigated. Several aspects of mitochondria fitness appear to be altered in animal models of cachexia. It was found that IL6 is responsible for the suppression of mitofusin 1, one of the main regulators of mitochondrial fusion and for the induction of FIS1 involved in mitochondrial fission in the *Apc<sup>Min/+</sup>* mouse model [64]. Disruption of mitochondrial dynamics and in particular of the fission machinery have been shown to directly promote mitochondrial dysfunction and skeletal muscle atrophy through the activation of the proteasome-ubiquitin system and the autophagy-lysosome axis [65]. Fragmented mitochondrial networks are also associated with selective removal of mitochondria through autophagy in cachectic muscle as seen with the increase in mitophagy markers p62 and BNIP3 [60,66]. Additionally, suppressed expression of the Peroxisome-Proliferator Gamma-Activated Receptor (Pgc1a) has been constantly reported in animal models of cancer cachexia indicating a drastic decrease in mitochondrial biogenesis [64,67,68] contributing to the general decreased in mitochondrial content observed in cachectic muscle [69]. Defective mitochondrial dynamics is further accompanied by a general dysfunction of the electron transport chain activity and ineffective ATP production [70,71]. It was notably shown that cachectic muscles express a higher level of mitochondrial uncoupling proteins (UCPs) promoting the dissociation of oxidative phosphorylation from respiration [69,72,73]. While UCP1 is responsible for dissipating the proton gradient energy through heat generation, UCP2 and UCP3 might be involved in the regulation of fatty acid transport to the mitochondria and the generation of ROS [74]. Interestingly, it has been shown that muscle from tumor bearing mice feature excessive fatty acid oxidation in the muscle leading to high levels of oxidative stress and impairment of muscle growth [75]. Excess ROS production has been tightly associated with mitochondrial dysfunction [76]. While ROS generation in the muscle is involved in cellular signaling supporting cell homeostasis [77], excessive ROS production can generate DNA damage, protein oxidation and apoptosis [78] and has been proven to directly cause muscle atrophy [79,80].



There is compelling evidence that high levels of oxidative stress are also involved in cancer induced muscle atrophy [81]. Alteration of the redox balance have been shown to regulate AMPK activity [82]. Activation of AMPK indicates the presence of an energetic stress where intracellular levels of ATP declines and intracellular AMP increase [83]. This energy sensing protein kinase has the ability to couple cellular energy status to protein synthesis by regulating the expression of Mtorc1, ubiquitin E3 ligase expression, autophagy, and mitophagy [84]. Several pre-clinical models of cancer cachexia feature chronically elevated levels of AMPK activity [64,85]. Chronic elevation of AMPK has been associated with skeletal muscle atrophy highlighting the importance of AMPK as a molecular hub between cellular metabolic control and protein homeostasis in muscle [86].

## **IV Iron metabolism in cachexia**

### **IV.1 Cellular iron metabolism**

Iron is an essential element for life, being indispensable for several cellular processes such as DNA synthesis, ATP production, or oxygen transport. To carry out those tasks, iron is incorporated into the heme groups of proteins like hemoglobin, myoglobin, and cytochromes or can be associated with iron sulfur cluster (Fe-S) motifs. Despite being an essential nutrient, it can also be a dangerous catalyst of the Fenton reaction leading to the formation of ROS and subsequent cell damages [87]. Therefore, organisms have developed a tight control of iron homeostasis. Multiple molecules cooperate to up take, utilize, and store iron while maintaining iron homeostasis. Iron is transported to cells bound to transferrin (Tf) and is mostly up taken by cells by endocytosis through the binding of transferrin to its receptor on cell membrane Transferrin Receptor (TfR). Within the endosome, iron is detached from Tf and released in the cytoplasm through Divalent Metal Transporter 1 (DMT1) joining the Labile Iron Pool (LIP), a pool of redox active iron which is transitory and constitutes a crossroad of metabolic pathways involving iron.[88] Because excess LIP gives rise to ROS, iron is safely stored in the different compartments of the cell through cytoplasmic ferritin (Ft), nuclear ferritin, and mitochondrial ferritin. Iron is particularly utilized by the mitochondria for the synthesis of heme and Fe-S which are both necessary for ATP production. Intracellular iron levels are reduced by efflux of iron via Ferroportin (FPN), and heme export through Feline Leukemia Virus subgroup C Cellular Receptor 1a (FLVCR1a). Intracellular iron homeostasis is maintained by Iron Regulatory Proteins (IRPs). IRPs can exert a post-transcriptional control on the expression of several mRNA encoding proteins of iron metabolism. Under iron starvation, IRP1 and IRP2

actively bind to the Iron Responsive Elements (IRE) located in the 5' or 3' untranslated region (UTR) of target transcripts promoting respectively a repression of its translation (such as for ferritin and ferroportin) or mRNA stabilization (such as for transferrin receptor) [89]. In this way, it will eventually increase iron uptake and availability within the cell. Contrarily, high iron levels decrease IRE-binding activity, leading to a decreased stability of TFR mRNA and an increase in translation of ferritin, therefore fostering iron sequestration upon uptake [89]. IRP1 and IRP2 exert a redundant function but present a different iron sensing mechanism. IRP1 is the cytoplasmic counterpart of mitochondrial aconitase and converts citrate to isocitrate; to do so it requires an Fe-S cluster. Therefore, in case of low cellular iron availability, the Fe-S cluster is lacking, and IRP1 functions as an mRNA binding protein [90]. IRP2 is highly homologous to IRP1 but does not possess aconitase activity, the protein accumulates in case of cellular iron deficiency and is rapidly degraded by the ubiquitin-proteasome system in case of iron repletion [91].

## **IV.2 Iron metabolism in cancer**

### **IV.2.1 Iron deficiency anemia in cancer patients**

Iron homeostasis and regulation is often disturbed in patients with chronic diseases or cancer. Indeed, iron deficiency and iron deficiency-related anemia are common comorbidities in cancer patients [92]. Epidemiologic studies revealed that about 40% of cancer patients are anemic [93]. The prevalence of anemia in cancer patients even increases in some specific cancer types such as pancreatic cancer patients (63%), colorectal cancer patients (52%), and lung cancer patients (51%) [92]. Iron deficiency anemia was also noted in 67% of patients receiving chemotherapy [92]. Anemia generally correlates with low performance status and was even associated with a higher mortality in cancer patients [94]. Interestingly, most patients suffer from Functional Iron Deficiency (FID) and not Absolute Iron Deficiency (AID) [95]. While AID is characterized by depleted iron stores and insufficient iron supply, in FID there is insufficient iron mobilization despite adequate iron stores in the body. This impairment of iron metabolism is due to the presence of pro-inflammatory cytokines causing iron to be diverted from erythropoiesis and retained within the reticuloendothelial system [96].

### **IV.2.2 Iron metabolism in cancer cells**

Iron metabolism is often dysregulated in the tumor itself. Indeed many types of cancer cells are able to reprogram iron metabolism by increasing the expression of proteins involved in iron uptake such as TfR, STEAP proteins, and lipocalin 2 while decreasing the expression of

proteins responsible for iron efflux such as ferroprotein. In this way, cancer cells secure themselves high levels of intracellular iron required for many fundamental cellular processes such as DNA synthesis, proliferation, ATP production, and cell cycle regulation[97]. Additionally, it was also shown that iron is actively exchanged between cells of the tumor microenvironment and cancer cells.

Collectively, the high prevalence of iron deficiency anemia in cancer patients and the cancer cells avidity for iron give evidence of strong alterations of iron metabolism in cancer.

### **IV.3 Iron and muscle function: Implication in cachexia?**

Skeletal muscle is among the more metabolically active tissue of the organism [98]. It requires high levels of energy to function at rest and even higher levels to support contraction and movement. In order to adapt to the rapidly changing energy demands, different types of muscle fibers generating energy in different ways co-exist within the muscle. The slow type I fibers have highly oxidative capacities and thus high mitochondrial content and high activity of iron dependent enzymes [99]. Contrarily the fast-glycolytic type IIx fibers generate ATP mostly by glycolysis. The fast-oxidative type IIa are mixed fibers and able to use both oxidative phosphorylation and glycolysis to produce energy [99]. Iron is a fundamental element to oxidative metabolism in skeletal muscle both for correct oxygen storage in myoglobin and for activity of mitochondrial enzymes. Indeed Fe-S cluster are incorporated in respiratory complexes I, II, and III of the electron transport chain and heme is part of the cytochromes in complex IV and V [100]. Therefore, we can expect that alterations in iron homeostasis alter the muscle's ability to produce ATP and more generally muscle function. It was shown indeed that cellular iron deficiency alters mitochondrial morphology [101] and decreases mitochondrial respiration [102]. Since iron deficiency constitutes a major energy challenge for the cell it was also shown to promote the activation of AMPK [103]. Cellular iron deficiency might also promote a shift in energy pathway production toward an increase in glycolysis. However, we know that iron deficiency in muscle decreases exercise capacity and muscle performance. Therefore, it remains to be determined if iron availability can also influence skeletal muscle mass and be involved in cancer-related atrophy.

## V References Introduction

1. Fearon, K.; Strasser, F.; Anker, S.D.; Bosaeus, I.; Bruera, E.; Fainsinger, R.L.; Jatoi, A.; Loprinzi, C.; MacDonald, N.; Mantovani, G., et al. Definition and classification of cancer cachexia: an international consensus. *Lancet Oncol* **2011**, *12*, 489-495, doi:10.1016/S1470-2045(10)70218-7.
2. Wallengren, O.; Lundholm, K.; Bosaeus, I. Diagnostic criteria of cancer cachexia: relation to quality of life, exercise capacity and survival in unselected palliative care patients. *Support Care Cancer* **2013**, *21*, 1569-1577, doi:10.1007/s00520-012-1697-z.
3. Wyart, E.; Bindels, L.B.; Mina, E.; Menga, A.; Stanga, S.; Porporato, P.E. Cachexia, a Systemic Disease beyond Muscle Atrophy. *Int J Mol Sci* **2020**, *21*, doi:10.3390/ijms21228592.
4. Utech, A.E.; Tadros, E.M.; Hayes, T.G.; Garcia, J.M. Predicting survival in cancer patients: the role of cachexia and hormonal, nutritional and inflammatory markers. *J Cachexia Sarcopenia Muscle* **2012**, *3*, 245-251, doi:10.1007/s13539-012-0075-5.
5. Baracos, V.E. Pitfalls in defining and quantifying cachexia. *J Cachexia Sarcopenia Muscle* **2011**, *2*, 71-73, doi:10.1007/s13539-011-0031-9.
6. Warren, S. The Immediate Causes of Death in Cancer. *The American Journal of the Medical Sciences* **1932**, *184*, 610-615, doi:10.1097/00000441-193211000-00002.
7. Togni, V.; Ota, C.C.; Folador, A.; Junior, O.T.; Aikawa, J.; Yamazaki, R.K.; Freitas, F.A.; Longo, R.; Martins, E.F.; Calder, P.C., et al. Cancer cachexia and tumor growth reduction in Walker 256 tumor-bearing rats supplemented with N-3 polyunsaturated fatty acids for one generation. *Nutr Cancer* **2003**, *46*, 52-58, doi:10.1207/S15327914NC4601\_07.
8. de Fatima Silva, F.; Ortiz-Silva, M.; de Souza Galia, W.B.; Cassolla, P.; Graciano, M.F.; Zaia, C.T.; Zaia, D.; Carpinelli, A.R.; da Silva, F.G.; de Souza, H.M. Pioglitazone improves insulin sensitivity and reduces weight loss in Walker-256 tumor-bearing rats. *Life Sci* **2017**, *171*, 68-74, doi:10.1016/j.lfs.2016.12.016.
9. Busquets, S.; Figueras, M.T.; Fuster, G.; Almendro, V.; Moore-Carrasco, R.; Ametller, E.; Argiles, J.M.; Lopez-Soriano, F.J. Anticachectic effects of formoterol: a drug for potential treatment of muscle wasting. *Cancer Res* **2004**, *64*, 6725-6731, doi:10.1158/0008-5472.CAN-04-0425.
10. Bonetto, A.; Rupert, J.E.; Barreto, R.; Zimmers, T.A. The Colon-26 Carcinoma Tumor-bearing Mouse as a Model for the Study of Cancer Cachexia. *J Vis Exp* **2016**, 10.3791/54893, doi:10.3791/54893.
11. Llovera, M.; Garcia-Martinez, C.; Lopez-Soriano, J.; Agell, N.; Lopez-Soriano, F.J.; Garcia, I.; Argiles, J.M. Protein turnover in skeletal muscle of tumour-bearing transgenic mice overexpressing the soluble TNF receptor-1. *Cancer Lett* **1998**, *130*, 19-27, doi:10.1016/s0304-3835(98)00137-2.
12. VanderVeen, B.N.; Hardee, J.P.; Fix, D.K.; Carson, J.A. Skeletal muscle function during the progression of cancer cachexia in the male Apc(Min/+) mouse. *J Appl Physiol (1985)* **2018**, *124*, 684-695, doi:10.1152/jappphysiol.00897.2017.
13. Talbert, E.E.; Cuitino, M.C.; Ladner, K.J.; Rajasekerea, P.V.; Siebert, M.; Shakya, R.; Leone, G.W.; Ostrowski, M.C.; Paleo, B.; Weisleder, N., et al. Modeling Human Cancer-induced Cachexia. *Cell Rep* **2019**, *28*, 1612-1622 e1614, doi:10.1016/j.celrep.2019.07.016.
14. Norton, J.A.; Moley, J.F.; Green, M.V.; Carson, R.E.; Morrison, S.D. Parabolic transfer of cancer anorexia/cachexia in male rats. *Cancer Res* **1985**, *45*, 5547-5552.
15. Ni, X.; Yang, J.; Li, M. Imaging-guided curative surgical resection of pancreatic cancer in a xenograft mouse model. *Cancer Lett* **2012**, *324*, 179-185, doi:10.1016/j.canlet.2012.05.013.
16. Smith, K.L.; Tisdale, M.J. Increased protein degradation and decreased protein synthesis in skeletal muscle during cancer cachexia. *Br J Cancer* **1993**, *67*, 680-685, doi:10.1038/bjc.1993.126.
17. Sandri, M. Protein breakdown in cancer cachexia. *Semin Cell Dev Biol* **2016**, *54*, 11-19, doi:10.1016/j.semcdb.2015.11.002.

18. Penna, F.; Costamagna, D.; Pin, F.; Camperi, A.; Fanzani, A.; Chiarpotto, E.M.; Cavallini, G.; Bonelli, G.; Baccino, F.M.; Costelli, P. Autophagic degradation contributes to muscle wasting in cancer cachexia. *Am J Pathol* **2013**, *182*, 1367-1378, doi:10.1016/j.ajpath.2012.12.023.
19. Glass, D.J. PI3 kinase regulation of skeletal muscle hypertrophy and atrophy. *Curr Top Microbiol Immunol* **2010**, *346*, 267-278, doi:10.1007/82\_2010\_78.
20. Llovera, M.; Garcia-Martinez, C.; Lopez-Soriano, J.; Carbo, N.; Agell, N.; Lopez-Soriano, F.J.; Argiles, J.M. Role of TNF receptor 1 in protein turnover during cancer cachexia using gene knockout mice. *Mol Cell Endocrinol* **1998**, *142*, 183-189, doi:10.1016/s0303-7207(98)00105-1.
21. Dogra, C.; Changotra, H.; Wedhas, N.; Qin, X.; Wergedal, J.E.; Kumar, A. TNF-related weak inducer of apoptosis (TWEAK) is a potent skeletal muscle-wasting cytokine. *FASEB J* **2007**, *21*, 1857-1869, doi:10.1096/fj.06-7537com.
22. Guttridge, D.C.; Mayo, M.W.; Madrid, L.V.; Wang, C.Y.; Baldwin, A.S., Jr. NF-kappaB-induced loss of MyoD messenger RNA: possible role in muscle decay and cachexia. *Science* **2000**, *289*, 2363-2366, doi:10.1126/science.289.5488.2363.
23. Scott, H.R.; McMillan, D.C.; Crilly, A.; McArdle, C.S.; Milroy, R. The relationship between weight loss and interleukin 6 in non-small-cell lung cancer. *Br J Cancer* **1996**, *73*, 1560-1562, doi:10.1038/bjc.1996.294.
24. Moses, A.G.; Maingay, J.; Sangster, K.; Fearon, K.C.; Ross, J.A. Pro-inflammatory cytokine release by peripheral blood mononuclear cells from patients with advanced pancreatic cancer: relationship to acute phase response and survival. *Oncol Rep* **2009**, *21*, 1091-1095, doi:10.3892/or\_00000328.
25. White, J.P.; Puppa, M.J.; Gao, S.; Sato, S.; Welle, S.L.; Carson, J.A. Muscle mTORC1 suppression by IL-6 during cancer cachexia: a role for AMPK. *Am J Physiol Endocrinol Metab* **2013**, *304*, E1042-1052, doi:10.1152/ajpendo.00410.2012.
26. Goodman, M.N. Interleukin-6 induces skeletal muscle protein breakdown in rats. *Proc Soc Exp Biol Med* **1994**, *205*, 182-185, doi:10.3181/00379727-205-43695.
27. Bonetto, A.; Aydogdu, T.; Jin, X.; Zhang, Z.; Zhan, R.; Puzis, L.; Koniaris, L.G.; Zimmers, T.A. JAK/STAT3 pathway inhibition blocks skeletal muscle wasting downstream of IL-6 and in experimental cancer cachexia. *Am J Physiol Endocrinol Metab* **2012**, *303*, E410-421, doi:10.1152/ajpendo.00039.2012.
28. Kandarian, S.C.; Nosacka, R.L.; Delitto, A.E.; Judge, A.R.; Judge, S.M.; Ganey, J.D.; Moreira, J.D.; Jackman, R.W. Tumour-derived leukaemia inhibitory factor is a major driver of cancer cachexia and morbidity in C26 tumour-bearing mice. *J Cachexia Sarcopenia Muscle* **2018**, *9*, 1109-1120, doi:10.1002/jcsm.12346.
29. Loumaye, A.; de Barsey, M.; Nachit, M.; Lause, P.; Frateur, L.; van Maanen, A.; Trefois, P.; Gruson, D.; Thissen, J.P. Role of Activin A and myostatin in human cancer cachexia. *J Clin Endocrinol Metab* **2015**, *100*, 2030-2038, doi:10.1210/jc.2014-4318.
30. Chen, J.L.; Walton, K.L.; Winbanks, C.E.; Murphy, K.T.; Thomson, R.E.; Makanji, Y.; Qian, H.; Lynch, G.S.; Harrison, C.A.; Gregorevic, P. Elevated expression of activins promotes muscle wasting and cachexia. *FASEB J* **2014**, *28*, 1711-1723, doi:10.1096/fj.13-245894.
31. Zhou, X.; Wang, J.L.; Lu, J.; Song, Y.; Kwak, K.S.; Jiao, Q.; Rosenfeld, R.; Chen, Q.; Boone, T.; Simonet, W.S., et al. Reversal of cancer cachexia and muscle wasting by ActRIIB antagonism leads to prolonged survival. *Cell* **2010**, *142*, 531-543, doi:10.1016/j.cell.2010.07.011.
32. Jones, J.E.; Cadena, S.M.; Gong, C.; Wang, X.; Chen, Z.; Wang, S.X.; Vickers, C.; Chen, H.; Lach-Trifilieff, E.; Hadcock, J.R., et al. Supraphysiologic Administration of GDF11 Induces Cachexia in Part by Upregulating GDF15. *Cell Rep* **2018**, *22*, 1522-1530, doi:10.1016/j.celrep.2018.01.044.
33. Zhang, G.; Liu, Z.; Ding, H.; Zhou, Y.; Doan, H.A.; Sin, K.W.T.; Zhu, Z.J.; Flores, R.; Wen, Y.; Gong, X., et al. Tumor induces muscle wasting in mice through releasing extracellular Hsp70 and Hsp90. *Nat Commun* **2017**, *8*, 589, doi:10.1038/s41467-017-00726-x.
34. Kim, J.; Won, K.J.; Lee, H.M.; Hwang, B.Y.; Bae, Y.M.; Choi, W.S.; Song, H.; Lim, K.W.; Lee, C.K.; Kim, B. p38 MAPK Participates in Muscle-Specific RING Finger 1-Mediated Atrophy in Cast-

- Immobilized Rat Gastrocnemius Muscle. *Korean J Physiol Pharmacol* **2009**, *13*, 491-496, doi:10.4196/kjpp.2009.13.6.491.
35. Calore, F.; Londhe, P.; Fadda, P.; Nigita, G.; Casadei, L.; Marceca, G.P.; Fassan, M.; Lovat, F.; Gasparini, P.; Rizzotto, L., et al. The TLR7/8/9 Antagonist IMO-8503 Inhibits Cancer-Induced Cachexia. *Cancer Res* **2018**, *78*, 6680-6690, doi:10.1158/0008-5472.CAN-17-3878.
  36. Yeh, S.S.; Blackwood, K.; Schuster, M.W. The cytokine basis of cachexia and its treatment: are they ready for prime time? *J Am Med Dir Assoc* **2008**, *9*, 219-236, doi:10.1016/j.jamda.2008.01.003.
  37. Penna, F.; Minero, V.G.; Costamagna, D.; Bonelli, G.; Baccino, F.M.; Costelli, P. Anti-cytokine strategies for the treatment of cancer-related anorexia and cachexia. *Expert Opin Biol Ther* **2010**, *10*, 1241-1250, doi:10.1517/14712598.2010.503773.
  38. Dodesini, A.R.; Benedini, S.; Terruzzi, I.; Sereni, L.P.; Luzi, L. Protein, glucose and lipid metabolism in the cancer cachexia: A preliminary report. *Acta Oncol* **2007**, *46*, 118-120, doi:10.1080/02841860600791491.
  39. Vazeille, C.; Jouinot, A.; Durand, J.P.; Neveux, N.; Boudou-Rouquette, P.; Huillard, O.; Alexandre, J.; Cynober, L.; Goldwasser, F. Relation between hypermetabolism, cachexia, and survival in cancer patients: a prospective study in 390 cancer patients before initiation of anticancer therapy. *Am J Clin Nutr* **2017**, *105*, 1139-1147, doi:10.3945/ajcn.116.140434.
  40. Kliewer, K.L.; Ke, J.Y.; Tian, M.; Cole, R.M.; Andridge, R.R.; Belury, M.A. Adipose tissue lipolysis and energy metabolism in early cancer cachexia in mice. *Cancer Biol Ther* **2015**, *16*, 886-897, doi:10.4161/15384047.2014.987075.
  41. Das, S.K.; Eder, S.; Schauer, S.; Diwoky, C.; Temmel, H.; Guertl, B.; Gorkiewicz, G.; Tamilarasan, K.P.; Kumari, P.; Trauner, M., et al. Adipose triglyceride lipase contributes to cancer-associated cachexia. *Science* **2011**, *333*, 233-238, doi:10.1126/science.1198973.
  42. Petruzzelli, M.; Schweiger, M.; Schreiber, R.; Campos-Olivas, R.; Tsoli, M.; Allen, J.; Swarbrick, M.; Rose-John, S.; Rincon, M.; Robertson, G., et al. A switch from white to brown fat increases energy expenditure in cancer-associated cachexia. *Cell Metab* **2014**, *20*, 433-447, doi:10.1016/j.cmet.2014.06.011.
  43. Kir, S.; White, J.P.; Kleiner, S.; Kazak, L.; Cohen, P.; Baracos, V.E.; Spiegelman, B.M. Tumour-derived PTH-related protein triggers adipose tissue browning and cancer cachexia. *Nature* **2014**, *513*, 100-104, doi:10.1038/nature13528.
  44. Vander Heiden, M.G.; Cantley, L.C.; Thompson, C.B. Understanding the Warburg effect: the metabolic requirements of cell proliferation. *Science* **2009**, *324*, 1029-1033, doi:10.1126/science.1160809.
  45. Khamoui, A.V.; Tokmina-Roszyk, D.; Rossiter, H.B.; Fields, G.B.; Visavadiya, N.P. Hepatic proteome analysis reveals altered mitochondrial metabolism and suppressed acyl-CoA synthetase-1 in colon-26 tumor-induced cachexia. *Physiol Genomics* **2020**, *52*, 203-216, doi:10.1152/physiolgenomics.00124.2019.
  46. Ishikawa, E. The regulation of uptake and output of amino acids by rat tissues. *Adv Enzyme Regul* **1976**, *14*, 117-136, doi:10.1016/0065-2571(76)90010-8.
  47. Goncalves, M.D.; Hwang, S.K.; Pauli, C.; Murphy, C.J.; Cheng, Z.; Hopkins, B.D.; Wu, D.; Loughran, R.M.; Emerling, B.M.; Zhang, G., et al. Fenofibrate prevents skeletal muscle loss in mice with lung cancer. *Proc Natl Acad Sci U S A* **2018**, *115*, E743-E752, doi:10.1073/pnas.1714703115.
  48. Halle, J.L.; Pena, G.S.; Paez, H.G.; Castro, A.J.; Rossiter, H.B.; Visavadiya, N.P.; Whitehurst, M.A.; Khamoui, A.V. Tissue-specific dysregulation of mitochondrial respiratory capacity and coupling control in colon-26 tumor-induced cachexia. *Am J Physiol Regul Integr Comp Physiol* **2019**, *317*, R68-R82, doi:10.1152/ajpregu.00028.2019.
  49. Bonetto, A.; Aydogdu, T.; Kunzevitzky, N.; Guttridge, D.C.; Khuri, S.; Koniaris, L.G.; Zimmers, T.A. STAT3 activation in skeletal muscle links muscle wasting and the acute phase response in cancer cachexia. *PLoS One* **2011**, *6*, e22538, doi:10.1371/journal.pone.0022538.

50. Flint, T.R.; Janowitz, T.; Connell, C.M.; Roberts, E.W.; Denton, A.E.; Coll, A.P.; Jodrell, D.I.; Fearon, D.T. Tumor-Induced IL-6 Reprograms Host Metabolism to Suppress Anti-tumor Immunity. *Cell Metab* **2016**, *24*, 672-684, doi:10.1016/j.cmet.2016.10.010.
51. Shimizu, N.; Yoshikawa, N.; Ito, N.; Maruyama, T.; Suzuki, Y.; Takeda, S.; Nakae, J.; Tagata, Y.; Nishitani, S.; Takehana, K., et al. Crosstalk between glucocorticoid receptor and nutritional sensor mTOR in skeletal muscle. *Cell Metab* **2011**, *13*, 170-182, doi:10.1016/j.cmet.2011.01.001.
52. Honors, M.A.; Kinzig, K.P. The role of insulin resistance in the development of muscle wasting during cancer cachexia. *J Cachexia Sarcopenia Muscle* **2012**, *3*, 5-11, doi:10.1007/s13539-011-0051-5.
53. Wang, X.; Hu, Z.; Hu, J.; Du, J.; Mitch, W.E. Insulin resistance accelerates muscle protein degradation: Activation of the ubiquitin-proteasome pathway by defects in muscle cell signaling. *Endocrinology* **2006**, *147*, 4160-4168, doi:10.1210/en.2006-0251.
54. Asp, M.L.; Tian, M.; Wendel, A.A.; Belury, M.A. Evidence for the contribution of insulin resistance to the development of cachexia in tumor-bearing mice. *Int J Cancer* **2010**, *126*, 756-763, doi:10.1002/ijc.24784.
55. Fernandes, L.C.; Machado, U.F.; Nogueira, C.R.; Carpinelli, A.R.; Curi, R. Insulin secretion in Walker 256 tumor cachexia. *Am J Physiol* **1990**, *258*, E1033-1036, doi:10.1152/ajpendo.1990.258.6.E1033.
56. Figueroa-Clarevega, A.; Bilder, D. Malignant Drosophila tumors interrupt insulin signaling to induce cachexia-like wasting. *Dev Cell* **2015**, *33*, 47-55, doi:10.1016/j.devcel.2015.03.001.
57. Asp, M.L.; Tian, M.; Kliewer, K.L.; Belury, M.A. Rosiglitazone delayed weight loss and anorexia while attenuating adipose depletion in mice with cancer cachexia. *Cancer Biol Ther* **2011**, *12*, 957-965, doi:10.4161/cbt.12.11.18134.
58. Trobec, K.; Palus, S.; Tschirner, A.; von Haehling, S.; Doehner, W.; Lainscak, M.; Anker, S.D.; Springer, J. Rosiglitazone reduces body wasting and improves survival in a rat model of cancer cachexia. *Nutrition* **2014**, *30*, 1069-1075, doi:10.1016/j.nut.2013.12.005.
59. VanderVeen, B.N.; Fix, D.K.; Carson, J.A. Disrupted Skeletal Muscle Mitochondrial Dynamics, Mitophagy, and Biogenesis during Cancer Cachexia: A Role for Inflammation. *Oxid Med Cell Longev* **2017**, *2017*, 3292087, doi:10.1155/2017/3292087.
60. Brown, J.L.; Rosa-Caldwell, M.E.; Lee, D.E.; Blackwell, T.A.; Brown, L.A.; Perry, R.A.; Haynie, W.S.; Hardee, J.P.; Carson, J.A.; Wiggs, M.P., et al. Mitochondrial degeneration precedes the development of muscle atrophy in progression of cancer cachexia in tumour-bearing mice. *J Cachexia Sarcopenia Muscle* **2017**, *8*, 926-938, doi:10.1002/jcsm.12232.
61. Argiles, J.M.; Lopez-Soriano, F.J.; Busquets, S. Muscle wasting in cancer: the role of mitochondria. *Curr Opin Clin Nutr Metab Care* **2015**, *18*, 221-225, doi:10.1097/MCO.000000000000164.
62. Hyatt, H.; Deminice, R.; Yoshihara, T.; Powers, S.K. Mitochondrial dysfunction induces muscle atrophy during prolonged inactivity: A review of the causes and effects. *Arch Biochem Biophys* **2019**, *662*, 49-60, doi:10.1016/j.abb.2018.11.005.
63. Abrigo, J.; Simon, F.; Cabrera, D.; Vilos, C.; Cabello-Verrugio, C. Mitochondrial Dysfunction in Skeletal Muscle Pathologies. *Curr Protein Pept Sci* **2019**, *20*, 536-546, doi:10.2174/1389203720666190402100902.
64. White, J.P.; Puppa, M.J.; Sato, S.; Gao, S.; Price, R.L.; Baynes, J.W.; Kostek, M.C.; Matesic, L.E.; Carson, J.A. IL-6 regulation on skeletal muscle mitochondrial remodeling during cancer cachexia in the ApcMin/+ mouse. *Skelet Muscle* **2012**, *2*, 14, doi:10.1186/2044-5040-2-14.
65. Romanello, V.; Guadagnin, E.; Gomes, L.; Roder, I.; Sandri, C.; Petersen, Y.; Milan, G.; Masiero, E.; Del Piccolo, P.; Foretz, M., et al. Mitochondrial fission and remodelling contributes to muscle atrophy. *EMBO J* **2010**, *29*, 1774-1785, doi:10.1038/emboj.2010.60.
66. Penna, F.; Ballaro, R.; Martinez-Cristobal, P.; Sala, D.; Sebastian, D.; Busquets, S.; Muscaritoli, M.; Argiles, J.M.; Costelli, P.; Zorzano, A. Autophagy Exacerbates Muscle Wasting in Cancer

- Cachexia and Impairs Mitochondrial Function. *J Mol Biol* **2019**, *431*, 2674-2686, doi:10.1016/j.jmb.2019.05.032.
67. Hardee, J.P.; Counts, B.R.; Gao, S.; VanderVeen, B.N.; Fix, D.K.; Koh, H.J.; Carson, J.A. Inflammatory signalling regulates eccentric contraction-induced protein synthesis in cachectic skeletal muscle. *J Cachexia Sarcopenia Muscle* **2018**, *9*, 369-383, doi:10.1002/jcsm.12271.
  68. Sun, R.; Zhang, S.; Hu, W.; Lu, X.; Lou, N.; Yang, Z.; Chen, S.; Zhang, X.; Yang, H. Valproic acid attenuates skeletal muscle wasting by inhibiting C/EBPbeta-regulated atrogin1 expression in cancer cachexia. *Am J Physiol Cell Physiol* **2016**, *311*, C101-115, doi:10.1152/ajpcell.00344.2015.
  69. Neyroud, D.; Nosacka, R.L.; Judge, A.R.; Hepple, R.T. Colon 26 adenocarcinoma (C26)-induced cancer cachexia impairs skeletal muscle mitochondrial function and content. *J Muscle Res Cell Motil* **2019**, *40*, 59-65, doi:10.1007/s10974-019-09510-4.
  70. Antunes, D.; Padrao, A.I.; Maciel, E.; Santinha, D.; Oliveira, P.; Vitorino, R.; Moreira-Goncalves, D.; Colaco, B.; Pires, M.J.; Nunes, C., et al. Molecular insights into mitochondrial dysfunction in cancer-related muscle wasting. *Biochim Biophys Acta* **2014**, *1841*, 896-905, doi:10.1016/j.bbali.2014.03.004.
  71. Padrao, A.I.; Oliveira, P.; Vitorino, R.; Colaco, B.; Pires, M.J.; Marquez, M.; Castellanos, E.; Neuparth, M.J.; Teixeira, C.; Costa, C., et al. Bladder cancer-induced skeletal muscle wasting: disclosing the role of mitochondria plasticity. *Int J Biochem Cell Biol* **2013**, *45*, 1399-1409, doi:10.1016/j.biocel.2013.04.014.
  72. Busquets, S.; Almendro, V.; Barreiro, E.; Figueras, M.; Argiles, J.M.; Lopez-Soriano, F.J. Activation of UCPs gene expression in skeletal muscle can be independent on both circulating fatty acids and food intake. Involvement of ROS in a model of mouse cancer cachexia. *FEBS Lett* **2005**, *579*, 717-722, doi:10.1016/j.febslet.2004.12.050.
  73. Tzika, A.A.; Fontes-Oliveira, C.C.; Shestov, A.A.; Constantinou, C.; Psychogios, N.; Righi, V.; Mintzopoulos, D.; Busquets, S.; Lopez-Soriano, F.J.; Milot, S., et al. Skeletal muscle mitochondrial uncoupling in a murine cancer cachexia model. *Int J Oncol* **2013**, *43*, 886-894, doi:10.3892/ijo.2013.1998.
  74. Schrauwen, P.; Hesselink, M. UCP2 and UCP3 in muscle controlling body metabolism. *J Exp Biol* **2002**, *205*, 2275-2285.
  75. Fukawa, T.; Yan-Jiang, B.C.; Min-Wen, J.C.; Jun-Hao, E.T.; Huang, D.; Qian, C.N.; Ong, P.; Li, Z.; Chen, S.; Mak, S.Y., et al. Excessive fatty acid oxidation induces muscle atrophy in cancer cachexia. *Nat Med* **2016**, *22*, 666-671, doi:10.1038/nm.4093.
  76. Xiao, Y.; Karam, C.; Yi, J.; Zhang, L.; Li, X.; Yoon, D.; Wang, H.; Dhakal, K.; Ramlow, P.; Yu, T., et al. ROS-related mitochondrial dysfunction in skeletal muscle of an ALS mouse model during the disease progression. *Pharmacol Res* **2018**, *138*, 25-36, doi:10.1016/j.phrs.2018.09.008.
  77. Ward, C.W.; Prosser, B.L.; Lederer, W.J. Mechanical stretch-induced activation of ROS/RNS signaling in striated muscle. *Antioxid Redox Signal* **2014**, *20*, 929-936, doi:10.1089/ars.2013.5517.
  78. Schieber, M.; Chandel, N.S. ROS function in redox signaling and oxidative stress. *Curr Biol* **2014**, *24*, R453-462, doi:10.1016/j.cub.2014.03.034.
  79. Li, Y.P.; Chen, Y.; Li, A.S.; Reid, M.B. Hydrogen peroxide stimulates ubiquitin-conjugating activity and expression of genes for specific E2 and E3 proteins in skeletal muscle myotubes. *Am J Physiol Cell Physiol* **2003**, *285*, C806-812, doi:10.1152/ajpcell.00129.2003.
  80. Powers, S.K.; Talbert, E.E.; Adihetty, P.J. Reactive oxygen and nitrogen species as intracellular signals in skeletal muscle. *J Physiol* **2011**, *589*, 2129-2138, doi:10.1113/jphysiol.2010.201327.
  81. Abrigo, J.; Elorza, A.A.; Riedel, C.A.; Vilos, C.; Simon, F.; Cabrera, D.; Estrada, L.; Cabello-Verrugio, C. Role of Oxidative Stress as Key Regulator of Muscle Wasting during Cachexia. *Oxid Med Cell Longev* **2018**, *2018*, 2063179, doi:10.1155/2018/2063179.



82. Irrcher, I.; Ljubicic, V.; Hood, D.A. Interactions between ROS and AMP kinase activity in the regulation of PGC-1alpha transcription in skeletal muscle cells. *Am J Physiol Cell Physiol* **2009**, *296*, C116-123, doi:10.1152/ajpcell.00267.2007.
83. Hardie, D.G.; Ross, F.A.; Hawley, S.A. AMPK: a nutrient and energy sensor that maintains energy homeostasis. *Nat Rev Mol Cell Biol* **2012**, *13*, 251-262, doi:10.1038/nrm3311.
84. Bergeron, R.; Ren, J.M.; Cadman, K.S.; Moore, I.K.; Perret, P.; Pypaert, M.; Young, L.H.; Semenkovich, C.F.; Shulman, G.I. Chronic activation of AMP kinase results in NRF-1 activation and mitochondrial biogenesis. *Am J Physiol Endocrinol Metab* **2001**, *281*, E1340-1346, doi:10.1152/ajpendo.2001.281.6.E1340.
85. Hall, D.T.; Griss, T.; Ma, J.F.; Sanchez, B.J.; Sadek, J.; Tremblay, A.M.K.; Mubaid, S.; Omer, A.; Ford, R.J.; Bedard, N., et al. The AMPK agonist 5-aminoimidazole-4-carboxamide ribonucleotide (AICAR), but not metformin, prevents inflammation-associated cachectic muscle wasting. *EMBO Mol Med* **2018**, *10*, doi:10.15252/emmm.201708307.
86. Thomson, D.M. The Role of AMPK in the Regulation of Skeletal Muscle Size, Hypertrophy, and Regeneration. *Int J Mol Sci* **2018**, *19*, doi:10.3390/ijms19103125.
87. Winterbourn, C.C. Toxicity of iron and hydrogen peroxide: the Fenton reaction. *Toxicol Lett* **1995**, *82-83*, 969-974, doi:10.1016/0378-4274(95)03532-x.
88. Pantopoulos, K. Iron metabolism and the IRE/IRP regulatory system: an update. *Ann N Y Acad Sci* **2004**, *1012*, 1-13, doi:10.1196/annals.1306.001.
89. Volz, K. The functional duality of iron regulatory protein 1. *Curr Opin Struct Biol* **2008**, *18*, 106-111, doi:10.1016/j.sbi.2007.12.010.
90. Takahashi-Makise, N.; Ward, D.M.; Kaplan, J. On the mechanism of iron sensing by IRP2: new players, new paradigms. *Nat Chem Biol* **2009**, *5*, 874-875, doi:10.1038/nchembio.261.
91. Ludwig, H.; Muldur, E.; Endler, G.; Hubl, W. Prevalence of iron deficiency across different tumors and its association with poor performance status, disease status and anemia. *Ann Oncol* **2013**, *24*, 1886-1892, doi:10.1093/annonc/mdt118.
92. Ludwig, H.; Van Belle, S.; Barrett-Lee, P.; Birgegard, G.; Bokemeyer, C.; Gascon, P.; Kosmidis, P.; Krzakowski, M.; Nortier, J.; Olmi, P., et al. The European Cancer Anaemia Survey (ECAS): a large, multinational, prospective survey defining the prevalence, incidence, and treatment of anaemia in cancer patients. *Eur J Cancer* **2004**, *40*, 2293-2306, doi:10.1016/j.ejca.2004.06.019.
93. Caro, J.J.; Salas, M.; Ward, A.; Goss, G. Anemia as an independent prognostic factor for survival in patients with cancer: a systemic, quantitative review. *Cancer* **2001**, *91*, 2214-2221.
94. Ludwig, H.; Evstatiev, R.; Kornek, G.; Aapro, M.; Bauernhofer, T.; Buxhofer-Ausch, V.; Fridrik, M.; Geissler, D.; Geissler, K.; Gisslinger, H., et al. Iron metabolism and iron supplementation in cancer patients. *Wien Klin Wochenschr* **2015**, *127*, 907-919, doi:10.1007/s00508-015-0842-3.
95. Grotto, H.Z. Anaemia of cancer: an overview of mechanisms involved in its pathogenesis. *Med Oncol* **2008**, *25*, 12-21, doi:10.1007/s12032-007-9000-8.
96. Torti, S.V.; Manz, D.H.; Paul, B.T.; Blanchette-Farra, N.; Torti, F.M. Iron and Cancer. *Annu Rev Nutr* **2018**, *38*, 97-125, doi:10.1146/annurev-nutr-082117-051732.
97. Zurlo, F.; Larson, K.; Bogardus, C.; Ravussin, E. Skeletal muscle metabolism is a major determinant of resting energy expenditure. *J Clin Invest* **1990**, *86*, 1423-1427, doi:10.1172/JCI114857.
98. Westerblad, H.; Bruton, J.D.; Katz, A. Skeletal muscle: energy metabolism, fiber types, fatigue and adaptability. *Exp Cell Res* **2010**, *316*, 3093-3099, doi:10.1016/j.yexcr.2010.05.019.
99. Levi, S.; Rovida, E. The role of iron in mitochondrial function. *Biochim Biophys Acta* **2009**, *1790*, 629-636, doi:10.1016/j.bbagen.2008.09.008.
100. Cartier, L.J.; Ohira, Y.; Chen, M.; Cuddihee, R.W.; Holloszy, J.O. Perturbation of mitochondrial composition in muscle by iron deficiency. Implications regarding regulation of mitochondrial assembly. *J Biol Chem* **1986**, *261*, 13827-13832.

101. Oexle, H.; Gnaiger, E.; Weiss, G. Iron-dependent changes in cellular energy metabolism: influence on citric acid cycle and oxidative phosphorylation. *Biochim Biophys Acta* **1999**, *1413*, 99-107, doi:10.1016/s0005-2728(99)00088-2.
102. Merrill, J.F.; Thomson, D.M.; Hardman, S.E.; Hepworth, S.D.; Willie, S.; Hancock, C.R. Iron deficiency causes a shift in AMP-activated protein kinase (AMPK) subunit composition in rat skeletal muscle. *Nutr Metab (Lond)* **2012**, *9*, 104, doi:10.1186/1743-7075-9-104.

-

# Aims of the work

## Chapter 1

While experimental research in cachexia is progressing, there is a substantial gap between experimental and clinical data. The knowledge of the complex biology of cachexia in humans remains elusive. This is partially due to the fact that cachectic cancer patients are extremely vulnerable therefore their participation in research is limited. But another issue might arise from the lack of clinical relevance between experimental models and human pathology. Indeed, most of our understanding of cachexia relies on a very small repertoire of animal models of cachexia inducing tumors such as Colon 26 adenocarcinoma and Lewis lung carcinoma. While these two models can potently induce skeletal muscle wasting and help to decipher some of the molecular mechanisms driving atrophy in cancer, they also come with a certain number of limitations and do not match all the criteria defining the human pathology. In particular, the rapid kinetic of wasting in animal models of cachexia contrasts with the slow development of the pathology in humans.

### Aim1

- To develop a new mouse model of cancer cachexia with a slow pace, closer to the human pathology in order to characterize early metabolic alterations corresponding to the pre-cachexia state.

## **Chapter 2**

The knowledge of the molecular mechanisms driving skeletal muscle wasting in cachexia is still scarce but accumulating evidence point at the central role played by mitochondrial dysfunction into promoting muscle atrophy. Nevertheless, there is a substantial need to identify and characterize new drivers of mitochondrial dysfunction in cachexia. Systemic iron metabolism is altered in cancer patients as seen by the high prevalence of iron deficiency anemia among cancer patients. Being a crucial component of heme and iron sulfur cluster, iron appears to be essential for mitochondrial function and adequate energy production. We therefore speculated that systemic iron alterations occurring in cancer could have a negative impact on mitochondrial function in skeletal muscle and be directly involved in the development of the atrophic process.

### **Aim 2**








- To identify the consequences of iron metabolism alterations in cancer for mitochondrial function in skeletal muscle and to determine the influence of iron availability on skeletal muscle mass maintenance.

# Chapter 1

Hindawi  
Oxidative Medicine and Cellular Longevity  
Volume 2018, Article ID 6419805, 10 pages  
<https://doi.org/10.1155/2018/6419805>

## Research Article

### Metabolic Alterations in a Slow-Paced Model of Pancreatic Cancer-Induced Wasting

Elisabeth Wyart,<sup>1</sup> Simone Reano,<sup>2</sup> Myriam Y. Hsu,<sup>1</sup> Dario Livio Longo ,<sup>3</sup> Mingchuan Li ,<sup>1</sup> Emilio Hirsch ,<sup>1</sup> Nicoletta Filigheddu ,<sup>2</sup> Alessandra Ghigo ,<sup>1</sup> Chiara Riganti ,<sup>4</sup> and Paolo Ettore Porporato <sup>1</sup>

<sup>1</sup>Department of Molecular Biotechnology and Health Science, Molecular Biotechnology Center, University of Torino, Torino, Italy

<sup>2</sup>Department of Translational Medicine, Istituto Interuniversitario di Miologia (IIM), University of Piemonte Orientale, Novara, Italy

<sup>3</sup>Department of Molecular Biotechnology and Health Science, Molecular Imaging Center, University of Torino, Torino, Italy

<sup>4</sup>Department of Oncology, University of Torino, Torino, Italy

Correspondence should be addressed to Chiara Riganti; chiara.riganti@unito.it  
and Paolo Ettore Porporato; paolo.porporato@unito.it

Received 27 October 2017; Accepted 31 December 2017; Published 26 February 2018

Academic Editor: Elisabetta Ferraro

Copyright © 2018 Elisabeth Wyart et al. This is an open access article distributed under the Creative Commons Attribution License, which permits unrestricted use, distribution, and reproduction in any medium, provided the original work is properly cited.

#### Abstract :

Cancer cachexia is a devastating syndrome occurring in the majority of terminally ill cancer patients. Notably, skeletal muscle atrophy is a consistent feature affecting the quality of life and prognosis. To date, limited therapeutic options are available, and research in the field is hampered by the lack of satisfactory models to study the complexity of wasting in cachexia-inducing tumors, such as pancreatic cancer. Moreover, currently used in vivo models are characterized by an explosive cachexia with a lethal wasting within few days, while pancreatic cancer patients might experience alterations long before the onset of overt wasting. In this work, we established and characterized a slow-paced model of pancreatic cancer-induced muscle wasting that promotes efficient muscular wasting in vitro and in vivo. Treatment with conditioned media from pancreatic cancer cells led to the induction of atrophy in vitro, while tumor-bearing mice presented a clear reduction in muscle mass and functionality. Intriguingly, several metabolic alterations in tumor-bearing mice were identified, paving the way for therapeutic interventions with drugs targeting metabolism.

## I Introduction

More than half of cancer patients are suffering from a systemic wasting disorder referred to as cachexia (from Greek “bad condition”), a syndrome strongly affecting the quality of life and prognosis in cancer patients. This syndrome is characterized by unstoppable consumption of adipose and skeletal muscle tissues leading to an excessive body weight loss that cannot be fully reverted by conventional nutritional support [1]. Cancer cachexia is a complex syndrome accounting for multiple organ dysfunction and systemic metabolic deregulations [2]. Cachectic patients experience symptoms ranging from anorexia, elevated inflammation, and insulin resistance to increased energy expenditure, which ultimately promote malaise, fatigue, and impaired tolerance to chemotherapy [3], further worsening patients’ prognosis. Besides being associated with a poor prognosis, cachexia is estimated to be the direct cause of one-third of cancer deaths [4]. Several tissue dysfunctions emerge during cachexia, such as liver steatosis, fat deposit lipolysis, intestinal dysbiosis, and, most notably, skeletal muscle wasting, which account for the steep decrease in quality of life, weakness, and respiratory distress of cancer patients.

Skeletal muscle atrophy is a highly regulated process driven by an unbalance between protein synthesis and degradation. Activation of the ubiquitin-dependent proteasome pathway (UPP) and the autophagy-lysosome system are two important mechanisms leading to increased protein breakdown. This process is orchestrated by a set of genes called atrogenes, such as Atrogin-1/MAFbx or Murf1 [5]. Compelling evidence shows that an impairment of mitochondrial metabolism and an increase in mitochondrial ROS are also strongly associated with the cachectic phenotype [6, 7]. Several tumor types, such as lung, gastrointestinal tract, and pancreatic cancer, are emerging as strong promoters of cancer cachexia [8]. In particular, pancreatic ductal adenocarcinoma (PDAC) presents a high penetrance of wasting, a process that seems to occur even in earlier phases of tumor transformation [9]. Despite the burden of cachexia in PDAC, there are still limited experimental models available.

Particularly, our understanding of the biology underlying cachexia is mostly based on the extensively used and well-characterized C26 carcinoma model, in which mice are drastically losing muscle and total body weight in a short period [10], thus contrasting with the progressive wasting occurring in the human pathology. It is known that the C26 model is associated with high levels of IL6 that play a central role in mediating muscle wasting [11], even though other inducers are probably involved in cachexia. In order to better characterize early stages of

cachexia, we established a model of pancreatic cancer-induced cachexia able to promote mitochondrial metabolic alterations and a progressive wasting both in vivo and in vitro.

## **II Materials and Methods**

### **Animals**

Young adult female C57BL/6J mice (9–12 weeks old) were used. All animal experiments were authorized by the Italian Ministry of Health and carried out according to the European Community guiding principles in the care and use of animals.

### **Generation of a PDAC Model.**

KPC tumor cells were derived from a primary culture of pancreatic tumor cells of the genetically engineered mouse model of PDAC (K-ras LSL.G12D/+ ; p53 R172H/+; Pdx-Cre (KPC)).  $0.7 \times 10^6$  KPC cells in 200  $\mu$ l PBS were injected subcutaneously into the flank of C57bl/6J mice. Mice were sacrificed 5 weeks after injection, when tumor volume was approaching 5 mm of radius.

### **In Vivo Assessment of Muscular Strength**

#### **Grip Test.**

An automatic grip strength meter was used to measure the maximum forelimb grip strength of mice. The machine measures the peak resistance force of the mouse while the latter is pulled away from the grid of the device. Each animal was assessed several times, and the final value corresponds to the average of 5 repeated force measurements in order to minimize procedure-related variability.

#### **Hanging Test.**

A wire-hanging test was used to assess whole-body muscle strength and endurance. The test was performed as previously described [12]. Briefly, mice were subjected to a 180-second hanging test on a wire, during which “falling” and “reaching” scores were recorded. When a mouse fell from the wire, the falling score was diminished by 1, and when a mouse reached one of the side of the wire, the reaching score was increased by 1. A final score was then established using both falling and reaching scores and was represented in the form of a Kaplan-Meier-like curve; scores have been normalized with respect to control.

## MRI

Magnetic resonance images were acquired on a 1 Tesla M2 system (Aspect, Israel) equipped with a 30 mm transmitter/receiver (TX/RX) solenoid coil to determine body composition [13]. T-weighted spin-echo images were acquired with high-resolution whole-body coronal orientation (repetition time/echo time/flip angle/number excitations [TR/TE/FA/NEX]: 400 ms/9.5 ms/90°/3, field of view [FOV]:10 cm, matrix: 192 × 192, number of slices: 18, slice thickness: 1.5 mm, in-plane spatial resolution: 521 μm, and acquisition time: 4 min). All T-weighted images were processed by an in-house Matlab-developed script (MATLAB R2008, The MathWorks Inc.). The T1-weighted image histogram has three dominating classes, background, lean mass, and fat, so the total fat volume was isolated by segmenting the image into three categories by using a k-means clustering algorithm [14, 15].

## Gene Expression Analysis

Gastrocnemii were harvested, frozen in liquid nitrogen, and crushed. Total RNA was extracted using TRIzol reagent (Invitrogen, Carlsbad, CA). cDNA was synthesized from 1000 ng of total RNA using cDNA reverse transcription kits (Applied Biosystems, Foster City, CA). Relative mRNA level was analyzed by real-time PCR (ABI 7900HT FAST Real-Time PCR system, Applied Biosystems, Foster City, CA) with TaqMan assays, using the Universal Probe Library system (Roche Applied Science, Penzberg, Germany). The 18S gene was used as a housekeeping control. The following primers were used: FBX030 (MUSA1): F:5'-gagaagccagggttgagc-3gagtgctgctg-3', FBX032 (atrogen 1): F:5'tgtg-3'and R: 5'-gatcaaacgcttgccaatct-3 F:5'-tgacatctacaagcaggagtg-3' and R: 5' and R: 5 '-tcatacagtg' - agtgaggaccggctac ' , TRIM63 (MuRF1):'-tcgtctctggttccttg-3', and cathepsin L F:5 '-caaataagaataaatattgcttgca-3 ' and R:5 ' -ttgatgtagcctccatccc-3

## Western Blot

Protein samples from gastrocnemius were extracted with RIPA lysis buffer (150 mM NaCl, 50 mM Tris- HCl, 0.5% sodium deoxycholate, 1.0% Triton X-100, 0.1% SDS, and 1 mM EDTA) supplemented with protease and phosphatase inhibitor cocktail (Roche). Protein concentration was determined using the BCA protein assay (Thermo Fisher Scientific). Lysates were subjected to SDS-PAGE and then transferred to the PVDF membrane for immunoblotting analysis. The following antibodies were used: monoband polyubiquitin (BML-PW8805, Enzo Life Sciences, 1 : 1000), p-AMPK (2535, Cell Signaling, 1 : 1000), and βactin (4967, Cell Signaling, 1 : 1000).



### Tissue Collection and Histology

Gastrocnemius muscle was excised, weighted, frozen in isopentane cooled in liquid nitrogen, and stored at -80 °C. Transverse sections (7  $\mu\text{m}$ ) from the medial belly were cut on a cryostat and collected on Superfrost plus glass slides. Cryosections were then processed for laminin staining. In detail, sections were fixed in 4% paraformaldehyde (PFA) for 10 min before being incubated

### Succinate Dehydrogenase Activity

Succinate dehydrogenase (SDH) enzymatic activity was determined on 15  $\mu\text{m}$  cryosections by specific staining (Bio-Optica, Milan, Italy) following the producer's instructions. Briefly, the cryosections were incubated with the rehydrated SDH solution for 45 min at 37°C, washed, fixed, and mounted on slides. Images were then acquired with the slide scanner Panoramic Midi 1.14.

### Cell Culture and Conditioned Medium (CM) Preparation.

C2C12 cells were cultured in DMEM/10% FBS and differentiated in DMEM/2% horse serum (HS) for 4 days as reported previously [16]. KPC cells were derived from a primary culture of pancreatic tumor cells of the genetically engineered mouse model of PDAC (K-ras<sup>LSL.G12D/+</sup>; p53<sup>R172H/+</sup>; PdxCre<sup>mice</sup> (KPC)). Conditioned medium (CM) was prepared as follows: KPC cells were grown in DMEM with 10% FBS supplemented with 1% penicillin and streptomycin. When cells reached full confluence, the medium was removed; cells were washed twice with phosphate-buffered saline (PBS) and once with serum-free DMEM. Cells were grown in serum-free DMEM for further 24 h; then, the medium was collected, centrifuged at 4000 rpm for 10 min, aliquoted, and stored at -80°C. Atrophy on C2C12 was induced with 10% CM treatment for 48 h.

### Myotube Diameter Quantification.

C2C12 myotubes were treated with differentiation medium supplemented with 10% conditioned medium from KPC for 48 h. Pictures of myotubes were taken with bright field microscopy (Zeiss), and diameters of myotubes were measured using the software JMicroVision as previously described [16].

### ROS Measurement In Vitro.

ROS production was assessed in C2C12 myotubes by using the oxidant sensitive fluorescent dye 2',7'-dichlorodihydro fluorescein diacetate (HDCFDA; Molecular Probes Inc., Eugene, OR). Cells were incubated with 10  $\mu\text{M}$  HDCFDA in PBS for 30 minutes at 37°C under 5% CO<sub>2</sub> atmosphere in darkness. An excess probe was

washed out with PBS. Fluorescence was recorded at excitation and emission wavelengths of 485 nm and 530 nm, respectively, by a fluorescence plate reader (Promega). Fluorescence intensity was expressed as arbitrary units.

#### Mitochondrial Isolation.

Mitochondrial fractions were isolated as previously reported [17], with minor modifications. Samples were lysed in 0.5 ml buffer A (50 mM Tris, 100 mM KCl, 5 mM MgCl<sub>2</sub>, 1.8 mM ATP, and 1 mM EDTA (pH 7.2)), supplemented with protease inhibitor cocktail III (Calbiochem), 1 mM PMSF, and 250 mM NaF. Samples were clarified by centrifuging at 650 ×g for 2 min at 4°C, and the supernatant was collected and centrifuged at 13,000 ×g for 5 min at 4°C. This supernatant was discarded, and the pellet containing mitochondria was washed in 0.5 ml buffer A and resuspended in 0.25 ml buffer B (250 mM sucrose, 15 mM K<sub>2</sub>HPO<sub>4</sub>, 2 mM MgCl<sub>2</sub>, 0.5 mM EDTA, and 5% BSA (w/v)). A 50 μl aliquot was sonicated and used for the measurement of protein content or Western blotting; the remaining part was stored at -80 °C.

#### Electron Transport Chain.

The activity of complexes I–III was measured on 25 μl of non sonicated mitochondrial samples resuspended in 145 μl buffer C (5 mM KH<sub>2</sub>PO<sub>4</sub>, 5 mM MgCl<sub>2</sub>, and 5% BSA (w/v)) and transferred into a 96well plate. Then, 100 μl buffer D (25% saponin (w/v), 50 mM KH<sub>2</sub>PO<sub>4</sub>, 5 mM MgCl<sub>2</sub>, 5% BSA (w/v), 0.12 mM cytochrome c-oxidized form, and 0.2 mM NaN<sub>3</sub>) was added for 5 min at room temperature. The reaction was started with 0.15 mM NADH and was followed for 5 min, and the absorbance was measured at 550 nm by a Synergy HT spectrophotometer (BioTek Instruments). Under these experimental conditions, the rate of cytochrome c reduction, expressed as nmol cyt c reduced/min/mg mitochondrial proteins, was dependent on the activity of both complex I and complex III [18].

#### Intramitochondrial ATP Levels.

The amount of ATP was measured on 20 μg of mitochondrial extracts with the ATPlite assay (PerkinElmer), according to the manufacturer's instructions. Data were converted into nmol/mg mitochondrial proteins, using a calibration curve previously set.

#### Intramitochondrial ROS Levels.

The amount of ROS in mitochondrial extracts was measured fluorimetrically incubating mitochondrial suspension at 37°C for 10 minutes with 10 μM of 5-(and-6)-chloromethyl-2,7-dichlorodihydro-fluorescein diacetate-acetoxymethyl ester (DCFDA-AM) and then washed and

resuspended in 0.5 ml of PBS. Results were expressed as nmol/mg mitochondrial proteins, using a calibration curve previously set with a serial dilution of H.

#### Fatty Acid $\beta$ -Oxidation.

Long-chain fatty acids were measured as described by Gaster et al. [19] with minor modifications. 100  $\mu$ l mitochondrial suspension was rinsed with 100  $\mu$ l of 20 mM HEPES, containing 0.24 mM fatty acid-free BSA, 0.5 mM L-carnitine, and 2  $\mu$ Ci [1- $^{14}$ C]palmitic acid (3.3 mCi/mmol, PerkinElmer). Samples were incubated at 37°C for 1 h; then, 100  $\mu$ l of 1 : 1 phenylethylamine (100 mM)/methanol solution (v/v) was added. After one hour at room temperature, the reaction was stopped by adding 100  $\mu$ l of 0.8 N HClO<sub>4</sub>. Samples were centrifuged at 13,000  $\times$ g for 10 min. Both the precipitates containing  $^{14}$ C acid-soluble metabolites (ASM) and the supernatants containing  $^{14}$ CO derived from oxidation (used as an internal control and expected to be less than 10% of ASM) were counted by liquid scintillation. Results are expressed as nmol/min/mg cellular proteins.

#### Statistics

Statistical significance was evaluated with one-way or two-way analysis of variance (ANOVA) for multiple groups, followed by a post hoc test as defined in the figure legends. Student's unpaired t-test was used to compare two groups. All error bars indicate SEM. Significance was established as  $P < 0.05$ . Data have been obtained from multiple independent experiments for an in vitro assay and from at least 4 mice for in vivo experiments. All the analyses were performed with the software PRISM5 (GraphPad Software).

### III Results

**Establishment of a Slow-Paced Cancer-Induced Muscle Wasting Model.** PDAC is known to induce muscle wasting with high penetrance [3]. Since cancer cachexia is a complex syndrome involving various pathological processes promoting wasting, such as anorexia and chronic inflammation, it is difficult to assess the direct contribution from the tumor. Therefore, we decided to assess the direct role of cancer cells in skeletal muscle atrophy via an in vitro model of atrophy, thus excluding other systemic confounding atrophic factors, hypothesizing that, in this type of cancer, atrophy can be mediated directly by tumor cell secreted factors. To this aim, we took advantage of KPC cells, a stable cell line derived from spontaneous primary tumor arising in C57BL/6 KRASG12DP53R172HPdx-Cre <sup>+/+</sup>(KPC) mouse [20], a genetically modified mouse model known to develop spontaneous wasting [9]. Similar to other cancer models[21], in our experimental conditions, KPC cells were able to directly promote muscle atrophy in vitro. Treatment of C2C12-derived myotubes with 10% KPC cell-conditioned media induced a consistent reduction in myotube thickness, similar to that elicited by dexamethasone, used as a positive control of atrophy induction (**Figure 1(a)**). A reduction in fiber thickness was associated with higher ROS generation (**Figure 1(b)**). A recent report from Michaelis et al. [20] showed that a subcutaneous injection of 5 million of these cells consistently promotes anorexia, hormonal dysfunctions, and lethal cachexia in 2 weeks. In order to establish a progressive model of wasting, we subcutaneously injected 0.7 million of KPC cells, which is the minimal amount able to consistently induce tumor growth without exacerbating factors such as excessive tumor burden and anorexia. Indeed, 5 weeks after KPC cell injection, neither food intake alteration (**Figure 1(c)**) nor macroscopic features of wasting were observed, despite a non significant decreasing trend in body weight (**Figure 1(d)**). Tumor weight at the end of the experiment was approximately 0.6 grams (**Figure 1(e)**), while in the other work, weight was between 1 and 2 grams [20]. Remarkably, despite the absence of overt signs of cachexia, skeletal muscle functionality, checked by rotarod evaluation twice a week (not shown), was drastically affected, but only at week 5, the week of the sacrifice. Accordingly, tumor-bearing mice showed reduced muscle performance, as assessed by the hanging-wire test [12] (**Figure 1(f)**), suggesting muscle deterioration in tumor-bearing animals. Along with reduced performance in stamina-related assays, mice displayed as well a reduction in grip strength indicating also that the maximal force developed was reduced (**Figure 1(g)**).

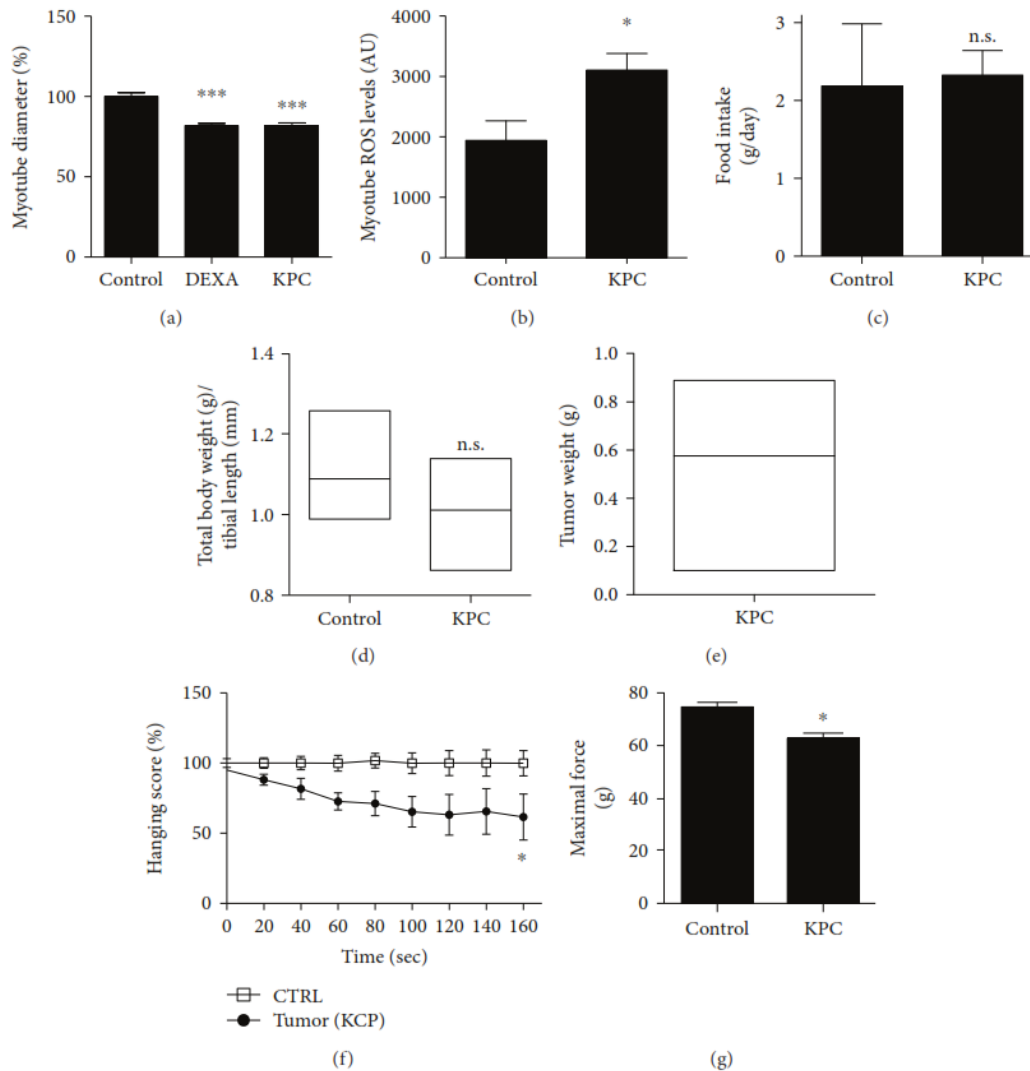


**Figure 1: Characterization of an in vitro and in vivo model of cancer-associated atrophy.** C2C12 myotubes treated for 48 h with 10% conditioned medium (CM) from KPC cells. Dexamethasone (DEXA) was used as a positive control of atrophy induction. Pictures were acquired at the brightfield microscope and (a) diameters were measured. (b) Increased ROS production in C2C12 myotubes treated with CM from KPC using oxidant-sensitive fluorescent dye H DCFDA. (c) No difference in food intake in tumor-bearing versus control mice at the end of the experiment. (d) No significant weight loss in KPC tumor-bearing versus control mice. (e) Average tumor weight (min max box plot). Upon tumor growth at the end stage, mice presented reduced muscular resistance as evidenced by (f) performance at the hanging test (reach/fall assay) and (g) maximal strength as performed by the grip test of the upper limbs. All experiments have been performed with N= 4 mice per group. All data are shown as means  $\pm$  SEM; n.s. = non significant; \* $P < 0.05$ ; \*\*\* $P < 0.001$ ; one-way ANOVA with Bonferroni correction for (a), two-way ANOVA with Dunnett's multiple comparison test for (e), and Student's t-test for (b), (c), (d), (f), and (g).

Coherently with the decrease in muscle functionality, 5 weeks after KPC injection, mice presented a consistent loss of gastrocnemius mass of roughly 20% (**Figure 2(a)**). The decrease was related to a reduction in average fiber size as detailed by histological analysis (**Figures 2(b)–2(d)**). Coherently, analysis of fiber cross-sectional area (CSA) distribution highlighted a shift towards smaller areas (**Figure 2(e)**). A reduction in muscle mass was not associated with transcriptional regulation of atrogenes Atrogin1, Musa, and Murf1 and of cathepsin L (**Figures 2(f)–2(i)**), nor with altered expression of ATG7, BECLIN1, and LC3 in gastrocnemii (not shown). Nevertheless, muscle protein lysates presented increased protein

ubiquitination (**Figure 2(j)**), indicative of an activation of the UPP. Along with increased protein ubiquitination, we identified higher AMPK phosphorylation, in line with the emerging role of AMPK as a functional player in cancer cachexia [22].

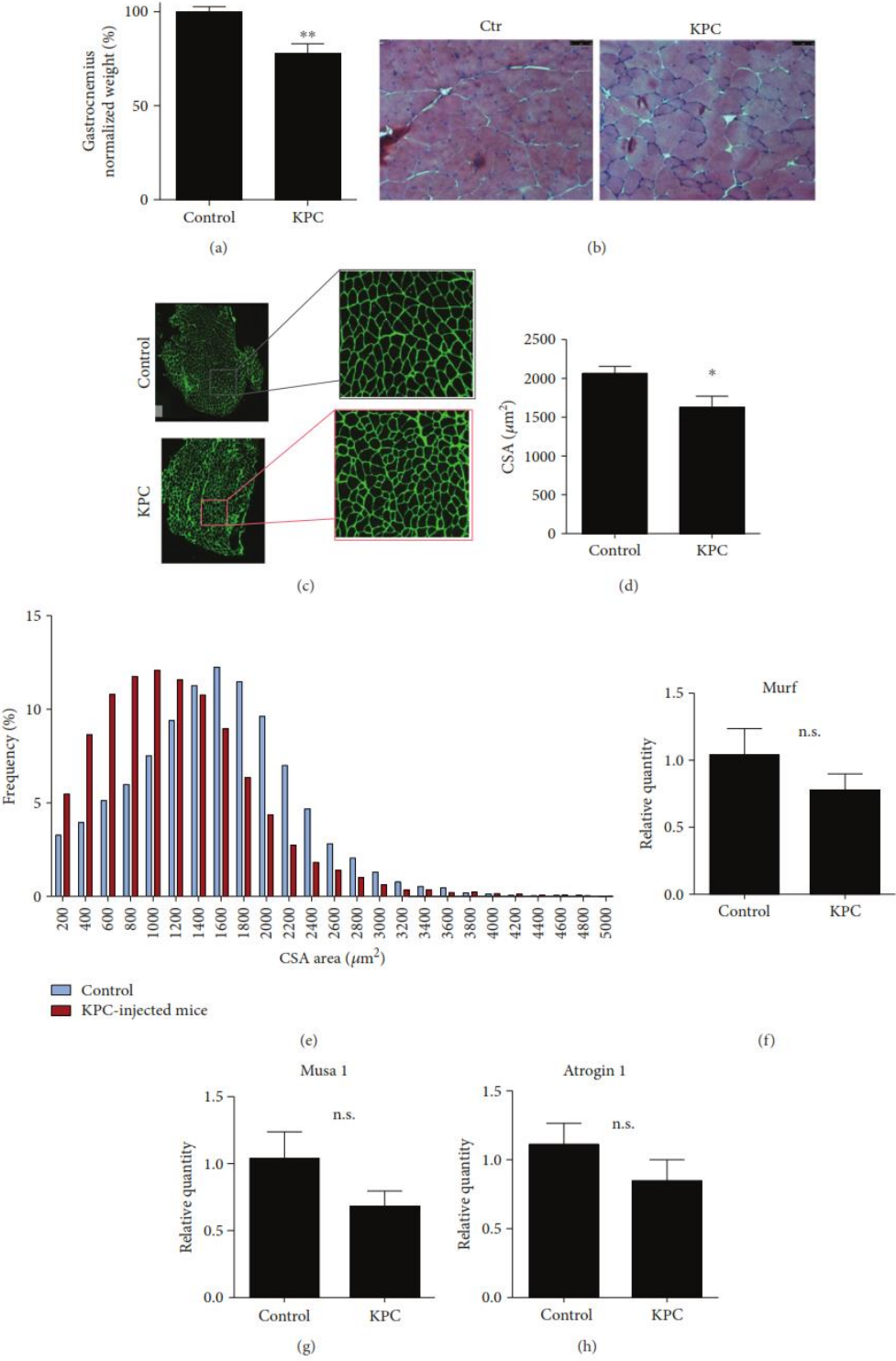
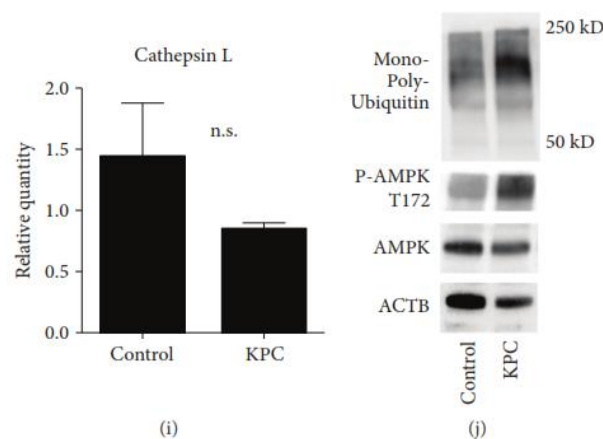


FIGURE 2: Continued.



**Figure 2: KPC cell injection promotes skeletal muscle atrophy.** (a) Gastrocnemius weight normalized on tibial length. (b) H&E representative pictures of muscle sections from control and KPC-injected mice. (c–e) Gastrocnemius myofiber membranes were stained for laminin, pictures of the whole muscle section were acquired, and the cross-sectional area (CSA) was measured (c). (d) Frequency histogram showing distribution of myofiber CSA in control and KPC-bearing mice.  $N=4$ . (e) Representative pictures of laminin staining for CSA analysis in control and KPC-bearing mice. (f–i) KPC injection does not upregulate atrogene expression.  $N=4$ . (j) Increased proteinubiquitination and AMPK (T172) phosphorylation in mice bearing tumor; blot representative of three independent experiments. All data are shown as means  $\pm$  SEM. Statistical analyses were conducted using two-tailed t-test. n.s. = nonsignificant.

**Mice Undergoing Muscle Dysfunction Present Altered Lipid Metabolism.** Given the importance of energy metabolism in regulating skeletal muscle mass and functionality [23, 24], we investigated potential alterations of mitochondrial metabolism in the skeletal muscle of KPC-bearing mice. To this aim, we assessed basal complex II activity in gastrocnemii by performing the succinate dehydrogenase (SDH) activity assay. Intriguingly, gastrocnemius sections from KPC-bearing animals presented increased complex II activity, as evidenced by the increased concentration of blue tetrazolium salt (**Figure 3(a)**). However, this increased activity was not coupled with elevated flux through the electron transport chain (ETC). Indeed, ETC, as measured by cytochrome c reduction rate in uncoupled mitochondria, was similar in the two groups (**Figure 3(b)**). While SDH activity supports ETC, it is also part of the tricarboxylic acid (TCA) cycle and it is linked to fatty acid oxidation, allowing ketone bodies generated by acetyl coenzyme A due to excessive fatty acid oxidation to enter the TCA. To clarify whether the increased SDH activity was indicative of increased fatty acid oxidation, we measured this metabolic pathway in isolated mitochondria from the gastrocnemius of either control or KPC-bearing mice and we observed a significant increase in fatty acid oxidation in muscles of tumor-bearing mice (**Figure 3(c)**), consistent with the increase in complex II activity. In order to identify if the altered intramuscular lipid oxidation was correlated with a systemic dysregulation during this precachectic process, we performed T-weighted magnetic resonance imaging (MRI). Intriguingly, 4 weeks post-KPC injection (one week before sacrifice), precachectic mice presented reduced bright hyperintensity regions, indicative of reduced fat deposits (**Figures**

**3(d) and 3(e)**). Coherently, at the time of sacrifice, KPC-bearing mice presented a significant reduction in inguinal fat tissue mass (**Figure 3(f)**). Therefore, we speculated that the reduced fat content might be related to increased fatty acid oxidation, a feature previously associated with cancer cachexia [23] in other tumor types. High SDH activity [25, 26] and excessive fatty acid oxidation might lead to ROS accumulation [27], ultimately promoting mitochondrial dysfunction [28] and fiber damage. Hence, we investigated the impact of tumor growth on mitochondrial ROS and energetic balance. Mitochondria extracted from KPC-bearing animals had indeed increased ROS (**Figure 3(g)**), coupled with reduced ATP (**Figure 3(h)**), suggesting that the increased fatty acid oxidation may have a detrimental rather than beneficial effect on mitochondria.

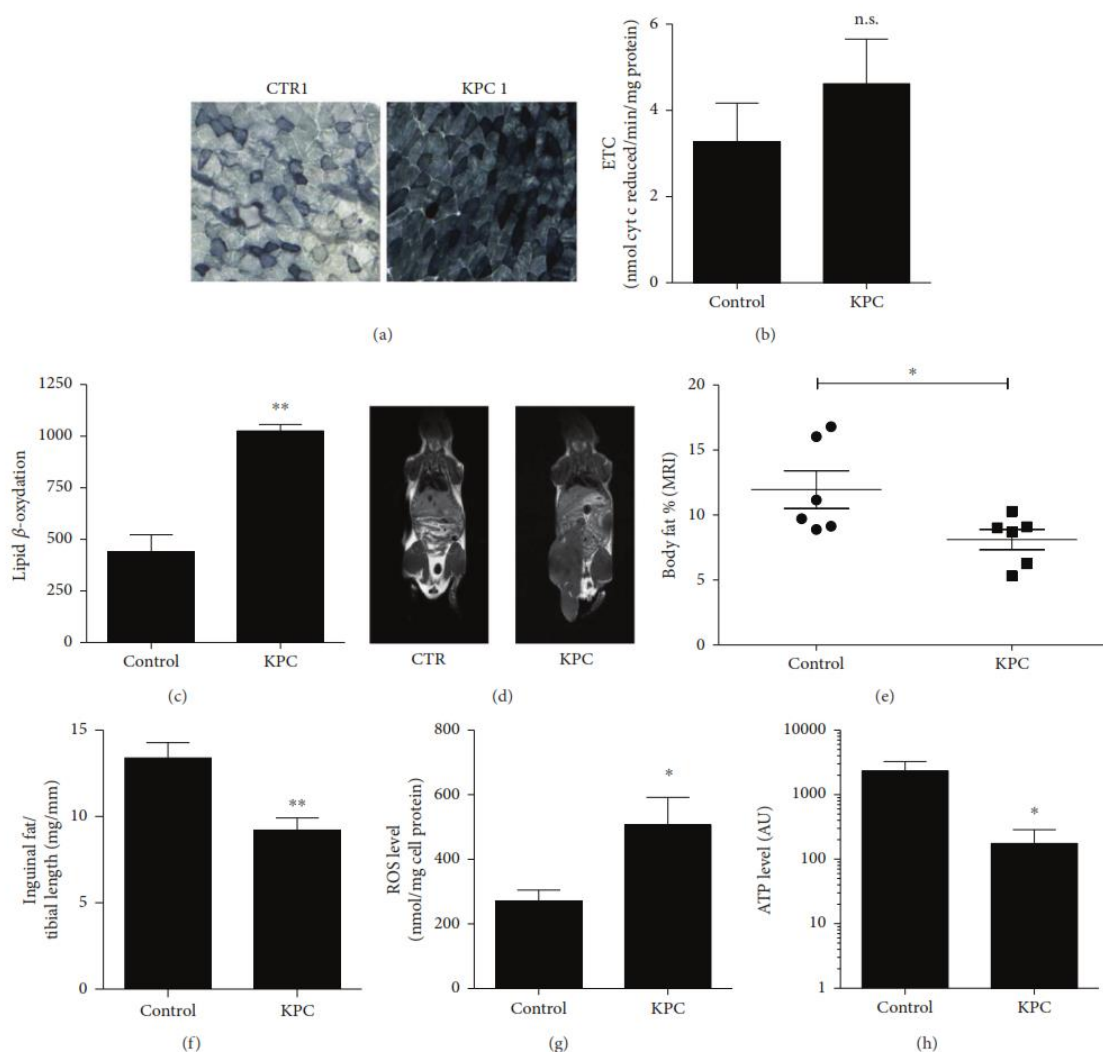


**Figure 3: Metabolic dysregulation of skeletal muscle in KPC-bearing mice.** (a) Representative images for succinate dehydrogenase (SDH) activity stain. (b) Gastrocnemius mitochondria were isolated, and ETC activity from complex I to complex III was assessed by evaluating cytochrome c reduction. (c)  $^{14}\text{C}$ -labeled palmitate was used as a substrate to measure lipid beta-oxidation in isolated mitochondria of gastrocnemius from control and KPC-bearing mice. (d) Representative T1-weighted MR images (brightest regions in T-weighted MR images correspond to adipose regions) and (e) in vivo measurement of adipose tissue using MR images in the control group versus KPC-bearing mice. (f) Weight of inguinal fat normalized to tibial length for control versus KPC-bearing mice. (g) Gastrocnemius mitochondria were isolated, and ATP level was assessed using the ATPlite kit (PerkinElmer, USA). (h) ROS measurement in isolated mitochondria from gastrocnemius using HDCFDA. N= 4. All data are shown as means  $\pm$  SEM. Statistical analysis was conducted using two-tailed t-test. n.s. = nonsignificant; \* $P < 0.05$ ; \*\* $P < 0.01$ .



## IV Discussion

Pancreatic cancer is a pathology with dismal prognosis associated with a stark decrease in quality of life, mostly because of cachexia development [29, 30]. While cachexia is considered the last step of cancer progression, it is important in PDAC to model the earliest steps of the disease (i.e., precachexia). Indeed, Mayers et al. [9] found that spontaneous PDAC mouse model presents an increased release of amino acids from the skeletal muscle months before the development of cachexia, which is consistent with the data from PDAC patients [9]. These data advocate for the importance of defining alterations in skeletal muscle occurring in the early phases of disease, before the establishment of overt cachexia. To this aim, we modified the cancer cachexia model described by Michaelis et al. to reproducibly induce cachexia with KPC cells [20]. Since KPC-bearing male mice present hormonal dysfunctions, we performed the study in female mice, although these animals are characterized by a moderate degree of wasting. While Michaelis and coworkers modeled cachexia by injecting up to  $5 \times 10^6$  cells per mouse, thus promoting anorexia and subsequent animal death starting from 11–14 days, we injected only  $0.7 \times 10^6$  cells (the minimal amount necessary to consistently promote tumor growth) in order to promote a slower tumor growth, thus allowing the characterization of precachectic events. This reduced cell number resulted in barely palpable tumors at 2 weeks after injection (the time point where mice from Michaelis et al. already started to die of cachexia). Moreover, in contrast to the effects reported with the injection of higher amount of KPC cells, smaller tumor mass (up to 75% reduction) and no effect on heart weight were observed (data not shown). Despite the moderate degree of wasting, mice presented reduced muscle function and strength. In order to detect alterations in muscle morphology occurring at early phases of wasting, we sacrificed the mice at the first sign of decreased performance. At necropsy, mice pre-sented a statistically significant reduction in gastrocnemius weight and fat deposit, but no signs of anorexia, excluding the involvement of food intake in the skeletal muscle mass reduction. Intriguingly, we found only a trend towards decreased body weight, similar to the findings of Brown and colleagues [7]. Of note, it is known that many tumors hijack organ function, especially the liver and spleen [3], by inducing increased organ size, which might counterbalance the drop in muscle and fat in the first phases. Muscle from tumor-bearing mice did not present any major transcriptional regulation of the investigated atrogenes. However, we identified increased levels of AMPK phosphorylation, indicative of ongoing energy stress, and protein ubiquitination indicating that the alterations present in muscle were mediated by a different pathway, that is, alternative ubiquitin ligase, a regulation at protein level, or alterations in protein deubiquitinases. As previously shown in clear cell kidney cancer, muscle undergoing wasting is causally linked to increased fatty acid oxidation [23, 31], potentially raising noxious ROS generation in the mitochondria. Noteworthy, also in our model, the significant drop in lipid was coupled with an

increased fatty acid utilization and mitochondrial ROS generation, indicating a potential source of oxidative stress causing reduced muscular function and degeneration. Intriguingly, we identified an increased activity of SDH, uncoupled with increased ETC flux. Moreover, ATP content was decreased, suggesting a profound mitochondrial alteration. This observation further supports the concept that mitochondrial alterations occur at the early phases of cachexia. While SDH does not contribute to increasing mitochondrial energy metabolism in cachectic muscles, it promotes the metabolism of ketone body derivatives that are produced in conditions of high fatty acid oxidation, that is, in the same metabolic conditions of KPC-bearing muscles. Redox cycles occurring at complex I and complex III of the ETC are generally considered the key sources of ROS within mitochondria. However, also, the SDH complex has been recognized as an important source of intramitochondrial ROS [25]. Taken together, our findings suggest that muscles consume fatty acids, forcing SDH activity in early cachexia. The final result is an energetic catastrophe that may severely impair muscle physiological performance.

Interestingly, *in vitro* myotubes did not show increased fatty acid oxidation during atrophy (not shown), in line with the fact that culture and differentiation media contain limited amount of fatty acids. However, C2C12 cells treated with the medium of pancreatic cancer cells displayed the same alterations observed in cachectic muscles, notably high ROS levels and AMPK phosphorylation (not shown), suggesting that common metabolic alterations in mitochondrial metabolism occur in the early phase of cachexia both *in vitro* and *in vivo*. In conclusion, we report a novel model of precachexia causing a drastic reduction in muscle function and an initial reduction in skeletal muscle mass. Interestingly, the onset of increased fatty acid oxidation and mitochondrial ROS generation occurs before the emergence of muscle mass reduction. Further test inhibiting fatty acid oxidation or mitochondrial ROS generation will be instrumental in understanding the relative contribution of such pathways to the pathogenesis of cachexia, as well as in the identification of the factors secreted by PDAC cells causing muscle atrophy, both *in vitro* and *in vivo*.

#### Conflicts of Interest

The authors declare no conflict of interest.

#### Acknowledgments

Paolo Ettore Porporato is supported by the Italian Ministries of Health, Research and Education (MIUR, Rita Levi-Montalcini program for young researchers, 2014), and Nicoletta Filigheddu is the recipient of Fondazione Cariplo Grant 2015-0634. The authors are grateful to Dr. Riccardo Taulli, Professor Maurizio Giustetto, and Professor Stefano Geuna for the helpful discussions and access to instrumentations and to Erica Mina and Edoardo Ratto for the valuable technical support.

## V References Chapter 1

- [1] N. Johns, N. A. Stephens, and K. C. H. Fearon, "Muscle wasting in cancer," *The International Journal of Biochemistry & Cell Biology*, vol. 45, no. 10, pp. 2215–2229, 2013.
- [2] M. J. Tisdale, "Wasting in cancer," *The Journal of Nutrition*, vol. 129, pp. 243S–246S, 1999.
- [3] P. E. Porporato, "Understanding cachexia as a cancer metabolism syndrome," *Oncogenesis*, vol. 5, no. 2, article e200, 2016.
- [4] K. Fearon, F. Strasser, S. D. Anker et al., "Definition and classification of cancer cachexia: an international consensus," *The Lancet Oncology*, vol. 12, no. 5, pp. 489–495, 2011.
- [5] S. H. Lecker, R. T. Jagoe, A. Gilbert et al., "Multiple types of skeletal muscle atrophy involve a common program of changes in gene expression," *The FASEB Journal*, vol. 18, no. 1, pp. 39–51, 2004.
- [6] E. Marzetti, M. Lorenzi, F. Landi et al., "Altered mitochondrial quality control signaling in muscle of old gastric cancer patients with cachexia," *Experimental Gerontology*, vol. 87, no. Part A, pp. 92–99, 2017.
- [7] J. L. Brown, M. E. Rosa-Caldwell, D. E. Lee et al., "Mitochondrial degeneration precedes the development of muscle atrophy in progression of cancer cachexia in tumour-bearing mice," *Journal of Cachexia, Sarcopenia and Muscle*, vol. 8, no. 6, pp. 926–938, 2017.
- [8] G. D. Stewart, R. J. Skipworth, and K. C. Fearon, "Cancer cachexia and fatigue," *Clinical Medicine*, vol. 6, no. 2, pp. 140–143, 2006.
- [9] J. R. Mayers, C. Wu, C. B. Clish et al., "Elevation of circulating branched-chain amino acids is an early event in human pancreatic adenocarcinoma development," *Nature Medicine*, vol. 20, no. 10, pp. 1193–1198, 2014.
- [10] A. Bonetto, J. E. Rupert, R. Barreto, and T. A. Zimmers, "The colon-26 carcinoma tumor-bearing mouse as a model for the study of cancer cachexia," *Journal of Visualized Experiments*, vol. 117, article e54893, 2016.
- [11] A. A. Narsale and J. A. Carson, "Role of interleukin-6 in cachexia: therapeutic implications," *Current Opinion in Supportive and Palliative Care*, vol. 8, no. 4, pp. 321–327, 2014.
- [12] S. Reano, E. Angelino, M. Ferrara et al., "Unacylated ghrelin enhances satellite cell function and relieves the dystrophic phenotype in Duchenne muscular dystrophy mdx model," *Stem Cells*, vol. 35, no. 7, pp. 1733–1746, 2017.
- [13] S. Geninatti-Crich, I. Szabo, D. Alberti, D. Longo, and S. Aime, "MRI of cells and mice at 1 and 7 tesla with Gd-targeting agents: when the low field is better!," *Contrast Media & Molecular Imaging*, vol. 6, no. 6, pp. 421–425, 2011.
- [14] L. Braccini, E. Ciraolo, C. C. Campa et al., "PI3K-C2 $\gamma$  is a Rab5 effector selectively controlling endosomal Akt2 activation downstream of insulin signalling," *Nature Communications*, vol. 6, p. 7400, 2015.
- [15] A. Perino, M. Beretta, A. Kili et al., "Combined inhibition of PI3K $\beta$  and PI3K $\gamma$  reduces fat mass by enhancing  $\alpha$ -MSH-dependent sympathetic drive," *Science Signaling*, vol. 7, no. 352, article ra110, 2014.
- [16] P. E. Porporato, N. Filigheddu, S. Reano et al., "Acylated and unacylated ghrelin impair skeletal muscle atrophy in mice," *The Journal of Clinical Investigation*, vol. 123, no. 2, pp. 611–622, 2013.
- [17] I. Campia, C. Lussiana, G. Pescarmona, D. Ghigo, A. Bosia, and C. Riganti, "Geranylgeraniol prevents the cytotoxic effects of mevastatin in THP-1 cells, without decreasing the beneficial effects on cholesterol synthesis," *British Journal of Pharmacology*, vol. 158, no. 7, pp. 1777–1786, 2009.
- [18] R. Wibom, L. Hagenfeldt, and U. von Döbeln, "Measurement of ATP production and respiratory chain enzyme activities in mitochondria isolated from small muscle biopsy samples," *Analytical Biochemistry*, vol. 311, no. 2, pp. 139–151, 2002.

- [19] M. Gaster, A. C. Rustan, V. Aas, and H. Beck-Nielsen, "Reduced lipid oxidation in skeletal muscle from type 2 diabetic subjects may be of genetic origin: evidence from cultured myotubes," *Diabetes*, vol. 53, no. 3, pp. 542–548, 2004.
- [20] K.A. Michaelis, X. Zhu, K. G. Burfeind et al., "Establishment and characterization of a novel murine model of pancreatic cancer cachexia," *Journal of Cachexia, Sarcopenia and Muscle*, vol. 8, no. 5, pp. 824–838, 2017.
- [21] D. N. Seto, S. C. Kandarian, and R. W. Jackman, "A key role for leukemia inhibitory factor in C26 cancer cachexia," *The Journal of Biological Chemistry*, vol. 290, no. 32, pp. 19976–19986, 2015.
- [22] M. Segatto, R. Fittipaldi, F. Pin et al., "Epigenetic targeting of bromodomain protein BRD4 counteracts cancer cachexia and prolongs survival," *Nature Communications*, vol. 8, no. 1, p. 1707, 2017.
- [23] T. Fukawa, B. C. Yan-Jiang, J. C. Min-Wen et al., "Excessive fatty acid oxidation induces muscle atrophy in cancer cachexia," *Nature Medicine*, vol. 22, no. 6, pp. 666–671, 2016.
- [24] C. T. Hensley, B. Faubert, Q. Yuan et al., "Metabolic heterogeneity in human lung tumors," *Cell*, vol. 164, no. 4, pp. 681–694, 2016.
- [25] M. Balietti, P. Fattoretti, B. Giorgetti et al., "A ketogenic diet increases succinic dehydrogenase activity in aging cardiomyocytes," *Annals of the New York Academy of Sciences*, vol. 1171, no. 1, pp. 377–384, 2009.
- [26] A. Edalat, P. Schulte-Mecklenbeck, C. Bauer et al., "Mitochondrial succinate dehydrogenase is involved in stimulus secretion coupling and endogenous ROS formation in murine beta cells," *Diabetologia*, vol. 58, no. 7, pp. 1532–1541, 2015.
- [27] A. Guaras, E. Perales-Clemente, E. Calvo et al., "The CoQH2/ CoQ ratio serves as a sensor of respiratory chain efficiency," *Cell Reports*, vol. 15, no. 1, pp. 197–209, 2016.
- [28] I. R. Indran, G. Tufo, S. Pervaiz, and C. Brenner, "Recent advances in apoptosis, mitochondria and drug resistance in cancer cells," *Biochimica et Biophysica Acta (BBA) - Bioenergetics*, vol. 1807, no. 6, pp. 735–745, 2011.
- [29] K. C. Fearon, M. D. Barber, J. S. Falconer, D. C. McMillan, J. A. Ross, and T. Preston, "Pancreatic cancer as a model: inflammatory mediators, acute-phase response, and cancer cachexia," *World Journal of Surgery*, vol. 23, no. 6, pp. 584–588, 1999.
- [30] X. Zhou, J. L. Wang, J. Lu et al., "Reversal of cancer cachexia and muscle wasting by ActRIIB antagonism leads to prolonged survival," *Cell*, vol. 142, no. 4, pp. 531–543, 2010.
- [31] R. J. Mailloux and M. E. Harper, "Mitochondrial proteolysis and ROS signaling: lessons from the uncoupling proteins," *Trends in Endocrinology and Metabolism*, vol. 23, no. 9, pp. 451–458, 2012.

# Chapter 2

## Iron metabolism dysregulation promotes cancer cachexia

Elisabeth Wyart<sup>1\*</sup>, Myriam Hsu<sup>1\*</sup>, Erica Mina<sup>1</sup>, Roberta Sartori<sup>2</sup>, Valentina Rausch<sup>1</sup>, Andrea Lauria<sup>3</sup>, Miriam Martini<sup>1</sup>, Salvatore Oliviero<sup>3,5</sup>, Riccardo Taulli<sup>4</sup>, Laure B Bindels<sup>6</sup>, Fabio Penna<sup>7</sup>, Nicoletta Filigheddu<sup>8</sup>, Emilio Hirsch<sup>1</sup>, Massimiliano Mazzone<sup>10,11</sup>, Hans Prenen<sup>9</sup>, Marco Sandri<sup>2</sup>, Antonella Roetto<sup>7</sup>, Alessio Menga<sup>1</sup>, and Paolo E Porporato<sup>1</sup>

1 Department of Molecular Biotechnology and Health Sciences, Molecular Biotechnology Center, University of Torino, Torino, Italy.

2 Department of Biomedical Sciences, University of Padova, 35131, Padova, Italy.

3 Department of Life Sciences and System Biology, University of Turin, Turin, Italy.

4 Department of Oncology, University of Torino, 10043 Orbassano, Italy.

5 IIGM

6 Metabolism and Nutrition Research Group, Louvain Drug Research Institute, UCLouvain, Université catholique de Louvain, Brussels, Belgium.

7 Department of Clinical and Biological Sciences, University of Torino, Torino, ITALY

8 Department of Translational Medicine, University of Piemonte Orientale, Novara, Italy.

9 Department of Medical Oncology, University Hospital Antwerp, Edegem, Belgium.

10 Laboratory of Tumor Inflammation and Angiogenesis, Center for Cancer Biology (CCB), VIB, Leuven, Belgium.

11 Laboratory of Tumor Inflammation and Angiogenesis, and Department of Oncology, KU Leuven, Belgium.

\*These authors contributed equally to this work

## Abstract

Cachexia is a systemic wasting syndrome characterized by irreversible skeletal muscle atrophy that dramatically increases both the morbidity and mortality in various diseases. Despite its high prevalence in cancer patients, knowledge regarding the mechanism of cancer-induced cachexia remains very scarce. Here, we report significant alterations in key regulators of iron metabolism, including transferrin receptor (TfR1), in skeletal muscle during cancer cachexia, both in mice models and in cancer patients. Surprisingly, systemic iron deprivation downregulates iron uptake from the skeletal muscle, indicating that muscle is an expendable tissue that supports systemic iron homeostasis in life-threatening condition. We further found that iron rescues AMPK activation and mitochondrial dysfunction that are major promoters of skeletal muscle wasting. Our findings establish a strong link between altered iron homeostasis and muscle functionality in cancer, with iron metabolism representing a promising therapeutic target to prevent or even reverse muscle wasting diseases.

## I Introduction

In healthy humans, skeletal muscle makes up to 40% of the total body mass [104], of which 20% are constituted by proteins. The balance between protein anabolism and catabolism is regulated by a variety of factors, including the endocrine system, dietary intake and physical activity that altogether make skeletal muscle a plastic organ. Progressive loss of skeletal muscle mass (muscle atrophy) commonly occurs upon aging, with sedentary lifestyle, immobilization, and in chronic and/or inflammatory pathologies, sepsis, cardiac failure, COPD, and notably cancer[105]. Typically, massive skeletal muscle atrophy is the hallmark of a multi-organ wasting disorder known as cachexia, which causes severe asthenia and decreased tolerance to therapies and leads to poor clinical outcomes [2,106]. In cancer patients, the prevalence of cachexia can reach 80% depending on the type of tumor and has been considered to cause directly at least 20% of all cancer-related deaths [107]

While muscle atrophy is the main hallmark of cachexia, systemic alterations contribute to the uncontrollable decrease in quality of life, notably insulin resistance, liver dysfunction, chronic inflammation, or even altered gut microbiota and nutrients absorption [106]. Remarkably, iron deficiency is commonly diagnosed in cancer types associated to high prevalence of cachexia[92]. Iron absorption is indeed blocked by inflammation, while cancer cells increase iron uptake to sustain unbridled proliferation [108], worsening the negative iron balance. Iron is an essential cofactor, mostly under the form of heme or iron-sulfur-clusters (ISC) in supporting mitochondrial metabolism [109-113]. Mitochondrial function is particularly important in skeletal muscle where the generation of energy is a prerequisite for every myofibrillar contraction. Mitochondrial dysfunction, that is characterized by decreased oxidative capacity, inefficient energy production, defective biogenesis or even increased mitophagy, is widely known to drive skeletal muscle wasting [61,63,114,115].

It is noteworthy that skeletal muscle is the biggest protein reservoir of the body that also contains up to 15% of total body iron [116,117]. However, whether skeletal muscle homeostasis is influenced by iron deficiency remains unknown. In this study, we found that regulation of iron metabolism was altered in the skeletal muscle during cancer cachexia. We further determined that iron deficiency, a common condition in cancer patients, drives cachexia, and establish that iron supplementation prevents skeletal muscle atrophy.

## **II Material and methods**

### **Human skeletal muscle biopsies**

The study enrolled patients (age > 18 years) with pancreatic cancer surgically treated at the 3rd Surgical Clinic of Padova University Hospital. Cancer patients were classified as severely cachectic in cases of >10% weight loss in the 6 months preceding surgery.

The study also enrolled control, healthy donors undergoing elective surgery for non-neoplastic and non-inflammatory diseases. Patients with signs of infection were excluded. All patients joined the protocol according to the guidelines of the Declaration of Helsinki and the research project has been approved by Ethical Committee for Clinical Experimentation of Provincia di Padova (protocol number 3674/AO/15). Written informed consent was obtained from participants. The biopsies were performed during elective surgery within 30 min of the start of the surgery by cold section of a rectus abdominal fragment of about 0.5-1 cm. The fragment was immediately frozen and conserved in liquid nitrogen for gene expression analysis.

### **Human handgrip strength**

Participants with either an absolute iron deficiency (AID) or a functional iron deficiency (FID) were included in the clinical study. AID is defined by an iron-saturation of transferrin (TSAT) <20% and serum ferritin level < 30 ng/ml. FID is defined by a TSAT <20% and serum ferritin levels of >30ng/ml. Patients were treated with a single infusion of 1000 mg of iron intravenously (ferric carboxymaltose) .

The participants were asked to perform two handgrip tests to measure their strength using a hand dynamometer. The first handgrip test (HG1) was conducted prior to iron administration. The second handgrip test (HG2) was conducted within 2-12 days after the iron IV administration.

The hand dynamometer was calibrated and the measurements have an accuracy of +/- 5%. The test-retest reliability is good ( $r > 0.80$ ) and the inter-rater reliability is excellent ( $r = 0.98$ ).

The handgrip test required the participants to be seated, positioning their forearm, of their dominant hand, in a 90° angle with their body. The arm should not be pressed to the body or supported by an armrest and the shoulders should be relaxed. The grip of the hand dynamometer was adjusted to the hand size of the participant. The hand dynamometer was placed in the dominant hand and the participant was asked to squeeze the hand dynamometer as hard as possible until the strength indicator was stabilized (this took approximately 3-5

seconds). This was repeated three times, in between each measurement the participant was given 30 seconds to relax the arm and hand muscles.

All participants gave written informed consent to participate in the study and the study was approved by the Antwerp University Hospital ethical committee in accordance with the ethical standards established by the 1964 Declaration of Helsinki.

### **Animal experimentation**

All animal experiments were authorized by the Italian Ministry of Health and carried out according to the European Community guiding principles in the care and use of animals. The BaF experiments performed in Belgium were approved by and performed in accordance with the guidelines of the local ethics committee from the UCLouvain, Belgium. Housing conditions were as specified by the Belgian Law of 29 May 2013, regarding the protection of laboratory animals. Cancer cell lines (C26 colon murine adenocarcinoma, and LLC Lewis lung carcinoma,  $1 \times 10^6$  cells/mouse) were injected subcutaneously in the flank of female 8 weeks old mice (BALB/C for C26, C57 BL/6 for LLC). Baf3 cachexia was induced as previously reported [118], injecting Bcr-Abl-transfected Baf3 intravenously in 6 weeks old Balbc mice. LLC (Lewis Lung Carcinoma) tumor-bearing mice were necropsied at day 24. For C26, all mice were necropsied at day 11 except for the survival experiment.

Ferric carboxymaltose (Ferrinject 15mg/kg) was injected in the tail vein every 5 days starting from day 6 post-C26 inoculation. Blood was collected by cardiac puncture, and perfusion with PBS after anesthesia was performed to obtain samples for iron quantification. For the phlebotomy experiment, retroorbital bleeding (400 $\mu$ l of blood) was performed under anesthesia, and mice were fed with iron-deprived diet (Mucedola) for 11 days before sacrifice. To quantify muscle wasting gastrocnemii and quadriceps were freshly isolated, weighted, and normalized to the respective tibial length. To measure strength, mice were held by the middle part of the tail and allowed to grab the metal grid in a parallel position before being gently pulled backwards. The maximal force generated by the grip was recorded, and the measure was repeated six times on a dynamometer (2Biol).

### **Cell Culture and *in vitro* treatments**

C2C12 myoblasts were purchased from ATCC and cultured in DMEM with 10% fetal bovine serum (FBS). After reaching full confluency, differentiation was induced by switching to 2% horse serum (HS) DMEM for 4 days. Human myoblast cell line, originated from the quadriceps of a 38-year-old donor, was kindly provided by Dr. Vincent Mouly. The cells were cultured in



Skeletal Muscle Cell Basal Medium (PromoCell, Heidelberg, Germany) containing 5% FBS and supplemented with hbFGF, hEGF, fetuin, insulin, and dexamethasone. Differentiation was induced by switching to DMEM containing 10µg/ml insulin for 7 days.

Conditioned medium (CM) was prepared as previously described [119]. Briefly, cancer cells were grown to high confluency, then conditioned in serum-free DMEM for 24h, medium was harvested and centrifuged at 500g for 10min. Supernatant was collected and used as conditioned medium at 10% final concentration. Deferoxamine (DFO, Sigma D9533) and bathophenanthroline disulphonic acid (BPS, Sigma 146617) were used at 100µM. Apotransferrin Hinokitiol (HNK, Sigma 469521) and ferric citrate (Sigma F3388) were used at 5µM and 250nM, respectively. Activin A (RnD Sytem 338-AC), Dexamethasone (DEXA, Sigma) were used at 1nM and 1µM, respectively. Myotubes were treated for 48h for all compounds. For cell transfection, C2C12 myoblasts were differentiated for 3 days prior to transfection with esiTFR1, esiNCOA4 or esiGFP using Lipofectamine 2000 (Invitrogen 11668019). Myotubes were photographed and lysed at 72h post-transfection. For myotube diameter quantification, pictures of myotubes were taken with bright field microscopy (Zeiss) at 20x magnification, and myotube diameter was measured using the software JMicroVision as previously described [120].

### **Western Blotting**

Frozen gastrocnemius samples were lysed in RIPA lysis buffer (150mM NaCl, 50mM Tris-HCl, 0.5% sodium deoxycholate, 1.0% Triton X-100, 0.1% SDS, and 1mM EDTA) supplemented with protease and phosphatase inhibitor cocktail (Roche). Protein concentration was determined using BCA assay (Thermo Fisher Scientific). 15 or 30µg of protein from cell or gastrocnemius lysates, respectively, were loaded per well for SDS-PAGE then transferred onto PVDF membranes prior to immunoblotting analysis. Blots were probed with the following primary antibodies: P-Thr172-AMPK (Cell Signaling 2535), Total-AMPK (Cell Signaling 2532), Ferritin (Sigma F5012), IRP2(PA-116544), Transferrin Receptor 1 (Santa Cruz sc65882), NCOA4 (ref) , Vinculin (Cell Signaling 4650). Protein carbonylation was assessed by measuring the levels of carbonyl groups using the OxyBlot protein oxidation detection kit (S7150, Sigma-Aldrich). Quantification analysis of blots was performed with Image Lab software (Biorad).

### **Iron quantification**

Iron content in skeletal muscle was quantified by ICP-MS (Element-2; Thermo-Finnigan, Rodano (MI), Italy) using medium mass resolution ( $M/\Delta M \sim 4,000$ ). 50 to 100mg of freshly

excised and snap-frozen quadriceps were submitted to overnight dialysis. Samples were collected before and after dialysis to assess total and protein-bound iron, respectively. Additionally, iron content was also measured in isolated mitochondria from quadriceps. All samples were digested overnight in 0.5mL of concentrated HNO<sub>3</sub> (70%) and mineralized by microwave heating for 6min at 150°C (Milestone, Ethos Up Microwave Digestion System). A natural abundance iron standard solution was analyzed in parallel in order to check for changes in the systematic bias. The calibration curve was obtained using four iron standard solutions (Sigma-Aldrich) in the range of 0.2–0.005 µg/mL. For liver and spleen iron, samples were heated at 180°C overnight and mineralized in 10mL HCl 3M, 10% trichloroacetic acid per gram of dry tissue overnight at 65°C with gentle shaking. 10µL of supernatants were mixed with a solution of 1.7% of thioglycolic acid (TGA), 84.7% of sodium acetate acetic acid pH 4.5, 13.6% of bathophenanthroline disulfonic acid (BPTS). After 1 hour of incubation at 37°C, absorbance was measured at 535nm. Iron content was determined using a standard curve of ferrous ammonium sulfate.

### **Heme assay**

Heme concentration was determined by fluorescence assay as previously described [121]. Saturated oxalic acid solution was added to 40ug proteins from gastrocnemius lysates prior to heating at 95C for 30min. Samples were loaded in triplicates and fluorescence was measured at 400nm excitation and 662nm emission wavelengths.

### **Mitochondria isolation and metabolic assays**

Mitochondria were isolated from snap-frozen quadriceps by Mitocheck Mitochondrial Isolation kit (Cayman chemical 701010). ATP content was quantified in 20 µg of fresh isolated mitochondria by CellTiter-Glo® Luminescent Cell Viability Assay (Promega G7570). Aconitase activity was measured in quadriceps homogenates by enzymatic assay (Cayman Chemical 705502). Oxygen Consumption Rate (OCR) measurements were conducted using a Seahorse XFe96 analyzer according to manufacturer's protocol. C2C12 cells were directly differentiated in XFe96 cell culture plates were treated with C26 CM alone or in combination with iron for 48h and incubated in 5% CO<sub>2</sub> at 37 °C. One hour prior to analysis, growth medium was replaced with assay medium (DMEM minus phenol red and sodium bicarbonate (Corning, Cat. No. 90-013-PB) that is supplemented with 1 mM pyruvate, 2 mM l-glutamine, and 10 mM glucose, pH 7.4) and incubated in a non-CO<sub>2</sub> incubator. During assay, 1 µM oligomycin (Sigma 495455), 1 µM FCCP (Sigma C2920), and 0.5 µM rotenone/antimycin A (Sigma R8875 and A8674) were sequentially injected into each well in accordance with standard protocols.

Absolute rates (p moles/min) were normalized to  $\mu\text{g}$  of protein determined by Bradford Assay (BioRad 5000006).

## **Histology**

Extracted gastrocnemii were immediately frozen in isopentane cooled in liquid nitrogen and stored at  $-80^{\circ}\text{C}$ . Transversal sections of  $5\mu\text{m}$  thickness were cut at the midbelly with a cryostat. Sections were fixed for 10 minutes in PFA 4%, then blocked with 0.1% triton x-100, 1% BSA in PBS before incubating with primary antibodies against fast/slow isoforms of myosin heavy chain and laminin (Abcam 91506, Abcam M8421, sc-59854), followed by incubation with the corresponding secondary antibodies (Alexa-488, Alexa-568). Pictures were taken with a fluorescent microscope and fiber areas were measured with ImageJ software (more than 500 fibers were analyzed per animal). The enzymatic activity of succinate dehydrogenase (SDH) was measured by Succinate Dehydrogenase Activity Colorimetric Assay Kit (BioVision K660-100).

## **RNA isolation and quantitative PCR**

Total RNA was isolated from snap-frozen tissue samples using TRIzol reagent (Invitrogen) according to the manufacturer's guidelines.  $1\mu\text{g}$  of total RNA was reverse-transcribed using the High Capacity cDNA Reverse Transcriptase kit (Applied Biosystems). cDNA was analyzed by Real Time Quantitative PCR (ABI PRISM 7900HT FAST Real-Time PCR system, Applied Biosystems) using the Luna Universal Probe qPCR master mix (NEB) and the Universal Probe Library system (Roche Applied Science), or with SYBR Green master mix (Applied Biosystems A25741). Relative mRNA levels were calculated using the  $2^{-\Delta\Delta\text{CT}}$  method and normalized to 18S or GAPDH mRNA, respectively. The following primers were used: For human skeletal muscle biopsies, 500 ng of RNA was reverse transcribed using SuperScript IV Reverse Transcriptase (ThermoFisher Scientific). Data were normalized to Actb gene expression.

| Gene       | Forward sequence (5'-3') | Reverse sequence (5'-3') |
|------------|--------------------------|--------------------------|
| Human TFR1 | aggaaccgagctccagtga      | atcaactatgatcaccgagt     |
| Human FPN  | cgagatggatgggtctccta     | accacattttcgacgtagcc     |
| Human ACTB | gggaaatcgtgcgtgaca       | ggactccatgcccagga        |
| mTFR1      | tcctttccttgcatattctgg    | ccaaataaggatagctgcatcc   |
| mFPN       | acccatccccatagtctctgt    | ccgattctagcagcaatgact    |
| mMFRN2     | tgtgtggcgacattacttcat    | gcctcctctgcttgacgact     |
| mALAS2     | ctcaccgtctttggttcgtc     | ggacaggaccgtagcaacat     |
| mFLVCR1A   | ccgtcgcctcgggatgg        | cactaaaacagggtggcaacaaaa |
| mATRO1     | agtgaggaccggctactgtg     | gatcaaacgcttgccaatct     |
| mMURF1     | tgacatctacaagcaggagtgc   | tcgtcttcgtgttcttgc       |
| mREDD1     | ccagagaagagggccttga      | ccatccaggatagaggagtctt   |
| mCPT1B     | aagagaccccgtagccatcat    | gacccaaaacagtatcccaatca  |
| mACOT1     | caactacgatgacctcccca     | gagccattgatgaccacagc     |
| mMCD       | gcacgtccgggaaatgaac      | gcctcacactcgtgatctt      |
| mGAPDH     | aggtcgggtgtgaacggatttg   | tgtagacctgtagttaggtca    |

## RNA-seq data processing and analysis

Following the isolation, the quantity and quality of the starting RNA were checked by Qubit and Bioanalyzer (Agilent). 1 µg of total RNA was subjected to poly(A) selection, and libraries were prepared using the TruSeq RNA Sample Prep Kit (Illumina) following the manufacturer's instructions. Sequencing was performed on the Illumina NextSeq 500 platform. After quality controls with FastQC (<https://www.bioinformatics.babraham.ac.uk/projects/fastqc/>), raw reads were aligned to the NCBI m37 mouse genome reference (mm9) using HiSat2 v2.2.0 [122] with options: `-N 1 -L 20 -i S,1,0.5 -D 25 -R 5 --pen-noncansplice 20 --mp 1,0 --sp 3,0` and providing a list of known splice sites extracted from RefSeq annotated genes (*hisat2\_extract\_splice\_sites.py* script). Gene expression levels were quantified with featureCounts v1.6.1 [123] (options: `-t exon -g gene_name`) using mm9 RefSeq gene annotation. Multi-mapped reads were excluded from quantification. Gene expression counts were next analyzed using the edgeR package [124]. Normalization factors were calculated using the trimmed-mean of M-values (TMM) method (implemented in the *calcNormFactors* function) and RPKM were obtained using normalized library sizes and gene lengths from RefSeq annotation (*rpkm* function). After filtering genes with low expression (1 count per million in less than 2 samples), differential expression analysis was carried out by fitting a Generalized Linear Model (GLM) to all groups and performing Likelihood Ratio Test to compare C26 treatment to the control. Genes with an absolute log<sub>2</sub>-Fold Change greater than 0.5 and False Discovery Rate (FDR) less than or equal to 0.05 were considered as differentially expressed. Hierarchical clustering of gene expression profiles was performed on differentially expressed genes only, using Euclidean distances and the complete linkage method. RPKM values were scaled as Z-scores across samples before computing distances. Gene expression heatmaps

were generated using the *ComplexHeatmap* [125] R package. Gene Ontology analysis and reactome pathways enrichment were performed on <https://tools.dice-database.org/GOnet/> and <http://pantherdb.org/>, respectively.

### **RNA Electrophoretic Mobility Shift Assay (REMSA)**

The fractionation method described by Rothermel *et al.* (2000) [126] was adopted with minor modification to extract the cytosolic protein fractions from the gastrocnemius muscle. Briefly, after removal of connective tissues, muscle was homogenized for 1 minute in ice-cold lysis buffer (25mM Hepes pH 8, 5mM KCl, 0.5mM MgCl, 1% NP-40, 1x protease inhibitors) using a tight-fitting Teflon pestle attached to a Potter S homogeniser (Sartorius Stedium) set to 1,000 rpm. Following centrifugation at 800 *g* for 15 min at 4°C to pellet the nuclei and cell debris, the supernatants were collected, subjected to further centrifugation three times at 500 *g* for 15 min at 4°C to remove residual nuclei and used for the REMSA as nuclei-free total cytosolic protein fractions. The IRP-IRE interactions were performed using LightShift Chemiluminescent RNA Electrophoretic mobility shift assay kit (REMSA, Pierce Biotechnology). Briefly, 20µL of reaction containing nuclease-free water, 5×REMSA Binding Buffer (50mM Tris-HCl pH 8.0, 750mM KCl, 0.5% Triton-X 100, 62.5% glycerol), tRNA (ThermoScientific 20158), 6 µg of muscle cytosolic extracts, biotinylated and unlabeled ferritin probe 5′ – UCCUGCUUCAACAGUGCUUGGACGGAAC – 3′ and where indicated 0.5 mM EDTA and 1 mM DTT, were incubated for 30 min at room temperature. Afterward, the samples were carefully mixed with 5µL of 5×REMSA Loading Buffer and resolved on 6% polyacrylamide gel and transferred on to nylon membrane (Roche Diagnostics, Indianapolis, IN). After the membrane was cross linked with UV-light, the IRP-IRE complexes were visualized by the chemiluminescent nucleic acid detection module (Thermo Scientific 20158).

### **Statistical analysis**

All graphs show mean ± SEM. N represents the total number of independent experiments. Statistical significance was tested as indicated in figure legends.

### III Results

#### **Altered iron metabolism in the skeletal muscle is a feature of cancer-induced cachexia**

Iron deficiency is highly prevalent in cancer patients and has been associated to advanced stage and poor prognosis [92]. To assess the effects of cancer-related iron-deficiency on skeletal muscle metabolism, we analyzed the transcript levels of the main players of iron metabolism in a cohort of cachectic patients presenting anemia defined by decreased hemoglobin levels and hematocrit (**Figures S1A and S1B**). During iron deficiency, cells normally increase iron import through transferrin receptor 1 (TFR1) and decrease efflux by ferroportin (FPN) to maintain homeostasis [127]. Surprisingly, the patients displayed decreased TFR1 and increased FPN levels in skeletal muscle (**Figures 1A and data not shown**). To reproduce cancer cachexia in mice, we used C26-colon cancer model in Balb/c mice, which led to significant total body weight loss and muscle mass reduction (**Figures S1C-E**). Coherently with human data, cachectic mice showed a drastic reduction of TFR1 and a significant increase of FPN in the muscle (**Figures 1B-C and S1F**). TFR1 downregulation was further confirmed in two different murine cachexia models, LLC (Lewis Lung Carcinoma) and BaF3 (murine interleukin 3-dependent pro-B cell line) (**Figures S1G-L**). Iron deprivation in healthy mice by phlebotomy and iron-free diet led to TFR1 mRNA downregulation and muscle wasting (**Figures S1M and S1N**), as in the C26 model.

Next, we measured the protein levels of iron-regulatory protein 2 (IRP2), a RNA-binding protein which is sensitive to iron status and drives post-transcriptional regulation of iron metabolism in mammals [128,129]. We found an upregulation of IRP2 (**Figure 1D**), indicating an iron-deficient state in the skeletal muscle of tumor-bearing mice. Despite the overexpression of IRP2, RNA electrophoretic mobility shift assay (REMSA) in native conditions revealed a lower RNA-binding activity to the iron-responsive element (IRE) site of ferritin in cachectic samples compared to control (**Figures 1E and S1O**). Interestingly, by performing the assay in reducing condition we evidenced the opposite pattern, with cachectic samples presenting a higher IRE-binding, suggesting an oxidative damage [130]. The oxidative stress in skeletal muscle of C26-bearing mice was confirmed by upregulated protein carbonylation (**Figure 1F**) as well as an overexpression of iron storage protein ferritin (FT), which is in line with IRP loss of activity [131] (**Figure 1G**). Coherently, cachectic muscles showed significantly increased protein-chelated iron despite no change in total iron content (**Figures 1H and 1I**). Furthermore, we found decreased mitochondrial iron and total heme content (**Figures 1J and 1K**), upregulated levels of mitochondrial iron importer mitoferrin 2 (MFRN2) and of the rate-limiting enzyme of heme synthesis aminolevulinic acid synthase 2 (ALAS2) (**Figures 1L and 1M**). Remarkably, the increase of ALAS2 expression confirmed impaired IRPs activity [132].

Heme deficiency was further supported by an increased expression of the heme exporter feline leukemia virus subgroup c cellular receptor 1a (FLVCR1a) (**Figure 1N**). Given that iron is essential for several enzymes involved in the TCA cycle and mitochondrial oxidative metabolism (OXPHOS) [133], we assessed the enzymatic activity of two iron-sulfur proteins, aconitase (ACO) and succinate dehydrogenase (SDH), and found, in cachectic muscles, a 50% reduction in the activity of both enzymes (**Figures 1O and 1P**). Along with these alterations, we observed a drop in mitochondrial ATP (**Figure 1Q**) and increased AMPK phosphorylation, denoting mitochondrial dysfunction in cachectic muscles [134] (**Figure 1R**). Interestingly, unlike the skeletal muscle, iron-deprivation increased hepatic TFR1 expression (**Figure S1P**) as expected. Likewise, tumor-bearing mice showed no change in liver TFR1 levels nor in total iron content (**Figures S1Q and S1R**), suggesting organ-specific regulation of iron metabolism during cancer cachexia. In summary, cachectic mice display remarkable alterations in muscle iron metabolism coupled with mitochondrial dysfunction.

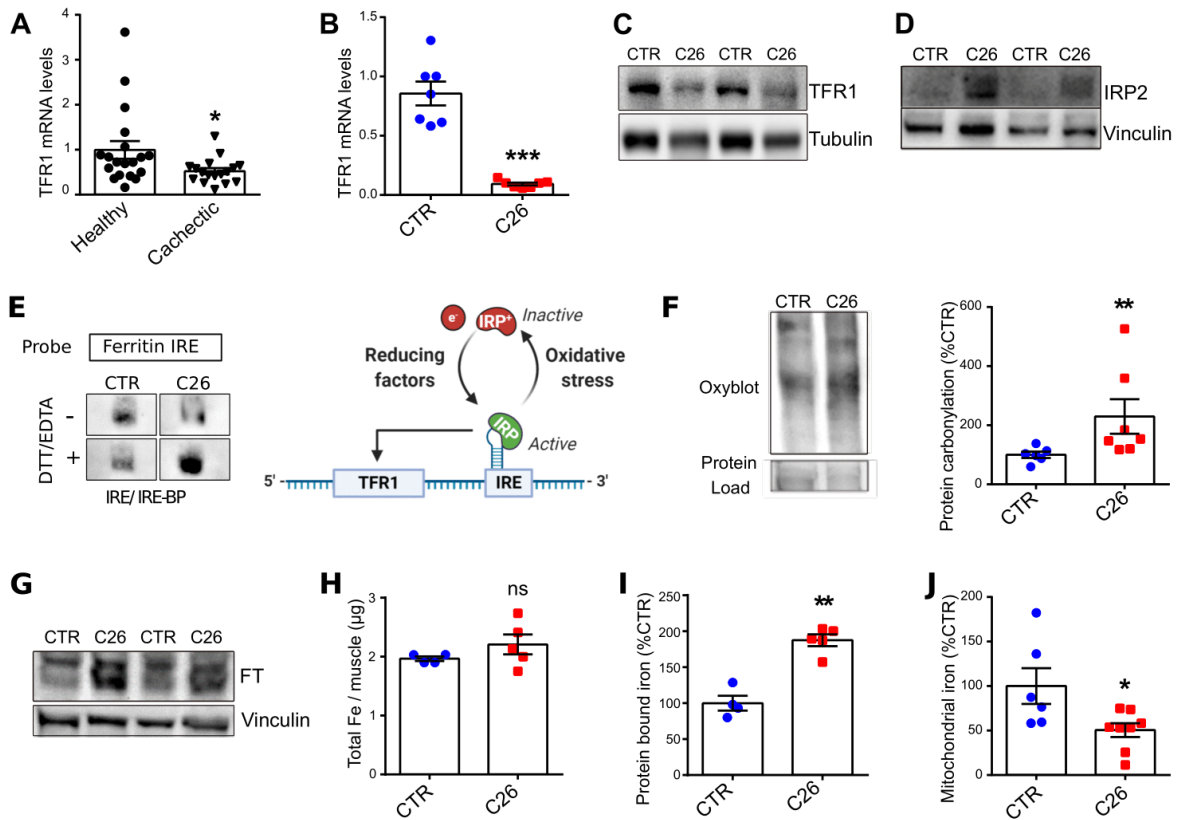


**Figure 1. Altered skeletal muscle iron metabolism is a feature of cachexia**

(A) TFR1 mRNA levels in muscle biopsies from cancer-patients of late stage cachexia (12 healthy subjects, 17 cachectic patients with at least 10% total body weight loss). (B) TFR1 mRNA levels normalized to 18s in mouse gastrocnemius (n=6). (C-D) Representative western blot of TFR1 (C) and IRP2 (D) in mouse gastrocnemius (n=4). (E) Binding of IRE-BPs to the ferritin IRE. The biotin labeled IRE probe was incubated with 6 µg of cytosolic gastrocnemius extracts from mice, in native or reducing conditions (with EDTA 0.5 mM and DTT 1 mM) (n=3). (F) Representative protein carbonylation blot and densitometric quantification in mouse quadriceps (n=6-7). (G) Representative western blot of ferritin H and L in mouse gastrocnemius (n=4) (H-J)



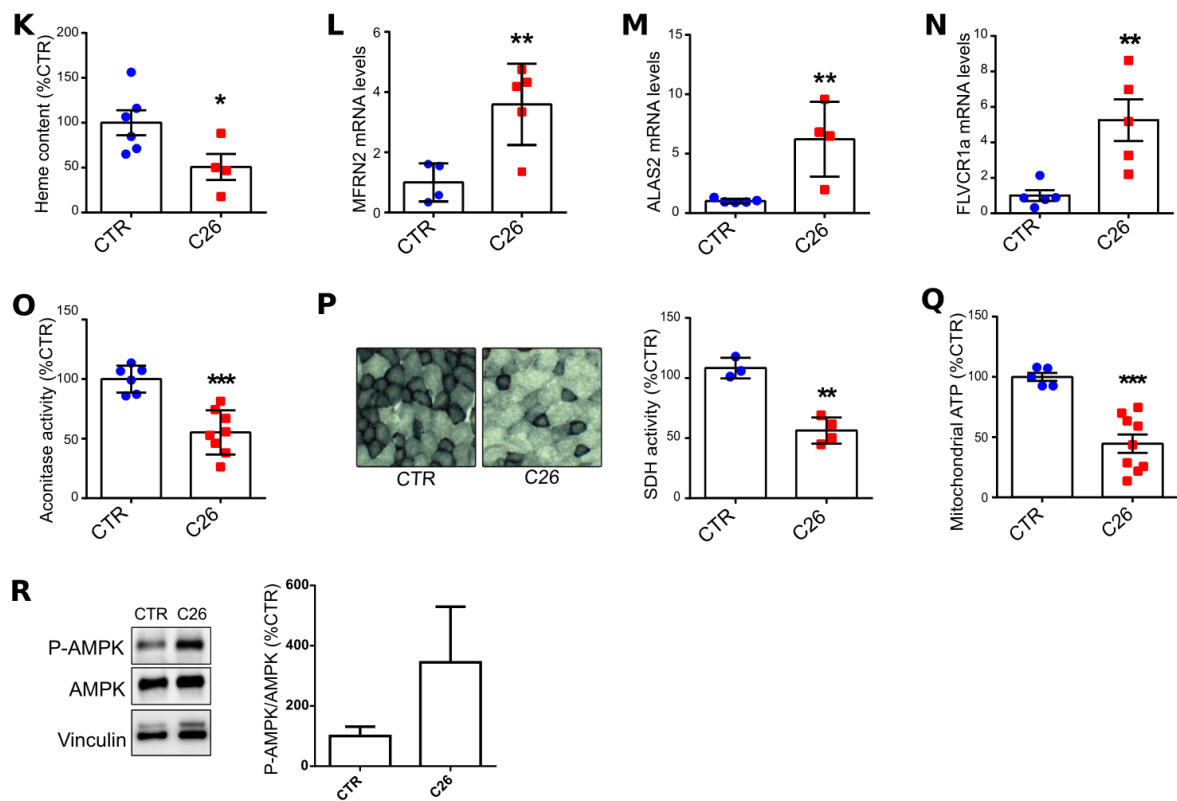


**Figure 1. Altered skeletal muscle iron metabolism is a feature of cachexia**

**(K)** Gastrocnemius heme content quantified by fluorescent heme assay (n=4-6). **(L-N)** mRNA levels of mitochondrial iron importer MFRN2 (L), the rate limiting enzyme of heme synthesis ALAS2 (M) and heme exporter FLVCR1A (N) normalized to 18s in mouse gastrocnemius (n=4-5). **(O)** Aconitase activity of mouse quadriceps lysates normalized to protein content (n=6-7). **(P)** Succinate Dehydrogenase activity staining in transversal sections of mouse gastrocnemius and corresponding intensity quantification (n=3-4). **(Q)** Mitochondrial ATP content in mouse quadriceps (n=5-9). **(R)** Representative western blot and densitometric quantification of phospho-AMPK and total AMPK in mouse gastrocnemius (n=3).

## Iron availability controls myotube size and mitochondrial function

To confirm these observations in a cell-based context amenable to deeper mechanistic studies, we performed RNAseq and GeneOntology (GO) analyses on C2C12 myotubes treated with C26-conditioned medium (C26 CM). Analysis of the transcriptomics results revealed a clear alteration of the transcriptional pattern, particularly affecting genes involved in electron transport chain, iron homeostasis (**Figures 2A and 2B**), and several pathways implicated in muscle functionality (Table S2). Therefore, we sought to assess the impact of iron availability on skeletal muscle cell fitness without other confounding variables such as inflammation. To this aim, we induced iron deprivation in C2C12 myotubes by iron-free iron chelators Desferoxamine (DFO), cell-impermeable bathophenanthroline disulfonic acid (BPS) and TFR1 competitor apotransferrin (Apo-Tf). All the three treatments confirmed what we previously observed with C26 CM treatment, a significant reduction in myotube diameter (Figure 2C). Consistently, iron chelation by DFO displayed the same atrophic effect on human myotubes (Figure 2D). To model the alterations occurring in C26-tumor bearing mice, we knocked down TFR1 in C2C12 myotubes and found a significant myotube atrophy (**Figures 2E and S2A**). To replicate ferritin accumulation in cachectic muscles, we silenced the expression of NCOA4, a cytoplasmic protein that mediates autophagic ferritin degradation, and consequent increase of bioavailable iron [135] ) also led to myotube atrophy (**Figures 2F and S2B**).

Interestingly, normalization of iron levels using the iron-ionophore hinokitiol rescued myotube atrophy induced by TFR1-silencing or C26 CM [136] (**Figures S2C and S2D**). Coherently, ferric citrate supplementation prevented cancer-CM and activin A (ActA) -induced atrophy [31] in murine and/or human myotubes (**Figures 2G-H and S2E-F**). To verify if iron alteration-linked atrophy was associated with mitochondrial metabolic dysfunction, the oxygen consumption rate (OCR) was measured in C2C12 myotubes using Seahorse XFe96 analyzer.. C26 CM treatment affected electron transport chain (ETC) activity which was rescued by iron supplementation (**Figures 2I**). Altogether, these data demonstrate that C26 CM treatment recapitulates the mitochondrial dysfunction observed *in vivo* (**Figures 1O-Q**), which can be fully rescued *in vitro* by iron supplementation.

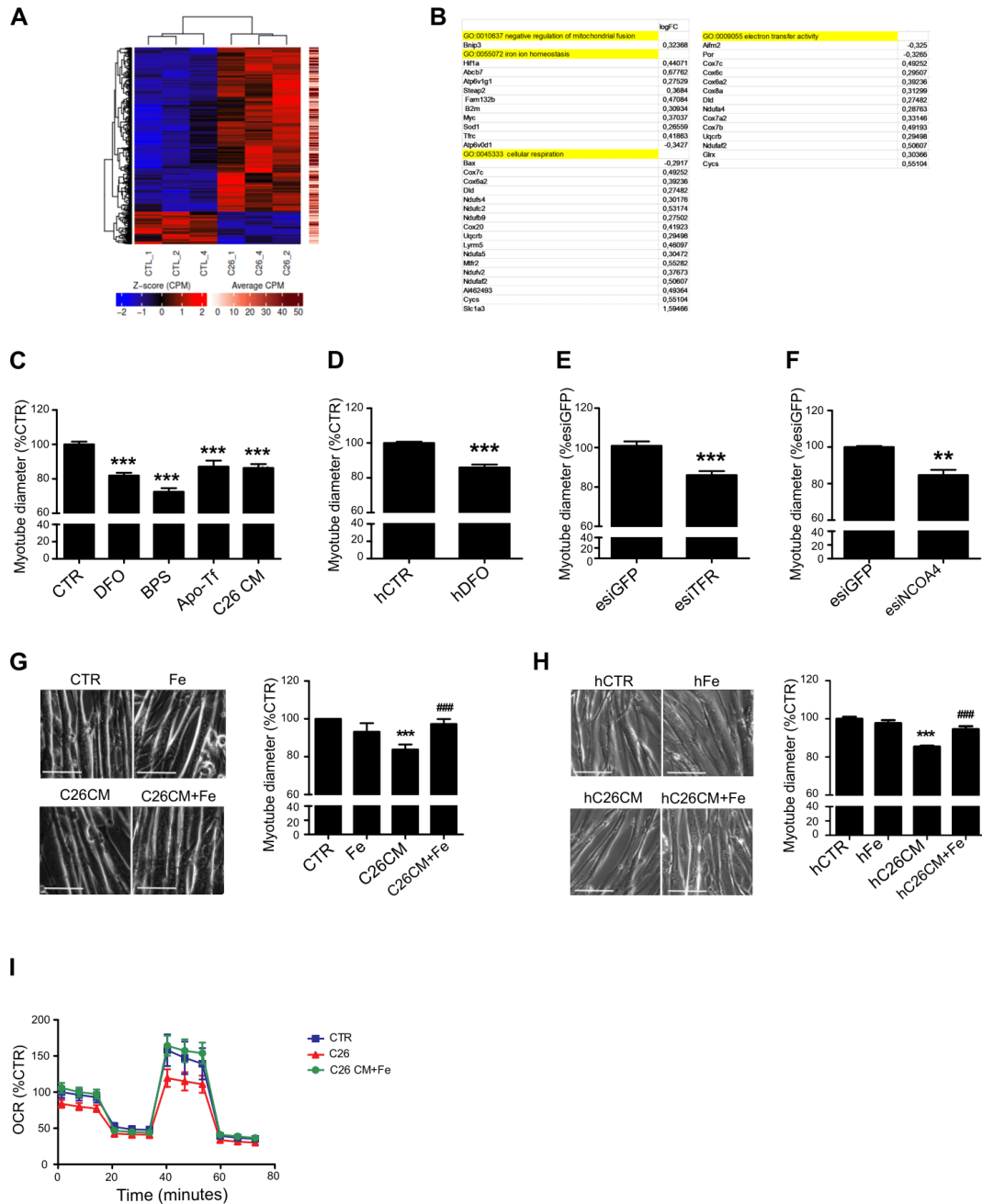


**Figure 2: Iron dependant mitochondrial function controls atrophy**

**(A)** Heatmap from RNA-seq of C26-conditioned medium (C26 CM, 10%) treated C2C12- myotubes. Each column represents a biological replicate and each row represents a gene. Pseudocolors indicate differential expression. Red indicates increased expression, blue indicates decreased expression and average expression levels are shown in black (n=3). **(B)** List of genes involved in iron homeostasis and mitochondrial oxidative metabolism significantly altered in C26 CM-treated C2C12 myotubes (n=3). **(C)** Diameter of C2C12 myotubes after 48h treatment with Desferoxamine 100uM (DFO), bathophenanthroline disulfonate 100uM (BPS), apo-transferrin (Apo-Tf) or C26 CM (n=3-4). **(D)** Diameter of human myoblast-derived myotubes after 48h treatment with DFO 100uM (n=3). **(E-F)** Representative pictures and diameter of TfR1 (E) or NCOA4 (F)-knocked down C2C12 myotubes at day 3 post-transfection (n=3-4). **(G-H)** Representative microscopic pictures and diameter of C2C12 (G) or human myoblast-derived myotubes (H) after 48h treatment with C26 CM and 250nM iron citrate (n=3 per condition). **(I)** Profile of oxygen consumption rate (OCR), in C2C12 myotubes after 48h treatment with C26 CM with ferric citrate supplementation. Data normalized to protein content (n=4-5).

## Iron supplementation counteracts muscle wasting in tumor-bearing mice

Based on these *in vitro* results, we wondered whether iron supplementation could also prevent skeletal muscle atrophy in C26-tumor bearing mice. Remarkably, repeated intravenous injection of iron resulted in healthier (smooth fur, no orbital discharge, no humpback) and more physically active mice that survived beyond the usually fatal two weeks (**Figures 3A-B**). Of note, iron improved the grip strength already from twenty-four hours after injection (**Figure S3A**) and the protection was preserved until the end point of the experiment at Day-12 post-C26 injection (**Figure 3C**).

In addition, the loss of body weight and muscle mass (gastrocnemius and quadriceps) was prevented (**Figures 3D-F**). Consistently, immunostaining for myosin heavy chain and cross-sectional area (CSA) revealed larger muscle fibers in the gastrocnemius of iron-treated mice (fibers involved in the atrophic process are mostly fast-twitch) (**Figures 3G-H and S3C-D**). These findings were further supported by a significant drop of ATRO1, MURF1 and REDD1 mRNA levels, which are indicators of skeletal muscle atrophy (**Figures 3I-K**). Importantly, the healthier status and the improvement of muscle function and mass following iron injection in C26-tumor bearing mice were not associated with changes in primary tumor growth (**Figure S3D**). On the basis of promising results obtained in pre-clinical models of cancer related cachexia, we measured the handgrip force in patients with severe anemia (all but one oncological) who reported muscle weakness, before and after iron injection. In both dominant and non-dominant hands, improved strength was found in most patients (**Figures 4A and 4B**) as short as 3 days after the injection. Together with our data reporting TfR downregulation in the skeletal muscle of cachectic patients (**Figure 1A**), these findings indicate that altered iron metabolism contributes to muscle weakness in cancer patients. All together, these results highlight the contribution of iron on both muscle mass and functionality and suggest a new promising therapeutic strategy to counteract cancer-induced skeletal muscle wasting.

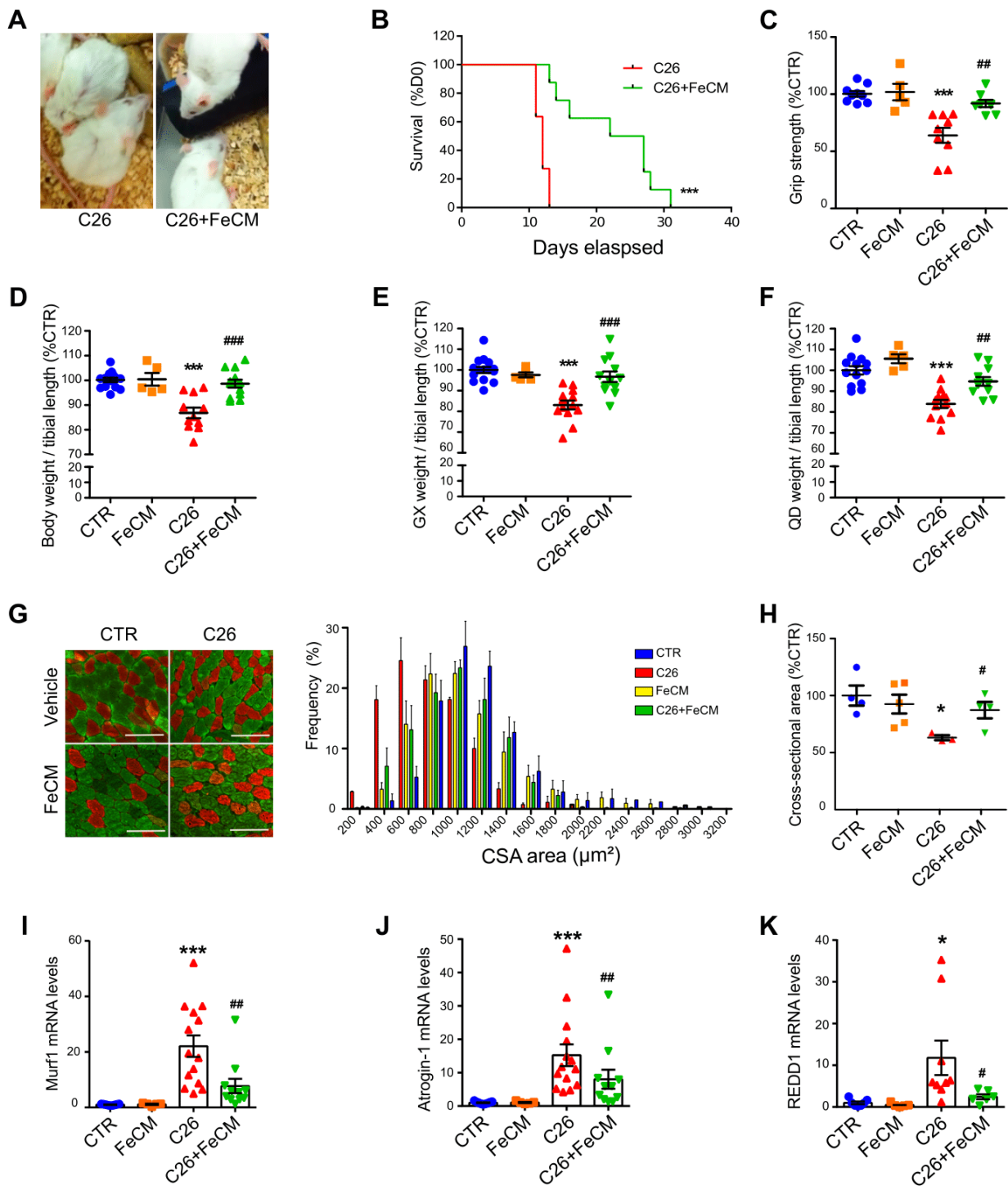


**Figure 3. Iron supplementation prevents cancer-induced cachexia**

(A) Representative photos of C26-tumor bearing mice receiving saline solution (left) or iron carboxymaltose 15mg/kg I.V. injection (right) taken at day 12 after C26 injection (n=3-4). (B) Kaplan-Meier depicting the survival of C26-tumor bearing mice after I.V. injection of saline or iron every 5 days post C26-injection (3-month-old BalbC, n=8-11). (C) Grip strength of mice measured at day 12 post C26 injection, normalized to average strength of the control group (n=5-9). (D-F) Final body weight (D), gastrocnemius weight (E) and quadriceps weight (F) normalized to tibial length of C26-tumor bearing mice after iron supplementation at day 12 post C26 injection (n=5-12). (G-H) Immunofluorescent staining of myosin heavy chain-fast (green) and slow (red) of transversal sections of gastrocnemius (midbelly) with corresponding frequency distribution (G) and average cross-sectional areas (H) (n=3-5). (I-K) mRNA levels of Murf1 (I), Atrogin 1 (H) and REDD1 (I) normalized to GAPDH in gastrocnemius (n=5-14).

## Iron rescues cancer-induced muscle mitochondrial dysfunction *in vivo*

To understand if iron supplementation leads to improved mitochondrial functionality, we next investigated the effects of iron supplementation on mitochondrial metabolism in cachectic mice. After verifying the replenishment of mitochondrial iron (**Figure 4C**), we measured the activity of aconitase and succinate dehydrogenase and observed a significant recovery of enzymatic functionality following iron injection (**Figures 4D and 4E**). In agreement with these *in vivo* results in mice (**Figures 2I and 2L**) showing restored mitochondrial metabolism upon iron treatment, we also found a significant increase in mitochondrial ATP content (**Figures 4F**) and coherently, a drop in AMPK activation (**Figures 4G**). These conditions are indicative of mitigated energetic stress and catabolic pathways. As AMPK drives fatty acid oxidation (FAO), which has been functionally linked to the cachectic process [75], we next evaluated the effect of iron injection on FAO. Consistently, iron supplementation reduced the upregulation of FAO genes (**Figures S4A-C**). All together, these findings show that iron supplementation prevents cancer-induced cachexia through a recovery of mitochondrial function.

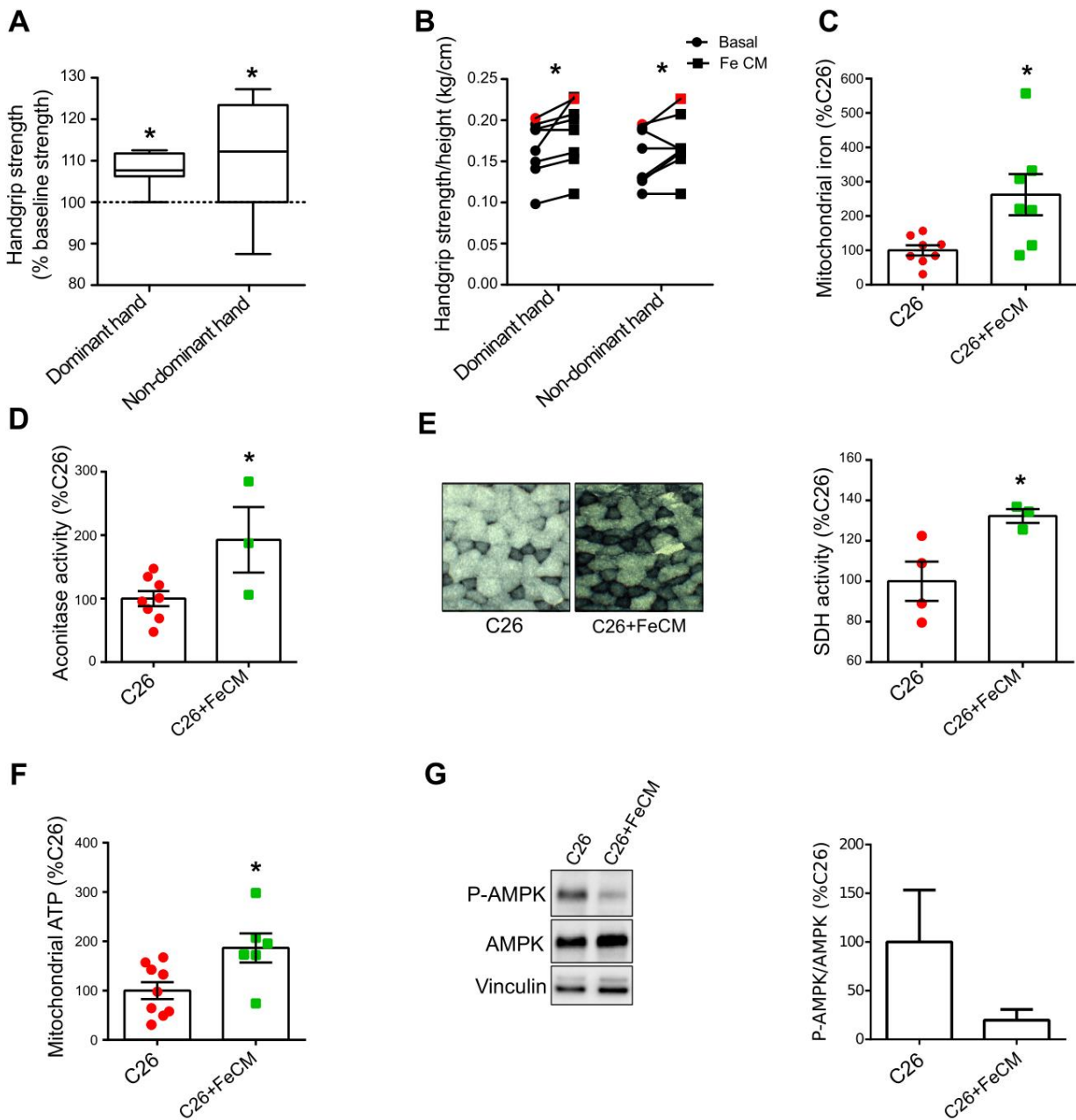


**Figure 4: Iron supplementation rescues mitochondrial function**

(A-B) Grip force of cancer patients and iron-deficient, otherwise healthy patient measured using dominant or non-dominant arm, before and after single dose of iron carboxymaltose 15mg/kg (L). Grip strength of cancer and non-cancer patients after iron injection expressed in percentage of baseline force measured before treatment (M) (8 patients). (C) Mitochondrial iron quantified by ICP-MS in quadriceps of C26-tumor bearing mice after iron carboxymaltose supplementation (n=7-8). (D) Succinate Dehydrogenase activity staining of gastrocnemius transversal sections and resulting intensity quantification (n=3-4). (E) Aconitase activity of quadriceps lysates normalized to protein content (n=3-7). (F) Mitochondrial ATP content determined by luminescence assay in the quadriceps (n=6-9). (G) Representative western blot and densitometric quantification of phospho-AMPK and total AMPK in the gastrocnemius of C26-tumor bearing mice after iron carboxymaltose supplementation (n=3).

## IV Discussion

In this study, we show that iron metabolism controls skeletal muscle homeostasis through the regulation of mitochondrial function. We evidenced striking iron dysregulation associated to cancer-induced muscle wasting that is rescued by iron supplementation. Despite being the biggest tissue in human body, the involvement of skeletal muscle in systemic iron homeostasis has been scarcely investigated. Nevertheless, skeletal muscle holds a substantial pool of iron that can be mobilized, as demonstrated by its ability to support erythropoiesis in healthy humans during high-altitude hypoxia [117]. Since iron-deficiency and anemia are common in cancer patients [92] and are associated with several features of cachexia such as impaired physical function, weakness and fatigue, we hypothesized a link between altered iron metabolism and muscle wasting. We found that both cancer and iron deficiency disrupt iron homeostasis in the skeletal muscle and lead to muscle atrophy in murine models. In both situations, the atrophic muscle paradoxically downregulated the iron importer TFR1 despite the lack of iron, highlighting the role of skeletal muscle as an expendable body compartment. Similarly, we found a consistent decrease of TFR1 in late-stage anemic cancer patients who presented at least 10% body weight loss. Our findings are in line with a previously published muscle-specific TFR1 KO mouse model characterized by muscle atrophy and severe systemic metabolic dysfunction [137]. Intriguingly, skeletal muscle from cachectic mice combines typical hallmarks of iron deficiency (i.e. IRP2 upregulation, decrease in aconitase activity and mitochondrial iron) with the ones of iron overload (i.e. TFR1 downregulation, increase in ferritin, ferroportin and in protein-bound iron). Such discrepancy can be explained by the impaired IRE-IRP system, due to a significant oxidative damage which is reversed by reducing conditions [138,139]. Consequently, cachectic muscles sequester intracellular iron, downregulate its import and increase the export despite the need for iron. This phenotype matches the observations reported in several IRP2 knockout models [113,129,140]. To understand whether the resulting inadequate levels of iron decrease muscle fitness, we focused on the *in vitro* C2C12-myotube model. Importantly, iron deprivation in myotubes induced by TFR1 or NCOA4 knockdown, apotransferrin, DFO, or BPS treatment was sufficient to trigger atrophy, whereas iron normalizing compounds hinokitiol or iron citrate proved to be protective. Thus, we speculated that iron availability directly influences muscle mass. Noteworthy, ferric carboxymaltose (FeCM) is a drug with well-established dosage and tolerability profile, that has been used for the treatment of anemia in patients with iron-deficiency [141]. Cellular uptake of FeCM is mediated by endocytosis, independently of TFR1 [142] which is depleted in the skeletal muscle of tumor-bearing mice. Surprisingly, repeated intravenous administration of



FeCM rescued body mass, muscle mass and function, and even increased the viability of mice. Furthermore, the striking alterations in iron metabolism and loss of muscle functionality could be coupled with mitochondrial dysfunction in tumor-bearing mice. Iron is essential to mitochondrial function [100] as it catalyzes several bioenergetic processes and its deprivation causes impaired mitochondrial biogenesis, enhanced mitophagy, and bioenergetic dysfunction [143-145]. In line with this, we found that reduced mitochondrial iron levels of cachectic mice impairs mitochondrial activity. The oxidative stress generated by dysfunctional mitochondria might reinforce iron dysregulation via IRPs inhibition, creating a vicious cycle. However, iron supplementation does not reconstitute the levels of key players in iron metabolism (such as FTN, data not shown) despite the rescue of muscle mass and function, implying that decreased iron availability is likely the direct cause of atrophy, rather than oxidative stress or impaired IRP. Furthermore, mitochondrial dysfunction is known to trigger catabolic signaling pathways, notably FAO [146] that has been widely associated with skeletal muscle wasting [60,63]. Our results pointed to two major Fe-S proteins of the TCA cycle and electron transport chain that have strongly reduced enzymatic activities, aconitase and SDH, corroborating the decreased oxidative capacities and energetic inefficiency as features of cachexia [69,147]. This confirms and extends early studies showing that iron deficiency decreases Fe-S proteins, cytochrome content, and total oxidative capacity in cancer cachexia [102,148]. Mitochondrial bioenergetics alone might not be sufficient to explain the wasting phenotype observed in our models, as fast-twitch fibers would be spared from mitochondria failure, but still represents a key point for muscle homeostasis preservation. Our data indicate that adequate iron supply restores mitochondrial function, as reflected by ATP production increase, AMPK deactivation and FAO reduction.

Although we found that iron supplementation can restore muscle mass homeostasis, we do not exclude other systemic effects of iron repletion, which might contribute to the better health and survival of tumor-bearing mice. For instance, it is known that iron availability can influence systemic metabolism by affecting liver [149] and adipose tissue function [150]. Nevertheless, we can rule out the influence by primary tumor growth since it is not affected, and Prussian blue staining revealed iron deposit mostly in immune cells (data not shown). As reported previously, iron loading in tumor-associated macrophages can polarize them towards a pro-inflammatory, anti-tumoral phenotype [151]. Of note, the beneficial effects of iron injection in vivo were unexpectedly fast as muscle strength was improved within 24 hours, hence the rescue is unlikely due to muscle stem cell differentiation/regeneration or erythropoiesis. Consistent with these findings, preliminary data from iron-deficient patients demonstrated an improvement of handgrip strength within few days after iron treatment, excluding the potential

involvement of erythropoiesis. However, further studies will be essential to better define the impact of short-term iron treatment on these patients.

In conclusion, our findings establish a direct role of iron availability in the control of skeletal muscle mass. Therefore, iron supplementation restores skeletal muscle homeostasis via mitochondrial metabolism normalization, paving the way to a new therapeutic strategy to fight muscle atrophy in cachectic patients, including those who are affected by non-cancer conditions but presenting iron deficiency, as co-morbidity such as COPD and chronic cardiac failure.

## Acknowledgments

We thank Dr. Sara Petrillo and Prof. Emanuela Tolosano for helpful discussion. VR is supported by FIRC, EH(LeDuq Grant). This work is supported by a MyFirstAircGrant by AIRC (PEP; MFAG Grant #21564).

## V References chapter 2

1. Wyart, E.; Bindels, L.B.; Mina, E.; Menga, A.; Stanga, S.; Porporato, P.E. Cachexia, a Systemic Disease beyond Muscle Atrophy. *Int J Mol Sci* **2020**, *21*, doi:10.3390/ijms21228592.
2. Fearon, K.; Strasser, F.; Anker, S.D.; Bosaeus, I.; Bruera, E.; Fainsinger, R.L.; Jatoi, A.; Loprinzi, C.; MacDonald, N.; Mantovani, G., et al. Definition and classification of cancer cachexia: an international consensus. *Lancet Oncol* **2011**, *12*, 489-495, doi:10.1016/S1470-2045(10)70218-7.
3. Wallengren, O.; Lundholm, K.; Bosaeus, I. Diagnostic criteria of cancer cachexia: relation to quality of life, exercise capacity and survival in unselected palliative care patients. *Support Care Cancer* **2013**, *21*, 1569-1577, doi:10.1007/s00520-012-1697-z.
4. Utech, A.E.; Tadros, E.M.; Hayes, T.G.; Garcia, J.M. Predicting survival in cancer patients: the role of cachexia and hormonal, nutritional and inflammatory markers. *J Cachexia Sarcopenia Muscle* **2012**, *3*, 245-251, doi:10.1007/s13539-012-0075-5.
5. Baracos, V.E. Pitfalls in defining and quantifying cachexia. *J Cachexia Sarcopenia Muscle* **2011**, *2*, 71-73, doi:10.1007/s13539-011-0031-9.
6. Warren, S. The Immediate Causes of Death in Cancer. *The American Journal of the Medical Sciences* **1932**, *184*, 610-615, doi:10.1097/00000441-193211000-00002.
7. Togni, V.; Ota, C.C.; Folador, A.; Junior, O.T.; Aikawa, J.; Yamazaki, R.K.; Freitas, F.A.; Longo, R.; Martins, E.F.; Calder, P.C., et al. Cancer cachexia and tumor growth reduction in Walker 256 tumor-bearing rats supplemented with N-3 polyunsaturated fatty acids for one generation. *Nutr Cancer* **2003**, *46*, 52-58, doi:10.1207/S15327914NC4601\_07.
8. de Fatima Silva, F.; Ortiz-Silva, M.; de Souza Galia, W.B.; Cassolla, P.; Graciano, M.F.; Zaia, C.T.; Zaia, D.; Carpinelli, A.R.; da Silva, F.G.; de Souza, H.M. Pioglitazone improves insulin sensitivity and reduces weight loss in Walker-256 tumor-bearing rats. *Life Sci* **2017**, *171*, 68-74, doi:10.1016/j.lfs.2016.12.016.

9. Busquets, S.; Figueras, M.T.; Fuster, G.; Almendro, V.; Moore-Carrasco, R.; Ametller, E.; Argiles, J.M.; Lopez-Soriano, F.J. Anticachectic effects of formoterol: a drug for potential treatment of muscle wasting. *Cancer Res* **2004**, *64*, 6725-6731, doi:10.1158/0008-5472.CAN-04-0425.
10. Bonetto, A.; Rupert, J.E.; Barreto, R.; Zimmers, T.A. The Colon-26 Carcinoma Tumor-bearing Mouse as a Model for the Study of Cancer Cachexia. *J Vis Exp* **2016**, 10.3791/54893, doi:10.3791/54893.
11. Llovera, M.; Garcia-Martinez, C.; Lopez-Soriano, J.; Agell, N.; Lopez-Soriano, F.J.; Garcia, I.; Argiles, J.M. Protein turnover in skeletal muscle of tumour-bearing transgenic mice overexpressing the soluble TNF receptor-1. *Cancer Lett* **1998**, *130*, 19-27, doi:10.1016/s0304-3835(98)00137-2.
12. VanderVeen, B.N.; Hardee, J.P.; Fix, D.K.; Carson, J.A. Skeletal muscle function during the progression of cancer cachexia in the male Apc(Min/+) mouse. *J Appl Physiol (1985)* **2018**, *124*, 684-695, doi:10.1152/jappphysiol.00897.2017.
13. Talbert, E.E.; Cuitino, M.C.; Ladner, K.J.; Rajasekera, P.V.; Siebert, M.; Shakya, R.; Leone, G.W.; Ostrowski, M.C.; Paleo, B.; Weisleder, N., et al. Modeling Human Cancer-induced Cachexia. *Cell Rep* **2019**, *28*, 1612-1622 e1614, doi:10.1016/j.celrep.2019.07.016.
14. Norton, J.A.; Moley, J.F.; Green, M.V.; Carson, R.E.; Morrison, S.D. Parabolic transfer of cancer anorexia/cachexia in male rats. *Cancer Res* **1985**, *45*, 5547-5552.
15. Ni, X.; Yang, J.; Li, M. Imaging-guided curative surgical resection of pancreatic cancer in a xenograft mouse model. *Cancer Lett* **2012**, *324*, 179-185, doi:10.1016/j.canlet.2012.05.013.
16. Smith, K.L.; Tisdale, M.J. Increased protein degradation and decreased protein synthesis in skeletal muscle during cancer cachexia. *Br J Cancer* **1993**, *67*, 680-685, doi:10.1038/bjc.1993.126.
17. Sandri, M. Protein breakdown in cancer cachexia. *Semin Cell Dev Biol* **2016**, *54*, 11-19, doi:10.1016/j.semcdb.2015.11.002.
18. Penna, F.; Costamagna, D.; Pin, F.; Camperi, A.; Fanzani, A.; Chiarpotto, E.M.; Cavallini, G.; Bonelli, G.; Baccino, F.M.; Costelli, P. Autophagic degradation contributes to muscle wasting in cancer cachexia. *Am J Pathol* **2013**, *182*, 1367-1378, doi:10.1016/j.ajpath.2012.12.023.
19. Glass, D.J. PI3 kinase regulation of skeletal muscle hypertrophy and atrophy. *Curr Top Microbiol Immunol* **2010**, *346*, 267-278, doi:10.1007/82\_2010\_78.
20. Llovera, M.; Garcia-Martinez, C.; Lopez-Soriano, J.; Carbo, N.; Agell, N.; Lopez-Soriano, F.J.; Argiles, J.M. Role of TNF receptor 1 in protein turnover during cancer cachexia using gene knockout mice. *Mol Cell Endocrinol* **1998**, *142*, 183-189, doi:10.1016/s0303-7207(98)00105-1.
21. Dogra, C.; Changotra, H.; Wedhas, N.; Qin, X.; Wergedal, J.E.; Kumar, A. TNF-related weak inducer of apoptosis (TWEAK) is a potent skeletal muscle-wasting cytokine. *FASEB J* **2007**, *21*, 1857-1869, doi:10.1096/fj.06-7537com.
22. Guttridge, D.C.; Mayo, M.W.; Madrid, L.V.; Wang, C.Y.; Baldwin, A.S., Jr. NF-kappaB-induced loss of MyoD messenger RNA: possible role in muscle decay and cachexia. *Science* **2000**, *289*, 2363-2366, doi:10.1126/science.289.5488.2363.
23. Scott, H.R.; McMillan, D.C.; Crilly, A.; McArdle, C.S.; Milroy, R. The relationship between weight loss and interleukin 6 in non-small-cell lung cancer. *Br J Cancer* **1996**, *73*, 1560-1562, doi:10.1038/bjc.1996.294.
24. Moses, A.G.; Maingay, J.; Sangster, K.; Fearon, K.C.; Ross, J.A. Pro-inflammatory cytokine release by peripheral blood mononuclear cells from patients with advanced pancreatic cancer: relationship to acute phase response and survival. *Oncol Rep* **2009**, *21*, 1091-1095, doi:10.3892/or\_00000328.
25. White, J.P.; Puppa, M.J.; Gao, S.; Sato, S.; Welle, S.L.; Carson, J.A. Muscle mTORC1 suppression by IL-6 during cancer cachexia: a role for AMPK. *Am J Physiol Endocrinol Metab* **2013**, *304*, E1042-1052, doi:10.1152/ajpendo.00410.2012.
26. Goodman, M.N. Interleukin-6 induces skeletal muscle protein breakdown in rats. *Proc Soc Exp Biol Med* **1994**, *205*, 182-185, doi:10.3181/00379727-205-43695.

27. Bonetto, A.; Aydogdu, T.; Jin, X.; Zhang, Z.; Zhan, R.; Puzis, L.; Koniaris, L.G.; Zimmers, T.A. JAK/STAT3 pathway inhibition blocks skeletal muscle wasting downstream of IL-6 and in experimental cancer cachexia. *Am J Physiol Endocrinol Metab* **2012**, *303*, E410-421, doi:10.1152/ajpendo.00039.2012.
28. Kandarian, S.C.; Nosacka, R.L.; Delitto, A.E.; Judge, A.R.; Judge, S.M.; Ganey, J.D.; Moreira, J.D.; Jackman, R.W. Tumour-derived leukaemia inhibitory factor is a major driver of cancer cachexia and morbidity in C26 tumour-bearing mice. *J Cachexia Sarcopenia Muscle* **2018**, *9*, 1109-1120, doi:10.1002/jcsm.12346.
29. Loumaye, A.; de Barsy, M.; Nachit, M.; Lause, P.; Frateur, L.; van Maanen, A.; Trefois, P.; Gruson, D.; Thissen, J.P. Role of Activin A and myostatin in human cancer cachexia. *J Clin Endocrinol Metab* **2015**, *100*, 2030-2038, doi:10.1210/jc.2014-4318.
30. Chen, J.L.; Walton, K.L.; Winbanks, C.E.; Murphy, K.T.; Thomson, R.E.; Makanji, Y.; Qian, H.; Lynch, G.S.; Harrison, C.A.; Gregorevic, P. Elevated expression of activins promotes muscle wasting and cachexia. *FASEB J* **2014**, *28*, 1711-1723, doi:10.1096/fj.13-245894.
31. Zhou, X.; Wang, J.L.; Lu, J.; Song, Y.; Kwak, K.S.; Jiao, Q.; Rosenfeld, R.; Chen, Q.; Boone, T.; Simonet, W.S., et al. Reversal of cancer cachexia and muscle wasting by ActRIIB antagonism leads to prolonged survival. *Cell* **2010**, *142*, 531-543, doi:10.1016/j.cell.2010.07.011.
32. Jones, J.E.; Cadena, S.M.; Gong, C.; Wang, X.; Chen, Z.; Wang, S.X.; Vickers, C.; Chen, H.; Lach-Trifilieff, E.; Hadcock, J.R., et al. Supraphysiologic Administration of GDF11 Induces Cachexia in Part by Upregulating GDF15. *Cell Rep* **2018**, *22*, 1522-1530, doi:10.1016/j.celrep.2018.01.044.
33. Zhang, G.; Liu, Z.; Ding, H.; Zhou, Y.; Doan, H.A.; Sin, K.W.T.; Zhu, Z.J.; Flores, R.; Wen, Y.; Gong, X., et al. Tumor induces muscle wasting in mice through releasing extracellular Hsp70 and Hsp90. *Nat Commun* **2017**, *8*, 589, doi:10.1038/s41467-017-00726-x.
34. Kim, J.; Won, K.J.; Lee, H.M.; Hwang, B.Y.; Bae, Y.M.; Choi, W.S.; Song, H.; Lim, K.W.; Lee, C.K.; Kim, B. p38 MAPK Participates in Muscle-Specific RING Finger 1-Mediated Atrophy in Cast-Immobilized Rat Gastrocnemius Muscle. *Korean J Physiol Pharmacol* **2009**, *13*, 491-496, doi:10.4196/kjpp.2009.13.6.491.
35. Calore, F.; Londhe, P.; Fadda, P.; Nigita, G.; Casadei, L.; Marceca, G.P.; Fassan, M.; Lovat, F.; Gasparini, P.; Rizzotto, L., et al. The TLR7/8/9 Antagonist IMO-8503 Inhibits Cancer-Induced Cachexia. *Cancer Res* **2018**, *78*, 6680-6690, doi:10.1158/0008-5472.CAN-17-3878.
36. Yeh, S.S.; Blackwood, K.; Schuster, M.W. The cytokine basis of cachexia and its treatment: are they ready for prime time? *J Am Med Dir Assoc* **2008**, *9*, 219-236, doi:10.1016/j.jamda.2008.01.003.
37. Penna, F.; Minero, V.G.; Costamagna, D.; Bonelli, G.; Baccino, F.M.; Costelli, P. Anti-cytokine strategies for the treatment of cancer-related anorexia and cachexia. *Expert Opin Biol Ther* **2010**, *10*, 1241-1250, doi:10.1517/14712598.2010.503773.
38. Dodesini, A.R.; Benedini, S.; Terruzzi, I.; Sereni, L.P.; Luzi, L. Protein, glucose and lipid metabolism in the cancer cachexia: A preliminary report. *Acta Oncol* **2007**, *46*, 118-120, doi:10.1080/02841860600791491.
39. Vazelle, C.; Jouinot, A.; Durand, J.P.; Neveux, N.; Boudou-Rouquette, P.; Huillard, O.; Alexandre, J.; Cynober, L.; Goldwasser, F. Relation between hypermetabolism, cachexia, and survival in cancer patients: a prospective study in 390 cancer patients before initiation of anticancer therapy. *Am J Clin Nutr* **2017**, *105*, 1139-1147, doi:10.3945/ajcn.116.140434.
40. Kliewer, K.L.; Ke, J.Y.; Tian, M.; Cole, R.M.; Andridge, R.R.; Belury, M.A. Adipose tissue lipolysis and energy metabolism in early cancer cachexia in mice. *Cancer Biol Ther* **2015**, *16*, 886-897, doi:10.4161/15384047.2014.987075.
41. Das, S.K.; Eder, S.; Schauer, S.; Diwoky, C.; Temmel, H.; Guertl, B.; Gorkiewicz, G.; Tamilarasan, K.P.; Kumari, P.; Trauner, M., et al. Adipose triglyceride lipase contributes to cancer-associated cachexia. *Science* **2011**, *333*, 233-238, doi:10.1126/science.1198973.
42. Petruzzelli, M.; Schweiger, M.; Schreiber, R.; Campos-Olivas, R.; Tsoli, M.; Allen, J.; Swarbrick, M.; Rose-John, S.; Rincon, M.; Robertson, G., et al. A switch from white to brown fat

- increases energy expenditure in cancer-associated cachexia. *Cell Metab* **2014**, *20*, 433-447, doi:10.1016/j.cmet.2014.06.011.
43. Kir, S.; White, J.P.; Kleiner, S.; Kazak, L.; Cohen, P.; Baracos, V.E.; Spiegelman, B.M. Tumour-derived PTH-related protein triggers adipose tissue browning and cancer cachexia. *Nature* **2014**, *513*, 100-104, doi:10.1038/nature13528.
  44. Vander Heiden, M.G.; Cantley, L.C.; Thompson, C.B. Understanding the Warburg effect: the metabolic requirements of cell proliferation. *Science* **2009**, *324*, 1029-1033, doi:10.1126/science.1160809.
  45. Khamoui, A.V.; Tokmina-Roszyk, D.; Rossiter, H.B.; Fields, G.B.; Visavadiya, N.P. Hepatic proteome analysis reveals altered mitochondrial metabolism and suppressed acyl-CoA synthetase-1 in colon-26 tumor-induced cachexia. *Physiol Genomics* **2020**, *52*, 203-216, doi:10.1152/physiolgenomics.00124.2019.
  46. Ishikawa, E. The regulation of uptake and output of amino acids by rat tissues. *Adv Enzyme Regul* **1976**, *14*, 117-136, doi:10.1016/0065-2571(76)90010-8.
  47. Goncalves, M.D.; Hwang, S.K.; Pauli, C.; Murphy, C.J.; Cheng, Z.; Hopkins, B.D.; Wu, D.; Loughran, R.M.; Emerling, B.M.; Zhang, G., et al. Fenofibrate prevents skeletal muscle loss in mice with lung cancer. *Proc Natl Acad Sci U S A* **2018**, *115*, E743-E752, doi:10.1073/pnas.1714703115.
  48. Halle, J.L.; Pena, G.S.; Paez, H.G.; Castro, A.J.; Rossiter, H.B.; Visavadiya, N.P.; Whitehurst, M.A.; Khamoui, A.V. Tissue-specific dysregulation of mitochondrial respiratory capacity and coupling control in colon-26 tumor-induced cachexia. *Am J Physiol Regul Integr Comp Physiol* **2019**, *317*, R68-R82, doi:10.1152/ajpregu.00028.2019.
  49. Bonetto, A.; Aydogdu, T.; Kunzevitzky, N.; Guttridge, D.C.; Khuri, S.; Koniaris, L.G.; Zimmers, T.A. STAT3 activation in skeletal muscle links muscle wasting and the acute phase response in cancer cachexia. *PLoS One* **2011**, *6*, e22538, doi:10.1371/journal.pone.0022538.
  50. Flint, T.R.; Janowitz, T.; Connell, C.M.; Roberts, E.W.; Denton, A.E.; Coll, A.P.; Jodrell, D.I.; Fearon, D.T. Tumor-Induced IL-6 Reprograms Host Metabolism to Suppress Anti-tumor Immunity. *Cell Metab* **2016**, *24*, 672-684, doi:10.1016/j.cmet.2016.10.010.
  51. Shimizu, N.; Yoshikawa, N.; Ito, N.; Maruyama, T.; Suzuki, Y.; Takeda, S.; Nakae, J.; Tagata, Y.; Nishitani, S.; Takehana, K., et al. Crosstalk between glucocorticoid receptor and nutritional sensor mTOR in skeletal muscle. *Cell Metab* **2011**, *13*, 170-182, doi:10.1016/j.cmet.2011.01.001.
  52. Honors, M.A.; Kinzig, K.P. The role of insulin resistance in the development of muscle wasting during cancer cachexia. *J Cachexia Sarcopenia Muscle* **2012**, *3*, 5-11, doi:10.1007/s13539-011-0051-5.
  53. Wang, X.; Hu, Z.; Hu, J.; Du, J.; Mitch, W.E. Insulin resistance accelerates muscle protein degradation: Activation of the ubiquitin-proteasome pathway by defects in muscle cell signaling. *Endocrinology* **2006**, *147*, 4160-4168, doi:10.1210/en.2006-0251.
  54. Asp, M.L.; Tian, M.; Wendel, A.A.; Belury, M.A. Evidence for the contribution of insulin resistance to the development of cachexia in tumor-bearing mice. *Int J Cancer* **2010**, *126*, 756-763, doi:10.1002/ijc.24784.
  55. Fernandes, L.C.; Machado, U.F.; Nogueira, C.R.; Carpinelli, A.R.; Curi, R. Insulin secretion in Walker 256 tumor cachexia. *Am J Physiol* **1990**, *258*, E1033-1036, doi:10.1152/ajpendo.1990.258.6.E1033.
  56. Figueroa-Clarevega, A.; Bilder, D. Malignant Drosophila tumors interrupt insulin signaling to induce cachexia-like wasting. *Dev Cell* **2015**, *33*, 47-55, doi:10.1016/j.devcel.2015.03.001.
  57. Asp, M.L.; Tian, M.; Kliewer, K.L.; Belury, M.A. Rosiglitazone delayed weight loss and anorexia while attenuating adipose depletion in mice with cancer cachexia. *Cancer Biol Ther* **2011**, *12*, 957-965, doi:10.4161/cbt.12.11.18134.
  58. Trobec, K.; Palus, S.; Tschirner, A.; von Haehling, S.; Doehner, W.; Lainscak, M.; Anker, S.D.; Springer, J. Rosiglitazone reduces body wasting and improves survival in a rat model of cancer cachexia. *Nutrition* **2014**, *30*, 1069-1075, doi:10.1016/j.nut.2013.12.005.

59. VanderVeen, B.N.; Fix, D.K.; Carson, J.A. Disrupted Skeletal Muscle Mitochondrial Dynamics, Mitophagy, and Biogenesis during Cancer Cachexia: A Role for Inflammation. *Oxid Med Cell Longev* **2017**, *2017*, 3292087, doi:10.1155/2017/3292087.
60. Brown, J.L.; Rosa-Caldwell, M.E.; Lee, D.E.; Blackwell, T.A.; Brown, L.A.; Perry, R.A.; Haynie, W.S.; Hardee, J.P.; Carson, J.A.; Wiggs, M.P., et al. Mitochondrial degeneration precedes the development of muscle atrophy in progression of cancer cachexia in tumour-bearing mice. *J Cachexia Sarcopenia Muscle* **2017**, *8*, 926-938, doi:10.1002/jcsm.12232.
61. Argiles, J.M.; Lopez-Soriano, F.J.; Busquets, S. Muscle wasting in cancer: the role of mitochondria. *Curr Opin Clin Nutr Metab Care* **2015**, *18*, 221-225, doi:10.1097/MCO.000000000000164.
62. Hyatt, H.; Deminice, R.; Yoshihara, T.; Powers, S.K. Mitochondrial dysfunction induces muscle atrophy during prolonged inactivity: A review of the causes and effects. *Arch Biochem Biophys* **2019**, *662*, 49-60, doi:10.1016/j.abb.2018.11.005.
63. Abrigo, J.; Simon, F.; Cabrera, D.; Vilos, C.; Cabello-Verrugio, C. Mitochondrial Dysfunction in Skeletal Muscle Pathologies. *Curr Protein Pept Sci* **2019**, *20*, 536-546, doi:10.2174/1389203720666190402100902.
64. White, J.P.; Puppa, M.J.; Sato, S.; Gao, S.; Price, R.L.; Baynes, J.W.; Kostek, M.C.; Matesic, L.E.; Carson, J.A. IL-6 regulation on skeletal muscle mitochondrial remodeling during cancer cachexia in the ApcMin/+ mouse. *Skelet Muscle* **2012**, *2*, 14, doi:10.1186/2044-5040-2-14.
65. Romanello, V.; Guadagnin, E.; Gomes, L.; Roder, I.; Sandri, C.; Petersen, Y.; Milan, G.; Masiero, E.; Del Piccolo, P.; Foretz, M., et al. Mitochondrial fission and remodelling contributes to muscle atrophy. *EMBO J* **2010**, *29*, 1774-1785, doi:10.1038/emboj.2010.60.
66. Penna, F.; Ballaro, R.; Martinez-Cristobal, P.; Sala, D.; Sebastian, D.; Busquets, S.; Muscaritoli, M.; Argiles, J.M.; Costelli, P.; Zorzano, A. Autophagy Exacerbates Muscle Wasting in Cancer Cachexia and Impairs Mitochondrial Function. *J Mol Biol* **2019**, *431*, 2674-2686, doi:10.1016/j.jmb.2019.05.032.
67. Hardee, J.P.; Counts, B.R.; Gao, S.; VanderVeen, B.N.; Fix, D.K.; Koh, H.J.; Carson, J.A. Inflammatory signalling regulates eccentric contraction-induced protein synthesis in cachectic skeletal muscle. *J Cachexia Sarcopenia Muscle* **2018**, *9*, 369-383, doi:10.1002/jcsm.12271.
68. Sun, R.; Zhang, S.; Hu, W.; Lu, X.; Lou, N.; Yang, Z.; Chen, S.; Zhang, X.; Yang, H. Valproic acid attenuates skeletal muscle wasting by inhibiting C/EBPbeta-regulated atrogen1 expression in cancer cachexia. *Am J Physiol Cell Physiol* **2016**, *311*, C101-115, doi:10.1152/ajpcell.00344.2015.
69. Neyroud, D.; Nosacka, R.L.; Judge, A.R.; Hepple, R.T. Colon 26 adenocarcinoma (C26)-induced cancer cachexia impairs skeletal muscle mitochondrial function and content. *J Muscle Res Cell Motil* **2019**, *40*, 59-65, doi:10.1007/s10974-019-09510-4.
70. Antunes, D.; Padrao, A.I.; Maciel, E.; Santinha, D.; Oliveira, P.; Vitorino, R.; Moreira-Goncalves, D.; Colaco, B.; Pires, M.J.; Nunes, C., et al. Molecular insights into mitochondrial dysfunction in cancer-related muscle wasting. *Biochim Biophys Acta* **2014**, *1841*, 896-905, doi:10.1016/j.bbalip.2014.03.004.
71. Padrao, A.I.; Oliveira, P.; Vitorino, R.; Colaco, B.; Pires, M.J.; Marquez, M.; Castellanos, E.; Neuparth, M.J.; Teixeira, C.; Costa, C., et al. Bladder cancer-induced skeletal muscle wasting: disclosing the role of mitochondria plasticity. *Int J Biochem Cell Biol* **2013**, *45*, 1399-1409, doi:10.1016/j.biocel.2013.04.014.
72. Busquets, S.; Almendro, V.; Barreiro, E.; Figueras, M.; Argiles, J.M.; Lopez-Soriano, F.J. Activation of UCPs gene expression in skeletal muscle can be independent on both circulating fatty acids and food intake. Involvement of ROS in a model of mouse cancer cachexia. *FEBS Lett* **2005**, *579*, 717-722, doi:10.1016/j.febslet.2004.12.050.
73. Tzika, A.A.; Fontes-Oliveira, C.C.; Shestov, A.A.; Constantinou, C.; Psychogios, N.; Righi, V.; Mintzopoulos, D.; Busquets, S.; Lopez-Soriano, F.J.; Milot, S., et al. Skeletal muscle

- mitochondrial uncoupling in a murine cancer cachexia model. *Int J Oncol* **2013**, *43*, 886-894, doi:10.3892/ijo.2013.1998.
74. Schrauwen, P.; Hesselink, M. UCP2 and UCP3 in muscle controlling body metabolism. *J Exp Biol* **2002**, *205*, 2275-2285.
  75. Fukawa, T.; Yan-Jiang, B.C.; Min-Wen, J.C.; Jun-Hao, E.T.; Huang, D.; Qian, C.N.; Ong, P.; Li, Z.; Chen, S.; Mak, S.Y., et al. Excessive fatty acid oxidation induces muscle atrophy in cancer cachexia. *Nat Med* **2016**, *22*, 666-671, doi:10.1038/nm.4093.
  76. Xiao, Y.; Karam, C.; Yi, J.; Zhang, L.; Li, X.; Yoon, D.; Wang, H.; Dhakal, K.; Ramlow, P.; Yu, T., et al. ROS-related mitochondrial dysfunction in skeletal muscle of an ALS mouse model during the disease progression. *Pharmacol Res* **2018**, *138*, 25-36, doi:10.1016/j.phrs.2018.09.008.
  77. Ward, C.W.; Prosser, B.L.; Lederer, W.J. Mechanical stretch-induced activation of ROS/RNS signaling in striated muscle. *Antioxid Redox Signal* **2014**, *20*, 929-936, doi:10.1089/ars.2013.5517.
  78. Schieber, M.; Chandel, N.S. ROS function in redox signaling and oxidative stress. *Curr Biol* **2014**, *24*, R453-462, doi:10.1016/j.cub.2014.03.034.
  79. Li, Y.P.; Chen, Y.; Li, A.S.; Reid, M.B. Hydrogen peroxide stimulates ubiquitin-conjugating activity and expression of genes for specific E2 and E3 proteins in skeletal muscle myotubes. *Am J Physiol Cell Physiol* **2003**, *285*, C806-812, doi:10.1152/ajpcell.00129.2003.
  80. Powers, S.K.; Talbert, E.E.; Adihetty, P.J. Reactive oxygen and nitrogen species as intracellular signals in skeletal muscle. *J Physiol* **2011**, *589*, 2129-2138, doi:10.1113/jphysiol.2010.201327.
  81. Abrigo, J.; Elorza, A.A.; Riedel, C.A.; Vilos, C.; Simon, F.; Cabrera, D.; Estrada, L.; Cabello-Verrugio, C. Role of Oxidative Stress as Key Regulator of Muscle Wasting during Cachexia. *Oxid Med Cell Longev* **2018**, *2018*, 2063179, doi:10.1155/2018/2063179.
  82. Irrcher, I.; Ljubicic, V.; Hood, D.A. Interactions between ROS and AMP kinase activity in the regulation of PGC-1 $\alpha$  transcription in skeletal muscle cells. *Am J Physiol Cell Physiol* **2009**, *296*, C116-123, doi:10.1152/ajpcell.00267.2007.
  83. Hardie, D.G.; Ross, F.A.; Hawley, S.A. AMPK: a nutrient and energy sensor that maintains energy homeostasis. *Nat Rev Mol Cell Biol* **2012**, *13*, 251-262, doi:10.1038/nrm3311.
  84. Bergeron, R.; Ren, J.M.; Cadman, K.S.; Moore, I.K.; Perret, P.; Pypaert, M.; Young, L.H.; Semenkovich, C.F.; Shulman, G.I. Chronic activation of AMP kinase results in NRF-1 activation and mitochondrial biogenesis. *Am J Physiol Endocrinol Metab* **2001**, *281*, E1340-1346, doi:10.1152/ajpendo.2001.281.6.E1340.
  85. Hall, D.T.; Griss, T.; Ma, J.F.; Sanchez, B.J.; Sadek, J.; Tremblay, A.M.K.; Mubaid, S.; Omer, A.; Ford, R.J.; Bedard, N., et al. The AMPK agonist 5-aminoimidazole-4-carboxamide ribonucleotide (AICAR), but not metformin, prevents inflammation-associated cachectic muscle wasting. *EMBO Mol Med* **2018**, *10*, doi:10.15252/emmm.201708307.
  86. Thomson, D.M. The Role of AMPK in the Regulation of Skeletal Muscle Size, Hypertrophy, and Regeneration. *Int J Mol Sci* **2018**, *19*, doi:10.3390/ijms19103125.
  87. Winterbourn, C.C. Toxicity of iron and hydrogen peroxide: the Fenton reaction. *Toxicol Lett* **1995**, *82-83*, 969-974, doi:10.1016/0378-4274(95)03532-x.
  88. Recalcati, S.; Gammella, E.; Buratti, P.; Cairo, G. Molecular regulation of cellular iron balance. *IUBMB Life* **2017**, *69*, 389-398, doi:10.1002/iub.1628.
  89. Pantopoulos, K. Iron metabolism and the IRE/IRP regulatory system: an update. *Ann N Y Acad Sci* **2004**, *1012*, 1-13, doi:10.1196/annals.1306.001.
  90. Volz, K. The functional duality of iron regulatory protein 1. *Curr Opin Struct Biol* **2008**, *18*, 106-111, doi:10.1016/j.sbi.2007.12.010.
  91. Takahashi-Makise, N.; Ward, D.M.; Kaplan, J. On the mechanism of iron sensing by IRP2: new players, new paradigms. *Nat Chem Biol* **2009**, *5*, 874-875, doi:10.1038/nchembio.261.
  92. Ludwig, H.; Muldur, E.; Endler, G.; Hubl, W. Prevalence of iron deficiency across different tumors and its association with poor performance status, disease status and anemia. *Ann Oncol* **2013**, *24*, 1886-1892, doi:10.1093/annonc/mdt118.

93. Ludwig, H.; Van Belle, S.; Barrett-Lee, P.; Birgegard, G.; Bokemeyer, C.; Gascon, P.; Kosmidis, P.; Krzakowski, M.; Nortier, J.; Olmi, P., et al. The European Cancer Anaemia Survey (ECAS): a large, multinational, prospective survey defining the prevalence, incidence, and treatment of anaemia in cancer patients. *Eur J Cancer* **2004**, *40*, 2293-2306, doi:10.1016/j.ejca.2004.06.019.
94. Caro, J.J.; Salas, M.; Ward, A.; Goss, G. Anemia as an independent prognostic factor for survival in patients with cancer: a systemic, quantitative review. *Cancer* **2001**, *91*, 2214-2221.
95. Ludwig, H.; Evstatiev, R.; Kornek, G.; Aapro, M.; Bauernhofer, T.; Buxhofer-Ausch, V.; Fridrik, M.; Geissler, D.; Geissler, K.; Gisslinger, H., et al. Iron metabolism and iron supplementation in cancer patients. *Wien Klin Wochenschr* **2015**, *127*, 907-919, doi:10.1007/s00508-015-0842-3.
96. Grotto, H.Z. Anaemia of cancer: an overview of mechanisms involved in its pathogenesis. *Med Oncol* **2008**, *25*, 12-21, doi:10.1007/s12032-007-9000-8.
97. Torti, S.V.; Manz, D.H.; Paul, B.T.; Blanchette-Farra, N.; Torti, F.M. Iron and Cancer. *Annu Rev Nutr* **2018**, *38*, 97-125, doi:10.1146/annurev-nutr-082117-051732.
98. Zurlo, F.; Larson, K.; Bogardus, C.; Ravussin, E. Skeletal muscle metabolism is a major determinant of resting energy expenditure. *J Clin Invest* **1990**, *86*, 1423-1427, doi:10.1172/JCI114857.
99. Westerblad, H.; Bruton, J.D.; Katz, A. Skeletal muscle: energy metabolism, fiber types, fatigue and adaptability. *Exp Cell Res* **2010**, *316*, 3093-3099, doi:10.1016/j.yexcr.2010.05.019.
100. Levi, S.; Rovida, E. The role of iron in mitochondrial function. *Biochim Biophys Acta* **2009**, *1790*, 629-636, doi:10.1016/j.bbagen.2008.09.008.
101. Cartier, L.J.; Ohira, Y.; Chen, M.; Cuddihy, R.W.; Holloszy, J.O. Perturbation of mitochondrial composition in muscle by iron deficiency. Implications regarding regulation of mitochondrial assembly. *J Biol Chem* **1986**, *261*, 13827-13832.
102. Oexle, H.; Gnaiger, E.; Weiss, G. Iron-dependent changes in cellular energy metabolism: influence on citric acid cycle and oxidative phosphorylation. *Biochim Biophys Acta* **1999**, *1413*, 99-107, doi:10.1016/s0005-2728(99)00088-2.
103. Merrill, J.F.; Thomson, D.M.; Hardman, S.E.; Hepworth, S.D.; Willie, S.; Hancock, C.R. Iron deficiency causes a shift in AMP-activated protein kinase (AMPK) subunit composition in rat skeletal muscle. *Nutr Metab (Lond)* **2012**, *9*, 104, doi:10.1186/1743-7075-9-104.
104. Janssen, I.; Heymsfield, S.B.; Wang, Z.M.; Ross, R. Skeletal muscle mass and distribution in 468 men and women aged 18-88 yr. *J Appl Physiol (1985)* **2000**, *89*, 81-88, doi:10.1152/jappl.2000.89.1.81.
105. von Haehling, S.; Anker, M.S.; Anker, S.D. Prevalence and clinical impact of cachexia in chronic illness in Europe, USA, and Japan: facts and numbers update 2016. *J Cachexia Sarcopenia Muscle* **2016**, *7*, 507-509, doi:10.1002/jcsm.12167.
106. Porporato, P.E. Understanding cachexia as a cancer metabolism syndrome. *Oncogenesis* **2016**, *5*, e200, doi:10.1038/oncsis.2016.3.
107. Tisdale, M.J. Cachexia in cancer patients. *Nat Rev Cancer* **2002**, *2*, 862-871, doi:10.1038/nrc927.
108. Torti, S.V.; Torti, F.M. Iron and cancer: more ore to be mined. *Nat Rev Cancer* **2013**, *13*, 342-355, doi:10.1038/nrc3495.
109. Rouault, T.A. Biogenesis of iron-sulfur clusters in mammalian cells: new insights and relevance to human disease. *Dis Model Mech* **2012**, *5*, 155-164, doi:10.1242/dmm.009019.
110. Chiabrando, D.; Vinchi, F.; Fiorito, V.; Mercurio, S.; Tolosano, E. Heme in pathophysiology: a matter of scavenging, metabolism and trafficking across cell membranes. *Front Pharmacol* **2014**, *5*, 61, doi:10.3389/fphar.2014.00061.
111. Paul, B.T.; Manz, D.H.; Torti, F.M.; Torti, S.V. Mitochondria and Iron: current questions. *Expert Rev Hematol* **2017**, *10*, 65-79, doi:10.1080/17474086.2016.1268047.

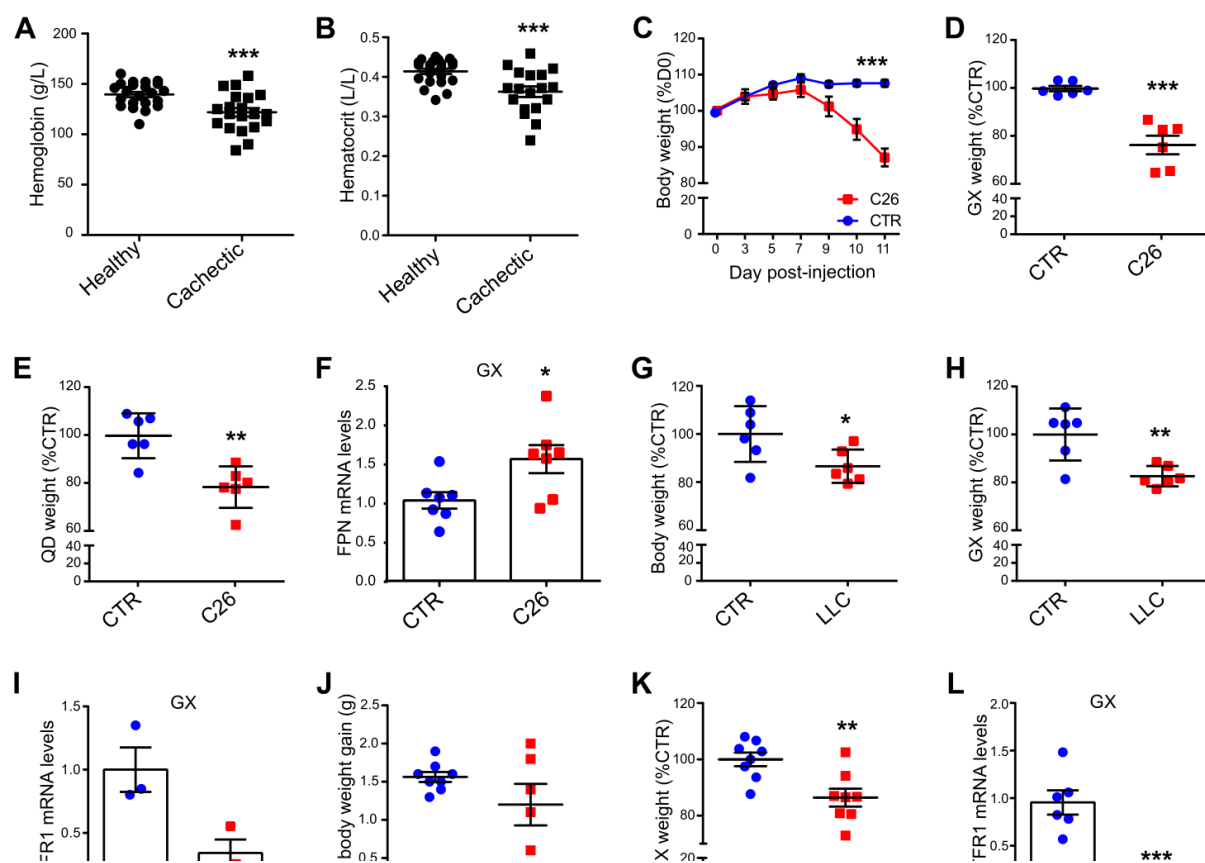


112. Rensvold, J.W.; Ong, S.E.; Jeevananthan, A.; Carr, S.A.; Mootha, V.K.; Pagliarini, D.J. Complementary RNA and protein profiling identifies iron as a key regulator of mitochondrial biogenesis. *Cell Rep* **2013**, *3*, 237-245, doi:10.1016/j.celrep.2012.11.029.
113. Galy, B.; Ferring-Appel, D.; Sauer, S.W.; Kaden, S.; Lyoumi, S.; Puy, H.; Kolker, S.; Grone, H.J.; Hentze, M.W. Iron regulatory proteins secure mitochondrial iron sufficiency and function. *Cell Metab* **2010**, *12*, 194-201, doi:10.1016/j.cmet.2010.06.007.
114. Boengler, K.; Kosiol, M.; Mayr, M.; Schulz, R.; Rohrbach, S. Mitochondria and ageing: role in heart, skeletal muscle and adipose tissue. *J Cachexia Sarcopenia Muscle* **2017**, *8*, 349-369, doi:10.1002/jcsm.12178.
115. Vitorino, R.; Moreira-Goncalves, D.; Ferreira, R. Mitochondrial plasticity in cancer-related muscle wasting: potential approaches for its management. *Curr Opin Clin Nutr Metab Care* **2015**, *18*, 226-233, doi:10.1097/MCO.000000000000161.
116. Sylven, C.; Jansson, E.; Book, K. Myoglobin content in human skeletal muscle and myocardium: relation to fibre size and oxidative capacity. *Cardiovasc Res* **1984**, *18*, 443-446, doi:10.1093/cvr/18.7.443.
117. Robach, P.; Cairo, G.; Gelfi, C.; Bernuzzi, F.; Pilegaard, H.; Viganò, A.; Santambrogio, P.; Cerretelli, P.; Calbet, J.A.; Moutereau, S., et al. Strong iron demand during hypoxia-induced erythropoiesis is associated with down-regulation of iron-related proteins and myoglobin in human skeletal muscle. *Blood* **2007**, *109*, 4724-4731, doi:10.1182/blood-2006-08-040006.
118. Bindels, L.B.; Beck, R.; Schakman, O.; Martin, J.C.; De Backer, F.; Sohet, F.M.; Dewulf, E.M.; Pachikian, B.D.; Neyrinck, A.M.; Thissen, J.P., et al. Restoring specific lactobacilli levels decreases inflammation and muscle atrophy markers in an acute leukemia mouse model. *PLoS One* **2012**, *7*, e37971, doi:10.1371/journal.pone.0037971.
119. Wyart, E.; Reano, S.; Hsu, M.Y.; Longo, D.L.; Li, M.; Hirsch, E.; Filigheddu, N.; Ghigo, A.; Riganti, C.; Porporato, P.E. Metabolic Alterations in a Slow-Paced Model of Pancreatic Cancer-Induced Wasting. *Oxid Med Cell Longev* **2018**, *2018*, 6419805, doi:10.1155/2018/6419805.
120. Murata, A.; Amaya, K.; Mochizuki, K.; Sotokawa, M.; Otaka, S.; Tani, K.; Nakagaki, S.; Ueda, T. Superior Mesenteric Artery-Pancreaticoduodenal Arcade Bypass Grafting for Repair of Inferior Pancreaticoduodenal Artery Aneurysm with Celiac Axis Occlusion. *Ann Vasc Dis* **2018**, *11*, 153-157, doi:10.3400/avd.cr.17-00113.
121. Sinclair, P.R.; Gorman, N.; Jacobs, J.M. Measurement of heme concentration. *Curr Protoc Toxicol* **2001**, *Chapter 8*, Unit 8 3, doi:10.1002/0471140856.tx0803s00.
122. Kim, D.; Paggi, J.M.; Park, C.; Bennett, C.; Salzberg, S.L. Graph-based genome alignment and genotyping with HISAT2 and HISAT-genotype. *Nat Biotechnol* **2019**, *37*, 907-915, doi:10.1038/s41587-019-0201-4.
123. Liao, Y.; Smyth, G.K.; Shi, W. featureCounts: an efficient general purpose program for assigning sequence reads to genomic features. *Bioinformatics* **2014**, *30*, 923-930, doi:10.1093/bioinformatics/btt656.
124. Robinson, M.D.; McCarthy, D.J.; Smyth, G.K. edgeR: a Bioconductor package for differential expression analysis of digital gene expression data. *Bioinformatics* **2010**, *26*, 139-140, doi:10.1093/bioinformatics/btp616.
125. Gu, Z.; Eils, R.; Schlesner, M. Complex heatmaps reveal patterns and correlations in multidimensional genomic data. *Bioinformatics* **2016**, *32*, 2847-2849, doi:10.1093/bioinformatics/btw313.
126. Rothermel, B.; Vega, R.B.; Yang, J.; Wu, H.; Bassel-Duby, R.; Williams, R.S. A protein encoded within the Down syndrome critical region is enriched in striated muscles and inhibits calcineurin signaling. *J Biol Chem* **2000**, *275*, 8719-8725, doi:10.1074/jbc.275.12.8719.
127. Camaschella, C.; Nai, A.; Silvestri, L. Iron metabolism and iron disorders revisited in the hepcidin era. *Haematologica* **2020**, *105*, 260-272, doi:10.3324/haematol.2019.232124.

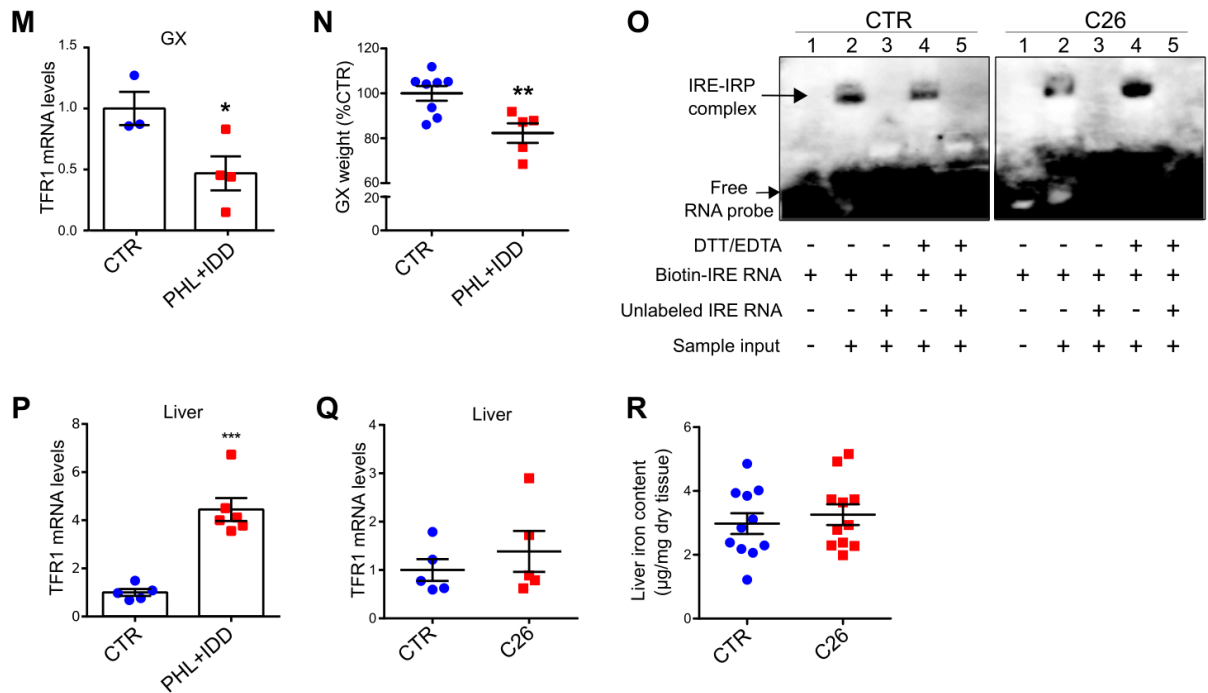
128. Wang, H.; Shi, H.; Rajan, M.; Canarie, E.R.; Hong, S.; Simoneschi, D.; Pagano, M.; Bush, M.F.; Stoll, S.; Leibold, E.A., et al. FBXL5 Regulates IRP2 Stability in Iron Homeostasis via an Oxygen-Responsive [2Fe2S] Cluster. *Mol Cell* **2020**, *78*, 31-41 e35, doi:10.1016/j.molcel.2020.02.011.
129. Meyron-Holtz, E.G.; Ghosh, M.C.; Iwai, K.; LaVaute, T.; Brazzolotto, X.; Berger, U.V.; Land, W.; Ollivierre-Wilson, H.; Grinberg, A.; Love, P., et al. Genetic ablations of iron regulatory proteins 1 and 2 reveal why iron regulatory protein 2 dominates iron homeostasis. *EMBO J* **2004**, *23*, 386-395, doi:10.1038/sj.emboj.7600041.
130. Gehring, N.H.; Hentze, M.W.; Pantopoulos, K. Inactivation of both RNA binding and aconitase activities of iron regulatory protein-1 by quinone-induced oxidative stress. *J Biol Chem* **1999**, *274*, 6219-6225, doi:10.1074/jbc.274.10.6219.
131. Cairo, G.; Tacchini, L.; Recalcati, S.; Azzimonti, B.; Minotti, G.; Bernelli-Zazzera, A. Effect of reactive oxygen species on iron regulatory protein activity. *Ann N Y Acad Sci* **1998**, *851*, 179-186, doi:10.1111/j.1749-6632.1998.tb08992.x.
132. Barman-Aksozen, J.; Halloy, F.; Iyer, P.S.; Schumperli, D.; Minder, A.E.; Hall, J.; Minder, E.I.; Schneider-Yin, X. Delta-aminolevulinic acid synthase 2 expression in combination with iron as modifiers of disease severity in erythropoietic protoporphyria. *Mol Genet Metab* **2019**, *128*, 304-308, doi:10.1016/j.ymgme.2019.04.013.
133. Xu, W.; Barrientos, T.; Andrews, N.C. Iron and copper in mitochondrial diseases. *Cell Metab* **2013**, *17*, 319-328, doi:10.1016/j.cmet.2013.02.004.
134. Zhao, B.; Qiang, L.; Joseph, J.; Kalyanaraman, B.; Viollet, B.; He, Y.Y. Mitochondrial dysfunction activates the AMPK signaling and autophagy to promote cell survival. *Genes Dis* **2016**, *3*, 82-87, doi:10.1016/j.gendis.2015.12.002.
135. Bellelli, R.; Federico, G.; Matte, A.; Colecchia, D.; Iolascon, A.; Chiariello, M.; Santoro, M.; De Franceschi, L.; Carlomagno, F. NCOA4 Deficiency Impairs Systemic Iron Homeostasis. *Cell Rep* **2016**, *14*, 411-421, doi:10.1016/j.celrep.2015.12.065.
136. Grillo, A.S.; SantaMaria, A.M.; Kafina, M.D.; Cioffi, A.G.; Huston, N.C.; Han, M.; Seo, Y.A.; Yien, Y.Y.; Nardone, C.; Menon, A.V., et al. Restored iron transport by a small molecule promotes absorption and hemoglobinization in animals. *Science* **2017**, *356*, 608-616, doi:10.1126/science.aah3862.
137. Barrientos, T.; Laothamatas, I.; Koves, T.R.; Soderblom, E.J.; Bryan, M.; Moseley, M.A.; Muoio, D.M.; Andrews, N.C. Metabolic Catastrophe in Mice Lacking Transferrin Receptor in Muscle. *EBioMedicine* **2015**, *2*, 1705-1717, doi:10.1016/j.ebiom.2015.09.041.
138. Cairo, G.; Castrusini, E.; Minotti, G.; Bernelli-Zazzera, A. Superoxide and hydrogen peroxide-dependent inhibition of iron regulatory protein activity: a protective stratagem against oxidative injury. *FASEB J* **1996**, *10*, 1326-1335, doi:10.1096/fasebj.10.11.8836047.
139. Mikhael, M.; Kim, S.F.; Schranzhofer, M.; Soe-Lin, S.; Sheftel, A.D.; Mullner, E.W.; Ponka, P. Iron regulatory protein-independent regulation of ferritin synthesis by nitrogen monoxide. *FEBS J* **2006**, *273*, 3828-3836, doi:10.1111/j.1742-4658.2006.05390.x.
140. Li, H.; Zhao, H.; Hao, S.; Shang, L.; Wu, J.; Song, C.; Meyron-Holtz, E.G.; Qiao, T.; Li, K. Iron regulatory protein deficiency compromises mitochondrial function in murine embryonic fibroblasts. *Sci Rep* **2018**, *8*, 5118, doi:10.1038/s41598-018-23175-y.
141. Scott, L.J. Ferric Carboxymaltose: A Review in Iron Deficiency. *Drugs* **2018**, *78*, 479-493, doi:10.1007/s40265-018-0885-7.
142. Marone, G.; Poto, S.; Giugliano, R.; Celestino, D.; Bonini, S. Control mechanisms of human basophil releasability. *J Allergy Clin Immunol* **1986**, *78*, 974-980, doi:10.1016/0091-6749(86)90288-5.
143. Rensvold, J.W.; Krautkramer, K.A.; Dowell, J.A.; Denu, J.M.; Pagliarini, D.J. Iron Deprivation Induces Transcriptional Regulation of Mitochondrial Biogenesis. *J Biol Chem* **2016**, *291*, 20827-20837, doi:10.1074/jbc.M116.727701.
144. Allen, G.F.; Toth, R.; James, J.; Ganley, I.G. Loss of iron triggers PINK1/Parkin-independent mitophagy. *EMBO Rep* **2013**, *14*, 1127-1135, doi:10.1038/embor.2013.168.

145. Bastian, T.W.; von Hohenberg, W.C.; Georgieff, M.K.; Lanier, L.M. Chronic Energy Depletion due to Iron Deficiency Impairs Dendritic Mitochondrial Motility during Hippocampal Neuron Development. *J Neurosci* **2019**, *39*, 802-813, doi:10.1523/JNEUROSCI.1504-18.2018.
146. Romanello, V.; Sandri, M. Mitochondrial Quality Control and Muscle Mass Maintenance. *Front Physiol* **2015**, *6*, 422, doi:10.3389/fphys.2015.00422.
147. Argiles, J.M.; Fontes-Oliveira, C.C.; Toledo, M.; Lopez-Soriano, F.J.; Busquets, S. Cachexia: a problem of energetic inefficiency. *J Cachexia Sarcopenia Muscle* **2014**, *5*, 279-286, doi:10.1007/s13539-014-0154-x.
148. Maguire, J.J.; Davies, K.J.; Dallman, P.R.; Packer, L. Effects of dietary iron deficiency of iron-sulfur proteins and bioenergetic functions of skeletal muscle mitochondria. *Biochim Biophys Acta* **1982**, *679*, 210-220, doi:10.1016/0005-2728(82)90292-4.
149. Klempa, K.L.; Willis, W.T.; Chengson, R.; Dallman, P.R.; Brooks, G.A. Iron deficiency decreases gluconeogenesis in isolated rat hepatocytes. *J Appl Physiol (1985)* **1989**, *67*, 1868-1872, doi:10.1152/jappl.1989.67.5.1868.
150. Gao, Y.; Li, Z.; Gabrielsen, J.S.; Simcox, J.A.; Lee, S.H.; Jones, D.; Cooksey, B.; Stoddard, G.; Cefalu, W.T.; McClain, D.A. Adipocyte iron regulates leptin and food intake. *J Clin Invest* **2015**, *125*, 3681-3691, doi:10.1172/JCI81860.
151. Serra, M.; Columbano, A.; Ammarah, U.; Mazzone, M.; Menga, A. Understanding Metal Dynamics Between Cancer Cells and Macrophages: Competition or Synergism? *Front Oncol* **2020**, *10*, 646, doi:10.3389/fonc.2020.00646.

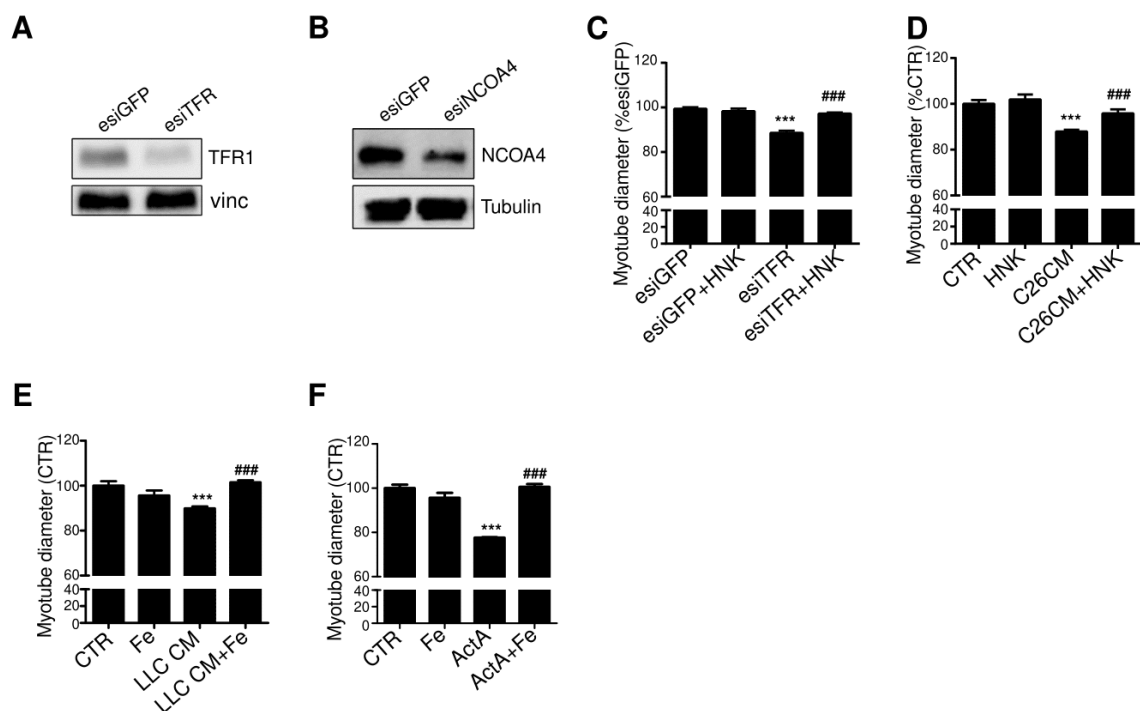
## VI Supplementary Material



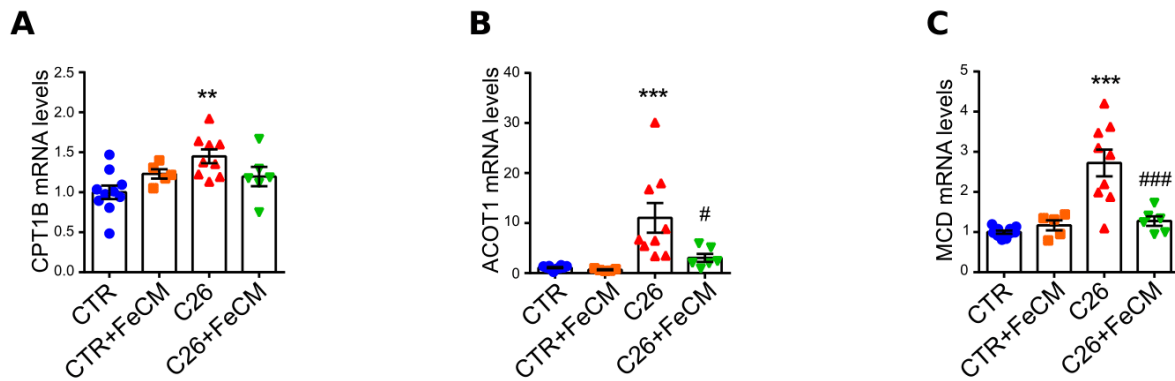
**Supplementary figure 1.** (A-B) Hemoglobin (A) and hematocrit (B) levels of healthy subjects and cachectic cancer patients presenting a body weight loss superior to 10% of initial body weight (n=12-17). (C) Body weight evolution of mice after C26-injection (n=5-6). (D-E) Gastrocnemius (D) and quadriceps (E) weights of C26 tumor-bearing mice at day 12 (n=4-6). (F) FPN1 mRNA levels normalized to 18s in gastrocnemius of C26-tumor bearing mice (n=6). (G-H) Total body weight and gastrocnemius weight in LLC-tumor bearing mice (n=5-6). (I) TFR1 mRNA levels normalized to 18s in the gastrocnemius of LLC-tumor bearing mice (n=3). (J-K) Total body weight gain and gastrocnemius weight of BaF-transplanted mice (n=6-8). (L) TFR1 mRNA levels normalized to 18s in the gastrocnemius of BaF-transplanted mice (n=6-8).



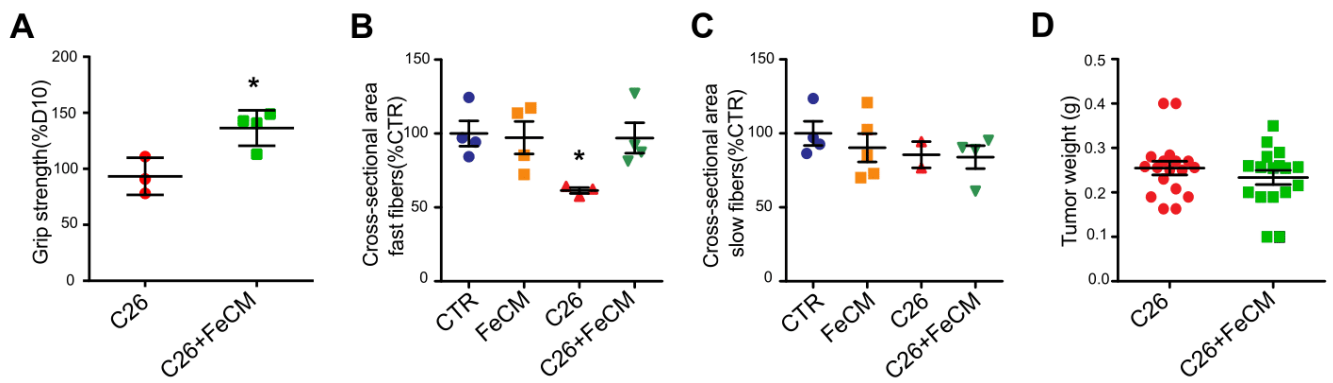
**Supplementary figure 1. (M)** Gastrocnemius TFR1 mRNA levels in mice after deprivation of iron by the combination of iron deficient diet and phlebotomy(n=3-4). **(N)** Gastrocnemius weight in mice subjected to iron deprivation(n=3-4). **(O)** Raw blots of RNA electrophoretic mobility shift assay (REMSA). The biotin labeled IRE probe was incubated without (lane 1) or with 6 µg of cytosolic gastrocnemius extracts from CTR and C26-tumor bearing mice, in native (lane 2) or reducing conditions (lane 4). Where indicated, unlabeled IRE probe was added in 200-fold molar excess (lanes 3 and 5) (n=3). **(P)** Hepatic TFR1 mRNA levels of mice subjected to iron deprivation (n=5-6). **(Q)** Hepatic TFR1 mRNA levels of C26-tumor bearing mice (n=4-5). **(R)** Hepatic liver content in C26-tumor bearing mice (n=11).



**Supplementary figure 2.** (A) Representative western blot of TFR1 after knockdown in C2C12 myotubes. (B) Representative western blot of NCOA4 after knockdown in C2C12 myotubes. (C) Diameter of TFR1-silenced C2C12 myotubes after 24h treatment with iron ionophore hinokitiol (HNK) (n=3). (D) Diameter of C2C12 myotubes treated with C26 conditioned medium and HNK for 48h (n=3). (E) Diameter of C2C12 myotubes treated with LLC conditioned medium and 250nM iron citrate (Fe) for 48h (n=3). (F) Diameter of C2C12 myotubes treated with Activin A (ActA) and 250nM ferric citrate (Fe) for 48h (n=3). (G-I) Basal respiration (G), maximal respiration (H) and spare capacity (I) of C2C12 myotubes treated with C26 conditioned medium and 250nM iron citrate (Fe) for 48h.



**Supplementary figure 3. (A)** Grip strength of C26 tumor-bearing mice 24h after iron injection (day 11 post C26-injection)(**B-C**) Average cross-sectional area of fast (**B**) and slow (**C**) –twitch muscle fibers (n=2-5) (**D**) Final weight of total tumor mass extracted from mice after sacrifice (n= 17)



**Supplementary figure 4**

(A-C) mRNA levels of Carnitine palmitoyltransferase I (CPT1B, **A**), Acyl-CoA thioesterase 1 (ACOT1, **B**), and malonyl-CoA decarboxylase (MCD, **C**) normalized to GAPDH in gastrocnemius (n=5-9)



# General Conclusion

Cancer is among the leading causes of death worldwide accounting for 9,6 million death in 2018. About half of cancer patients develop cachexia, a wasting disorder causing extreme body weight loss and muscle wasting. Importantly, cachexia is associated with a reduced quality of life, a decreased resistance to treatment and a shorter survival. The molecular mechanisms driving cachexia are scarce and to date, there is no approved therapy.

In the present work we addressed two different issues. The first one was to generate a novel mouse model of cancer cachexia. Indeed, the cachexia research field is hampered by the lack of animal models. Most studies rely on a very limited number of models which were used in early studies and then adopted as general models. However, there is a need to develop new models to reflect the wide heterogeneity of cachexia in patients. We therefore established a model of pancreatic cancer related wasting; pancreatic cancer being one of cancer with the highest penetrance of cachexia. By injecting the KPC tumor cells (a clone endowed of high metastatic potential) in mice, we triggered an efficient muscle wasting and importantly with a more progressive pace than in current available models. Unfortunately, we did not managed to obtain overt wasting as the tumor growth was too fast. Nevertheless, we identified several early metabolic alterations in tumor bearing mice such as an increase in fatty acid utilization and ROS generation, a drop in ATP content and the activation of AMPK. Collectively these alterations clearly indicate a mitochondrial dysfunction. Interestingly the onset of these alterations occurs before the emergence of muscle atrophy and atrogenes regulation suggesting that mitochondrial dysfunction is an early event in the pathophysiology of cachexia.

In a second time we hypothesized that systemic alterations of iron occurring in cancer patients could potentially play a role in the development of muscle wasting in cancer, given the crucial role of iron in controlling muscle bioenergetics. To investigate on the influence of iron metabolism dysfunction in cancer related atrophy, we used a well characterized model of cancer cachexia, the C26 model. We found strong alterations of key players in iron metabolism in the skeletal muscle such as a drastic reduction of Tfr1 and an increase of FPN. We identified a mis-compartmentalization of iron in the muscle where oxidative stress impedes the correct regulation of iron by IRP2 resulting in an increased chelated iron in ferritin despite a low iron availability in the cytosol. Those impairments in muscle iron metabolism contribute to a decreased pool of iron in the mitochondria and negatively affect its function. As a result, mitochondrial ATP formation is compromised by the decreased activity of iron-dependent enzymes. We confirmed in cellular models, that iron availability could directly influence muscle

mass. Remarkably, iron supplementation restored mitochondrial function and skeletal mass in C26 tumor bearing mice. Finally, we found that muscle iron metabolism alteration was also a feature of cachexia in humans and preliminary data from iron deficient patients suggest that iron supplementation could be beneficial to restore strength in patients.

Taking together these two pieces of work stress the importance of mitochondrial dysfunction in the development of cancer related muscle atrophy. They are in line with a growing body of literature identifying mitochondrial dysfunction as a key element driving muscle wasting in cancer. Interestingly, we found similarities despite using two different mouse models of cachexia. In particular, we found in both models an increase in oxidative stress, a decrease in ATP generation, an activation of the energy stress sensor AMPK and an increase in fatty acid oxidation. Unexpectedly, we observed a strong difference in SHD activity, while in KPC mice SDH was increased, in C26 mice it was strongly decreased. This difference might be explained by the different kinetic of the two models with KPC corresponding to a pre-cachexia model while C26 to a full cachexia model thus suggesting that SDH activity might vary depending on the stage of cachexia. In the second work, iron supplementation correctly replenished the mitochondrial iron pool and restored mitochondrial function and muscle mass suggesting that mitochondria might be a suitable target to treat or prevent cachexia. Importantly preliminary data of increased strength after iron supplementation in human patients indicate that iron treatment might be clinically relevant. However, further studies will be essential to confirm the critical role played by mitochondria in triggering muscle wasting in cachectic cancer patients, and to determine if iron supplementation might be a suitable strategy to counteract human cachexia.